CALIBRATION AND USE OF GEOLYSIMETERS FOR THE MEASUREMENT OF HYDROLOGIC FLUXES IN MINE CLOSURE LANDFORMS

A Thesis Submitted to the
College of Graduate and Postdoctoral Studies
In Partial Fulfillment of the Requirements
For the Degree of Master of Science
In the Department of Civil, Geological and Environmental Engineering
University of Saskatchewan
Saskatoon

By

JAMES TIPMAN

PERMISSION TO USE

In presenting this thesis/dissertation in partial fulfillment of the requirements for a Postgraduate degree from the University of Saskatchewan, I agree that the Libraries of this University may make it freely available for inspection. I further agree that permission for copying of this thesis/dissertation in any manner, in whole or in part, for scholarly purposes may be granted by the professor or professors who supervised my thesis/dissertation work or, in their absence, by the Head of the Department or the Dean of the College in which my thesis work was done. It is understood that any copying or publication or use of this thesis/dissertation or parts thereof for financial gain shall not be allowed without my written permission. It is also understood that due recognition shall be given to me and to the University of Saskatchewan in any scholarly use which may be made of any material in my thesis/dissertation.

DISCLAIMER

The [name of company/corporation/brand name and website] were exclusively created to meet the thesis and/or exhibition requirements for the degree of Master of Science at the University of Saskatchewan. Reference in this thesis to any specific commercial products, process, or service by trade name, trademark, manufacturer, or otherwise, does not constitute or imply its endorsement, recommendation, or favoring by the University of Saskatchewan. The views and opinions of the author expressed herein do not state or reflect those of the University of Saskatchewan, and shall not be used for advertising or product endorsement purposes.

Requests for permission to copy or to make other uses of materials in this thesis/dissertation in whole or part should be addressed to:

Head of the Department of Civil, Geological and Environmental Engineering
University of Saskatchewan
3B48.3 Engineering Building
57 Campus Drive,
Saskatoon, Saskatchewan, S7N 5A9, Canada

OR

Dean
College of Graduate and Postdoctoral Studies
University of Saskatchewan
116 Thorvaldson Building, 110 Science Place
Saskatoon, Saskatchewan S7N 5C9
Canada

ABSTRACT

The use of geolysimeters as a hydrologic instrument has generally been limited to academic studies. To determine usefulness of geolysimeters in mining reclamation applications, a series of geolysimeters were installed into mine tailing landforms. These were compared to traditional hydrologic instruments over the course of three years.

The geolysimeters installed into aquitards using a fully grouted method had several examples of sensors that provide useful hydrologic data. They compared well to rain gauge readings and show potential to compliment traditional methods of measuring evapotranspiration data. Three sensors showed good potential for use as hydrologic instruments.

Several errors were encountered over the course of the program, and they are described in detail. Errors range from installation into unsaturated zones, shielding failure of wires, data collector errors, extreme weather conditions, and unknown hydrogeological conditions. Based on these errors, several recommendations were made to improve the efficacy of future programs. These recommendations cover program design, instrumentation selection, logger programming, calibration of data, and logger placement.

ACKNOWLEDGEMENTS

Many people have supported me in this endeavor, I would like to acknowledge and thank:

- Syncrude Canada Ltd. for providing funding and support for this project;
- My Supervisors, Dr. Lee Barbour and Dr. Garth van der Kamp;
- Dr. Dyan Pratt for logistical support;
- Dr. Sophie Kessler for help accessing site instrumentation; and,
- My committee members for their patience and understanding.

DEDICATION

To my parents.

And to all the rest who help me to be better.

TABLE OF CONTENTS

LIST OF TABLES

LIST OF FIGURES

LIST OF EQUATIONS

LIST OF ABBRIEVATIONS

AET	actual evapotranspiration
BRF	barometric response function
CPD	cycles per day
EC	eddy covariance
ET	evapotranspiration
GL	geological lysimeter
KC	Clearwater formation - deep marine heavily over-consolidated clay shale
LE	loading efficiency
ML	moisture loading
MFT	mature fine tailings
NaN	not a number
OKC	O'Kane Consultants
PET	potential evapotranspiration
PI	Glacially deposited lacustrine lake clay
P-M	Penman-Monteith
SBH	South Bison Hills
SCL	Syncrude Canada Ltd.
SVAT	soil vegetation atmosphere transfer
SWSS	Southwest Sand Storage
VWP	vibrating wire piezometer
WIP	West in Pit

LIST OF SYMBOLS

A	Coefficient relating the change in deviator stress to a change in confining stress (-)
B	Coefficient relating the change in confining stress to the change in pore pressure (-)
B	Barometric pressure (kPa)
$\underline{B}$	Ratio of pore pressure response to an applied load (-)
BET	Vertical dissipation of excess pore pressure (mm)
BRF	Barometric response function (-)
C_e	Expansion index (m^2/s)
C_v	Coefficient of consolidation (m^2/s)
ET	Evapotranspiration (mm)
LE	Loading efficiency (-)
NP	Net Percolation (mm)
n	Porosity (m^3/m^3)
P	Pore pressure (kPa)
P	Precipitation (mm)
P*	Barometric removed pore pressure (kPa)
dp/dt	Change in pore pressure per change in time
dpa/dt	Change in atmospheric pressure in time
dpe/dt	Change in pressure induced by earth time strains with time
dP	Rainfall impulse (mm)
R	Runoff (mm)
R^2	Proportion of variance for a dependent variable that is explained by an independent variable
ΔS	Change in surficial soil water storage
Sy	Specific yield (cm3/cm3)
t	Time (days)
u	Pore pressure (kPa)
α	Time step coefficient relating pore pressure to barometric pressure
β	Octahedral normal stress loading efficiency (kPa)
γ	Vertical loading efficiency (-)

σ_1 Vertical stress(kPa)

σ_3 Confining stress (kPa)

σ_1-σ_3 Deviator stress (kPa)

σ_b Vertical stress (kPa)

σ_t Octahedral normal stress (kPa)

1 INTRODUCTION

The closure of oil sands mines requires that the reclaimed land be returned to an 'equivalent capability' (Province of Alberta 1993, 2017) to the natural system that existed prior to mining. This equivalent capability includes the ability to support vegetation and hydrological function of the closure landscape over a long time into the future. It is generally understood that monitoring the hydrological performance of these landforms may be required for many decades following closure (Morgenstern 2012). Undertaking decadal or longer-term monitoring using conventional methods of meteorological measurement and reclamation cover modeling may be difficult to sustain.

This research program undertakes to evaluate an alternative method of monitoring the hydrological performance of reclaimed mine waste using what will be described later as a 'geological lysimeter' (GL). This method provides the advantages, over conventional monitoring methods, of having a relatively low cost and maintenance requirements while integrating hydrological observations over a larger ground surface area.

1.1 Objectives

The overall goal of this thesis is to evaluate the use of GLs for monitoring components of the surface water balance at reclaimed mine sites using grouted-in geotechnical vibrating wire piezometer (VWP) installations. Both VWPs specifically purposed for use as GLs and some existing VWP installations used for geotechnical monitoring will be evaluated.

The specific objectives of this study are as follows:

i) Develop a set of recommended procedures for installation, data collection and data interpretation for GLs used to quantify components of soil moisture loading such as precipitation/infiltration and evapotranspiration.

ii) Quantify the lower limit of daily precipitation that can be monitored using GLs based on a comparison to conventional monitoring of rainfall using tipping bucket rain gauges.

iii) Quantify rates of daily evapotranspiration monitored with GLs and compare these rates of evapotranspiration to estimates obtained from site monitoring such as eddy covariance and soil water storage.

1.2 Overview of approach being taken

The approach of this project is to interpret monitoring data from a number of VWPs which have been previously installed for geotechnical monitoring within different oil sands mine waste containment areas as well as a number of VWPs specifically installed for use as GLs. These data records will be evaluated using several different interpretative methods recommended in the literature and the estimated magnitude of soil moisture loading from precipitation or evaporation will be compared to independent measurements of these hydrological processes undertaken on the same sites. Based on the experience gained through the data reduction and interpretation, the final part of the thesis will compile key recommendations as to how this monitoring approach might be implemented at a mine site for long-term closure monitoring.

2 BACKGROUND AND LITERATURE REVIEW

Hydrogeologists and geotechnical engineers have long recognized that the application of an aerially extensive surface load will result in an immediate increase in pore pressure within underlying formations. For example, Jacob (1940) and others observed that water wells in confined aquifers underwent a rapid drop in water level which was proportional to the increase in surface barometric pressure. They referred to this as the barometric well efficiency of the aquifer. The water level in the well drops because only a portion of the barometric load is transmitted to the pore water of the formation while the full barometric load is applied to the water in the riser pipe. This causes water to flow from the riser pipe into the formation resulting in a rapid drop in the observed water level.

The change in pressure within the formation expressed as a fractional portion of the change in barometric pressure is referred to as the barometric loading efficiency. This ratio is the same as the b-bar ($\bar{B}$) pore pressure coefficient described by Skempton (1954). This coefficient is defined as the ratio of the pore pressure response to an applied surface load. In this chapter, we will review the underlying principles that can be used to explain this phenomenon and illustrate a few of the ways it has been used in hydrogeology and geotechnical engineering. We will also review the various methods that have been developed in the literature to interpret the loading efficiency of a formation.

2.1 Theoretical Considerations for Barometric Loading Efficiency

The relationship between barometric loading and the soil pore pressure response has been examined in the literature extensively. The fundamental behavior is the result of soil or porous rock being comprised of two phases - a compressible soil structure which contains a compressible fluid. This saturated system undergoes compression (i.e. one-dimensional volumetric strain) when loaded, with the volumetric strain of the soil being equal to the volumetric strain within the pore fluid (assuming the soil particles themselves as relatively incompressible). Although the volumetric strain of both the soil structure and water are the same, the applied load (stress) must be distributed between these two phases as a function of

their relative stiffness. For an example of this theory: in conventional geotechnical engineering, application of this phenomena has been used to explain the induced pore-pressure within a soft clay resulting from the application of a surface load (Bishop 1954). In this case, because the soil structure is far more compressible than the water, the full surface load is transmitted only to the pore-water; this results in a $\bar{B}$ value of one. In hydrogeology, as noted previously, this phenomenon has been used to explain water level responses in wells to both barometric pressure changes or tidal loading (Jacob 1940, van der Kamp and Gale 1983).

The geomechanics describing this phenomenon rely on effective stress theory (Terzaghi 1943) but with incorporation of fluid compressibility (Biot 1941). Effective stress theory describes stress on a soil element as having three parts: Total stress, which is the force balance of all stresses in a soil; effective stress, which is the stress borne by the soil structure, and pore pressure; the stress borne by the pore fluid. In the case of the soft clay undergoing surface loading, there is initially no change in effective stress as the surface load is transferred almost entirely to the pore-pressure. As the pore-pressure dissipates because of flow to adjoining formations; however, the effective stress increases and the soil skeleton compresses.

Jacob (1940) examined flow in confined, elastic, artesian aquifers and noted compression due to an applied atmospheric load resulted in an associated change in pore pressure, but this pore pressure response was less than the applied barometric pressure. He developed a one dimensional force balance showing that the total stress within an aquifer is split between the soil skeleton and pore pressure; introducing a coefficient, functionally a loading efficiency, that he treated as a mathematical abstract related to the contact area of the soil skeleton with the confining layers over which the hydrostatic pressure was effective (Jacob 1940).

Skempton (1954) worked on undrained pore pressure changes induced by changes in applied stresses in a triaxial apparatus. He related a change in stress to a change in pore pressure (u) by separating stress changes into changes in confining stress (σ_3) and deviator stress (σ_1-σ_3) (Skempton 1954). Changes in deviator stress are related to a change in confining stress using the coefficient A; then the coefficient B is used to relate the change in confining stress to a change in pore pressure (Skempton 1954):

$$\Delta u = B[\Delta\sigma_3 + A(\Delta\sigma_1 - \Delta\sigma_3)] \quad (2.1)$$

In a perfectly elastic soil, A will have a value of 1/3; assigning a coefficient in its place indicates that the soil is behaving in an inelastic manner, and therefore A must be determined through triaxial testing (Skempton 1954). Skempton's definition of B was the ratio of change in the pore pressure due to a change in mean confining pressure. The significance of B is its use in quantifying the relationship of the stressing of the soil skeleton to the stressing of the pore pressure by invoking strain compatibility to find that (Skempton 1954):

$$B = \frac{1}{1+\frac{nC_v}{C_e}} \quad (2.2)$$

Skempton (1954) provided a third coefficient, $\bar{B}$, to relate a change in applied vertical stress to a change in pore pressure. This coefficient is much more useful for field analysis, as a change in vertical stress at a point is the observable change for an aerially extensive loading. Skempton (1954) provides a conversion between $\bar{B}$ and B:

$$\bar{B} = B\left[1 - (1 - A)\left(1 - \frac{\Delta\sigma_3}{\Delta\sigma_1}\right)\right] \quad (2.3)$$

It is worth noting that Skempton's (1954) approach is rooted in empirical determination of the pore-pressure parameters rather than in fundamental elasticity theory.

van der Kamp and Gale (1983) derived a framework to utilize both barometric fluctuations and tidal fluctuations as independent tests to determine formation properties. To do this they introduced Nur and Byerlee (1971) and Rice and Cleary's (1976) extensions of Biot's (1941) consolidation framework to determining the formation properties of specific storage and rigidity modulus from applied tidal loadings and barometric fluctuations. In the process, van der Kamp and Gale (1983) reaffirmed loading efficiencies describing the pore pressure (p) response to changes in octahedral normal stress (mean confining stress) (σ_t) and vertical stress (σ_b). The loading efficiencies are γ for vertical loadings and β for octahedral normal stress. The set of equations specifically relating changes in stress to pore pressure (p) responses are:

$$p = \gamma \sigma_b \tag{2.4}$$

$$p = \beta \sigma_t \tag{2.5}$$

The approaches of Skempton (1954) and van der Kamp and Gale (1983) show how the increase in pore pressure due to an applied vertical total stress can be described using elasticity theory and characterized simply using a loading efficiency. For the remainder of this thesis, van der Kamp and Gale's (1983) loading efficiency (γ) notation will be used for instantaneous, linear loading.

The loading efficiency, once defined through observations of formation pore pressure to a known surface load (i.e. barometric loading), are then applied to estimate other types of areally extensive surface loading (e.g. soil moisture loading). For example, van der Kamp and Maathuis (1991) demonstrated that seasonal fluctuations in the pore pressure record could be used to estimate changes in moisture loading.

A necessary condition for this application is that the total stress change must propagate to the depth of interest. Propagating a detectable stress change to a depth generally happens in two ways: by having a large load placed over a finite surface area (i.e. idealized as a point load) or by having an areally extensive distributed load so that there is no dissipation of the applied load with depth (i.e. idealized as a one-dimensional force balance). Most detectable changes in pore pressure due to surface loading are of the latter type; however, van der Kamp and Schmidt (1997) also conducted a successful field experiment for detecting pore pressure change due to a heavy point load.

Changes in moisture loading due to soil vegetation atmosphere transfer (SVAT) are often considered to be areally extensive. It is of note; however, that the contributing area to a pore pressure response at depth could be inferred from stress redistribution theory. In this manner, the representative area associated with an estimated soil moisture loading can be constrained using stress redistribution theory. This allows the contributing area for any specific location of pore pressure changes to be estimated.

Although the change in pore-pressure associated with a change in surface load is instantaneous (Jacob 1940, Ferris et al. 1962) there may be a time lag associated with the response of the pore pressure measurement (e.g. VWP pressure transducer). This is complicated by the fact that the changes in surface load (e.g. barometric pressure fluctuations) are also transient and consequently the observed pore pressure response is transient. To be a candidate for investigation of surface loadings in the pore pressure, excess pore pressure must be present for long enough after the change in surface loading that it can be measured; i.e. it must not have dissipated before it can be measured. Ideal hydrogeologic conditions for measuring barometric loading, then, are a fully confined, homogenous, artesian aquifer with little lateral groundwater flow or a thick, laterally extensive, and saturated aquitard.

2.2 Methods of Obtaining Loading Efficiency

There are a number of different ways proposed in the literature for estimating barometric loading efficiency from VWP and barometric pressure observations; however, no single approach works in all cases. Several phenomena are potentially observable in the time series for raw pore pressure and, as such, may obscure the loading phenomena. The pore pressure may be trending, noisy, lagged, or may be affected by some other signal which masks the determination of γ. If the pore pressure is stable, the typical methodology used to obtain γ is to create a plot of the change in barometric pressure and cross plot it with the change in pore pressure (Marefat et al. 2015). This method will also reduce trending in the pore pressure; however, trending may also be removed by linear removal of the trend before subjecting the pore pressure to a loading analysis. In general, for softer soils, this should only be necessary if the trending is large (i.e. on the scale of tenths of meters to meters of pressure change over the period analyzed).

General sensor noise may also obscure the barometric loading signal. In this case, it may be necessary to cross plot the raw values of barometric pressure and pore pressure (Tipman et al. 2017). Such a method will not account for sensor drift; however, the change in relative value of the noise relative to the value of the sensor response will enable an indication of the pressure to be observed in this case. For this to work clearly, a shorter window of analysis will reduce the

effect of drift. Combined with linear detrending of the pore pressure time series, this may give a good approximate value for γ (Tipman et al. 2017).

Time lag is an additional effect that may obscure the loading efficiency. As the barometric pressure over the ground surface changes, the pore pressure response within the formation is instantaneous. There is often an initial instantaneous change in the observed pressures as a result of lateral stress transfer to the grouted borehole annulus and this is then followed by a classic exponential pattern of recovery with time back to the formation pore pressures. This phenomenon is a coupled transient stress – pore fluid phenomena, similar to consolidation from geotechnical theory.

This time dependent recovery of the observed pore pressure with time in response to an instantaneous change in barometric pressure is referred to as a barometric response function (BRF). A typical BRF is shown in Figure 2.1. The three key features of a BRF are the initial instantaneous response, the time lag for full recovery and the final equilibrated pore pressure which represents the barometric loading efficiency (LE). This form of loading recovery is referred to as the 'wellbore storage model' (Hvorslev 1951, Rasmussen and Crawford 1997) and represents the pressure difference created by differential stiffnesses between the well completion materials and the surrounding formation equalizing over time through fluid flow between the well and formation.

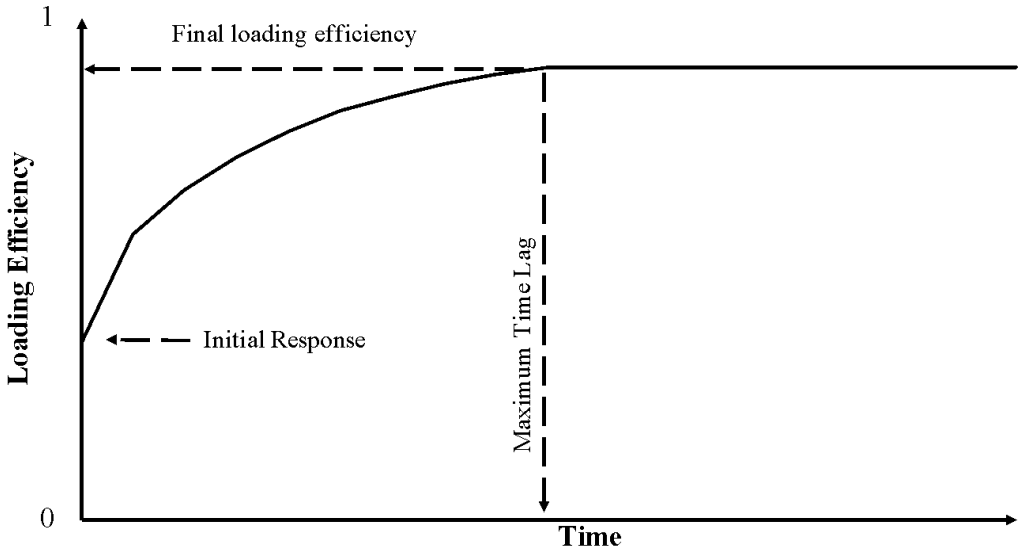

Figure 2.1 – Typical BRF showing a wellbore storage effect

The BRF is typically generated through a linear regression analysis of the time series pore and barometric pressure such as the one presented by Box and Jenkins (1976). Each change in pore pressure (p) at a time (t) is compared to a series of barometric pressure changes (B) extending from some prior time to the change in W. This forms a set of linear equations where each change in p is related to the set of changes in B by some coefficient (α) (Toll and Rasmussen 2007):

$$\Delta p(t) = \sum_{i-0}^{m} \alpha(i) \Delta B(t-i) \tag{2.6}$$

In this equation, m is the oldest time point examined and the number of intervals, while t is the current point. The interval points (i) in the middle are of a consistent time step between each. If this time step is multiplied by the total examined time (m), or the calibration window, of the barometric influence is calculated. The set of α coefficients are calculated for each Δp in the data set that has a continuous set of B observations the size of the calibration window. These compiled α values are regressed by a liner least squares method applied such that the average value for α at each time step is calculated. The BRF value at each time step is the sum of all the α coefficients to that time step, and as such the ultimate loading efficiency is the sum of all alpha values.

A number of studies have use the BRF to help define the hydrogeologic conditions adjacent to the pore-pressure observation. For example, the wellbore storage model shows that the dominant physical phenomenon observed is differences in stiffness and conductivity allowing a very slow equalization of induced pressure differentials between the well pack/standpipe and the formation (Hvorslev 1951, Rasmussen and Crawford 1997). The well may behave in other ways for other settings like unsaturated horizons, or installation into an aquifer; however, for a well installation into an aquitard, the wellbore storage response is typical. The BRF may be calculated using a least squares regression algorithm, as described above, and barometric transients may be removed (i.e. deconvoluted) using the BRF to remove portions of the prior barometric changes proportion to the changes in the value of the BRF at each point.

Another phenomenon that may obscure γ is earth tides. Solid earth tides affect the pore pressure in the earth by causing a regular expansion and contraction of the earth which will cause a correlated fluctuation in the pore pressure (Melchior 1978). Depending on the relative magnitude of the high frequency changes in the pore pressure, tidal fluctuations may add to the 'noise' in the time series pore pressure reading. The influence of earth tides is easily detected, generally, by obtaining a Fourier transform of the pore pressure time series. If the pore pressure is being influenced by earth tides, then power spikes will be seen in the Fourier transform correlating to the major components of the tidal influence. The five largest tidal components are shown in Table 2.1 (Merritt 2004).

Table 2.1 - Tidal components (after Merritt 2004)

Symbol	Frequency (cpd)	Period (hours)	Explanation
O_1	0.92953574	25.819341	Main lunar diurnal
K_1	1.00273794	23.934469	Lunar-solar diurnal
M_2	1.93227356	12.420602	Main lunar semi-diurnal
S_2	2.00000000	12.000000	Main solar semidiurnal
N_2	1.89598199	12.658348	Lunar elliptic (lunar semi-diurnal) component caused by monthly variation in the moon's distance

There are two straightforward ways to remove earth tides from the pore pressure record. Firstly, using signal filtering; this method is to take a Fourier transform and apply band filters tightly around the frequency bands that appear in the transform and Table 2.1. This should be done after barometric removal because barometric pressure is also influenced by tidal forces. With standard signal analysis analytical software, this process is quite simple; however, the main disadvantage that non-pure signals that have been transformed, filtered and inverse-transformed back to their original signal lose their "realness" because non-harmonic data may be lost. A second method for tidal removal is to use publicly available software (TSoft version 2.2.0, 2013) to generate a synthetic tidal force time series for the subject site. This force is then multiplied by an adjustable scaling coefficient and subtracted from the pore pressure time series. The scaling factor is varied to achieve the optimum removal of the earth tide signal from the pore pressure record. Some tidal influence may also be seen in the barometric series, so changing the removal of tidal influence may have a different effect before or after barometric removal.

To verify any mechanically achieved loading efficiency number, a visual inspection should be performed. To do this, the time series raw pore pressure, barometric pressure, and raw pore pressure with barometric transients removed at some loading efficiency are all plotted on the same chart. The loading efficiency is changed until a the 'corrected' pore pressure shows the minimum influence of barometric pressure (Smith et al. 2013).

2.3 Applications of Barometric Loading Efficiency

The two most common ways that barometric loading efficiency has been applied in hydrogeology and geotechnical engineering have been in estimating *in situ* hydromechanical properties of geologic units (e.g. compressibility) and the measurement of surface moisture loading. Moisture loading is defined as change in weight in the overlying profile as a result of change in stored water volume. These would most commonly be due to increases in stored water as a result of precipitation events or loss of water from evaporation (e.g. van der Kamp and Schmidt 1997). It is for this reason that the latter application is often described as a 'geological weighing lysimeter' or 'geolysimeter' since it mimics the function of a weighing lysimeter, which is a hydrological tool for measuring infiltration into a soil profile; in this case by using the response of the geologic medium as the lysimeter.

Laboratory methods for determining the elastic properties of field samples have historically been used in hydrogeological problems. Laboratory testing has problems in terms of sample distortion, scale problems, and so on; leading such measurements to overestimate compressibility. Hydrogeologists have been pursuing field tests that can overcome some of these problems and give a more representative bulk value. Van der Kamp (2001) identifies several in situ methods for determining specific storage, slug testing, constant head pumping tests, permeability testing with pumped wells and observation wells, and pore pressure response to loading. In-situ tests have the advantage that they are not necessarily influenced by sample disturbance. Van der Kamp (2001) discusses the results of in situ methods compared to laboratory methods, generally finding in situ values of compressibility to be up to several orders of magnitude smaller than values obtained by laboratory tests such as oedometer tests.

Methods to determine material properties using surface loading have been discussed in theory by Jacob (1940), van der Kamp and Gale (1983), and Rojstaczer and Agnew (1989). van der Kamp (2001) takes studies by van der Kamp and Schmidt (1997) and Barr et al. (2000) and calculates their specific storage (Ss) values from loading efficiencies. Smith et al. (2013) used the method outlined in van der Kamp and Gale (1983) to determine the compressibility of a thick clay shale aquitard and found that these field based values provided more consistent trending with depth

than laboratory test methods. Marefat et al. (2015) studied the compressibility of Champlain clays to determine their elastic properties. This study was significant because the laboratory testing of highly sensitivity clays is very difficult due to sample distortion.

van der Kamp and Maathuis (1991) showed that soil moisture loading fluctuations could be detected over large time scales by interpretation of the pore pressure record in subsurface confined aquifers. Bardsley and Campbell (1994) showing correlation of the pore pressure record to loading events in the short term in a thick aquifer and suggested that GLs could provide a useful check on hydrologic inputs such as evapotranspiration (ET). This indicates that in the right settings, pore pressure monitoring could be used as an additional input check on surficial hydrologic values. van der Kamp and Gale (1983) provide a governing differential equation for pore pressure distribution in a one-dimensional column, with Barr et al. (2000) revising this equation. It shows the effect that surficial inputs, along with tidal strain, have on the pore pressure.

$$\frac{\partial p}{\partial t} = \gamma\left(\frac{\partial p_a}{\partial t} + \frac{\partial p_e}{\partial t} + P + ET + R\right) + \beta \qquad (2.7)$$

For Equation 2.7, p is the formation pressure, p_a is atmospheric pressure, p_e is induced pressure due to tidal strain, P is the transient pressure induced due to precipitation, ET is the transient pressure induced due to evapotranspiration, and R is the transient pressure induced due to surface runoff. β is the dissipation of pore pressure over time and γ is the loading efficiency.

The β component, of Equation 2.7, is the effect of the formation attempting to returned to a fully drained state from the undrained loading by equalizing the excess pore pressure with surrounding formations. This process is governed by flow properties of the formation, and therefore is proportional to the hydraulic conductivity, amount of excess pore pressure and thickness of the formation. Smith et al. (2013) notes that this could take months to years in low conductivity formations.

The appropriate hydrogeological conditions were extended to thick clay aquitards, indicating that the actual requirement is sufficient hydraulic isolation from neighboring hydrogeological events

(van der Kamp and Schmidt 1997). The van der Kamp and Maathuis (1991) study also indicated that the area over which the surface load was being integrated was consistent with geotechnical stress distribution methodology, and therefore the reading area of a GL can be on the order of hectares. The pore pressure has been recorded showing fluctuations due to rainfall as deep as 300 m (Sophocleous et al. 2006). Barr et al. (2000) extended the concept of confirming individual hydrological inputs with a GL to attempting to confirm multiple inputs using a superposition assumption. Smith et al. (2017) used GL data to measure solid precipitation; comparing the moisture loading change to snow measurement showing a small amount of undercatch. Van der Kamp and Schmidt (2017) presents precipitation and evapotranspiration surface loading for yearly cumulative loads and short-term cumulative precipitation results (van der Kamp and Schmidt 2017).

When a GL is placed into a complex situation with a fluctuating ground water table, the pressure from those fluctuations will propagate downwards through the various formations from the ground water table as pressure waves. This results in pore pressure fluctuations with a lagged response from the surficial input. Anochikwa et al. (2012) used a computer model to determine the lagged response due to the hydraulic diffusivity of the GL's formation by modeling the best relationship between the input and the observed response. Bardsley and Campbell (2007) used a set of nested piezometers to provide a combined GL response that is more accurate than either individual response. Those authors, and others, also used GLs in aquifers to attempt to calibrate gravity methods of estimating surficial water balance (GRACE) (Bardsley and Campbell 2000, Lambert et al. 2013)

2.4 Summary

Barometric loading can be explained from the theory of elasticity as applied to a compressible porous medium such as soil or rock. The theory allows a loading coefficient to relate pore pressure increase to an applied load and allows for an increase in pore pressure to be interpreted as a surface load. This methodology has since been used to detect surface loadings such as precipitation or evapotranspiration and hydromechanical properties. For this technique to work, site selection, equipment selection and field techniques must be carefully planned and executed

to identify the relatively small loadings of SVAT phenomena compared to other observable pore pressure changes. With data collected, several methods of determining loading efficiency are possible, including linear correction, calibration using the slop of a plot of transients, or deconvolution using the time domain.

3 SITE DESCRIPTION AND INSTRUMENTATION

This chapter will describe the site location, geology, specific site descriptions, exploration details, installation details, and field techniques used in this study.

3.1 Mildred Lake Mine Site

This chapter describes the site location and instrumentation used in this study. This project was carried out at the SCL Base Mine Lake site. This is an oil sands mine site which is located approximately 45 km north of Fort McMurray, Alberta, Canada. This site has been in operation since 1978, processing oil sands deposits in the Athabasca river basin into petroleum products. The site location is shown in Figure 3.1.

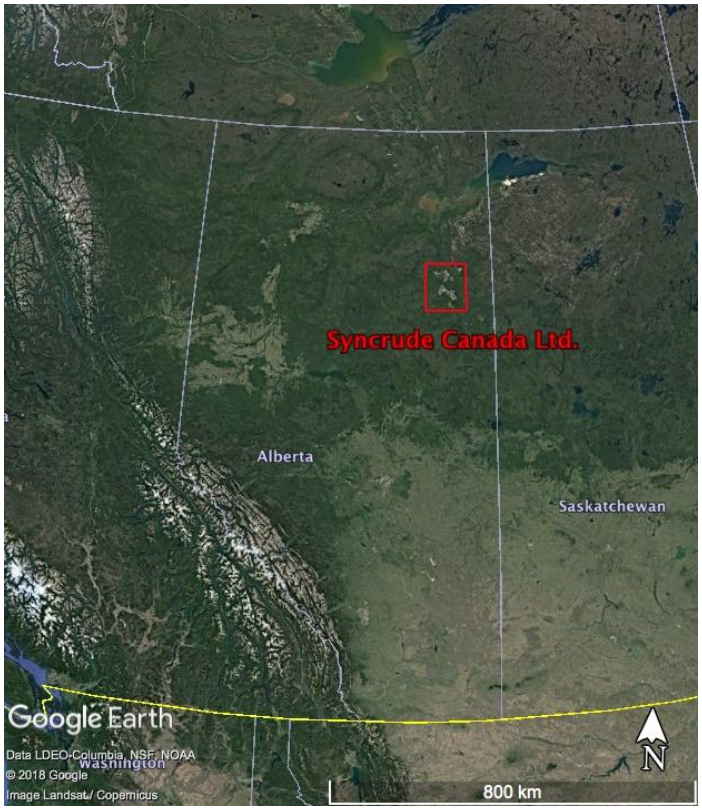

Figure 3.1– SCL Geographic location (Google Earth)

3.2 General Geology

The SCL Base Mine Lake site is extensive and, owing to that, has varied surficial deposits overlying bedrock with the upper bedrock sequence being the Cretaceous Clearwater formation shales. In general, the area surrounding the study area has been well described by SCL. The surficial geology generally indicates that the surficial units are Pleistocene in origin, composed of glacio-lacustrine (Pl) units overlying glacial deposits (Pg). There are some meltwater (glaciofluvial) (Gf) channels within the Pleistocene deposits which are sand and gravel with cobbles and boulders. In areas of topographic lows, organic Holocene (Ho) deposits can be found near to the surface.

The upper bedrock underlying the study area is Cretaceous deposits of the Clearwater formation. The entire unit is described as Kc and has been subdivided into 1 member and 7 units. The Wabaskaw (Kcw) member forms the base of the Clearwater formation. Overlying the Wabaskaw member are the Clearwater units, referred to as Kca – Kcg in ascending order. The Clearwater formation is composed of silty shale, laminated siltstone, and fine-grained sandstone of marine origin. The contact between the Clearwater formation and overlying Pleistocene deposits is rafted in some places due to glacial action. Below the Clearwater formation is the McMurray formation, which underlies the study site. In general, for the remainder of this examination, Pl, Pg, and Kc are the descriptors of note.

3.3 Site Locations

The Mildred Lake mine site is undergoing progressive reclamation from the south end of the mine towards the north end. The location of a number of the key reclaimed landforms on which GL monitoring was installed are shown in Figure 3.2. These landforms include:

- Southwest Sands Storage (SWSS) - a sand tailings dyke which forms a large structure in the south west portion of SCL's site;
- W1 and W2 – Out of Pit shale overburden dumps (stockpiles);
- South Bison Hills (SBH) - a reclaimed set of landforms on the south edge of the site; and,

- An undisturbed site labeled as the “Natural” site which is included in the discussion of the SWSS locations. This site is intended to provide a background data set.

Figure 3.2 – View of SCL site highlighting landforms instrumented for this project (Google Earth)

3.4 Field Instrumentation

The installation of the VWPs used during this investigation is composed of a number of time spans and methods. The VWPs installed specifically for this project were installed over approximately a month and a half, from June 22 through August 03, 2013. These VWPs were identified by a prefix designator BHLB. The drilling method used for these installations was sonic drilling. The holes were drilled deeper than the installation horizon and completed in the following manner:

- Backfilled with Bentonite Holeplug (natural smectitic clay chips) to the depth of VWP sand filter;
- The VWPs were installed within approximately 1 m of frac sand (sand designed for filter packs with consistent grain sizes);
    - All VWPs installed specifically for this project were Geokon 4500s with a 350 kPa full scale pressure rating;
- The frac sand pack was then covered by approximately 1 m of Bentonite Holeplug; and,
- The remainder of the hole was backfilled with Bentonite EZ seal, a low permeability bentonite-cement grout mixture.

In the case of BHLB08, the backfill above the sand pack was completed entirely with Bentonite Holeplug.

The SCL geotechnical monitoring sensors were not installed specifically for this study but were a standard installation for geotechnical monitoring of the various structures. The VWPs were installed as multiple stacked VWPs in one borehole and where designated as:

- VP-12-32-02 - 2 piezometer stack in the SWSS landform;
- VP-09-32-03 – A 3 piezometer stack on the SWSS landform;
- SIVP080046 - A 3 piezometer stack on the W1 landform; and,
- SIVP080069R – A 2 piezometer stack on the W1 landform.

Due to the multiple VWPs per installation, the specific VWP is indicated as upper, lower, or middle to refer to the shallowest, deepest and middle sensor, respectively. Locations with 2 sensors will have an upper and lower, while 3 sensor locations will have upper, lower and middle, as outlined below.

VP12-32-02 is a 2-piezometer stack. The borehole was drilled using wet rotary methods. The borehole records show the following installation details:

- Bentonite Holeplug from surface to just above a layer of Bentonite EZ-Seal (1.5 m minimum thickness), ending at a depth of 31.9 mbgl.
- A sand pack from 31.9 mbgl to 33.3 mbgl. The upper piezometer is within the sand at 32.6 mbgl.
- A layer of Bentonite Holeplug (minimum thickness 0.5 m) underlain by Bentonite EZ-Seal and a second layer of Bentonite Holeplug (minimum thickness 1.5 m) to a depth of 54.4 mbgl.
- A sand layer from 54.4 mbgl to 55.4 mbgl with a piezometer within at 55.1 mbgl.
- Bentonite Holeplug to the termination depth of 66 mbgl.

VP-09-32-03 was drilled using coring methods. The completion details are outlined below:

- Bentonite (Type unknown) from ground to 15.24 mgbl;
- Sand from 15.24 to 16.17 mbgl; a piezometer (denoted Upper Tip) in the sand at 16.00 mbgl;
- Bentonite from 16.17 to 22.09 mbgl;
- Sand from 22.09 to 22.25 mbgl with a piezometer (denoted Middle Tip) in the sand at 22.2 mbgl;
- Bentonite from 22.25 to 29.84 mbgl;
- Sand from 29.84 to 30.18 mbgl with a piezometer (denoted Lower Tip) at 30.02 mbgl;
- Bentonite from 30.18 mbgl to the bottom of the drill hole at 35.02 mbgl;
- A 2" PVC casing pipe is used to protect the VWP wires from damage near the ground surface (from an unknown stickup to an unknown depth below the ground level but above the upper tip sand horizon) was set into the Bentonite and has been filled with Bentonite chips.

SIVP080046 is a 3-piezometer stack that was drilled using dual rotary drilling methods. The piezometer stack was installed as supporting instrumentation for a slope inclinometer installation, and therefore was attached to the SI casing and grouted in place without a sand filter pack.

SIVP080049R is a 2-piezometer stack that was drilled using a coring method (exact method is unknown). It was installed as a Slope Inclinometer with two supporting piezometers. This hole was completed with full grouting, with a small layer of frac sand and a Bentonite plug at the surface.

All the SCL piezometers were SI 52611030 model, which has a full scale of 690 kPa. All instrumented piezometers in these stacks were completed in KC completion horizon, with the exception of SIVP080069R's upper tip, which was completed in a redeposited "PI" clay dump.

3.5 Installation Locations

South West Sand Storage (SWSS)

SWSS is a sand tailings storage structure designed to be approximately 60 m high with 20H:1V side slopes. The pond in the middle of the structure was originally designed to have very small amounts of fine tailings; however, some mature fine tailings (MFT) is stored within the development pond. Drill logs show that the structure is primarily fine to medium grained sand overlying KC material. Figure 3.3 shows the overall layout of SWSS as well as the area of focus in this study, Cell 32. The actual line of boreholes drilled for this project is close to the Cell 31 area; however, for the purpose of this thesis all SWSS instrumentation will be noted as Cell 32. Figure 3.4 shows the specific locations of sensors at within the structure.

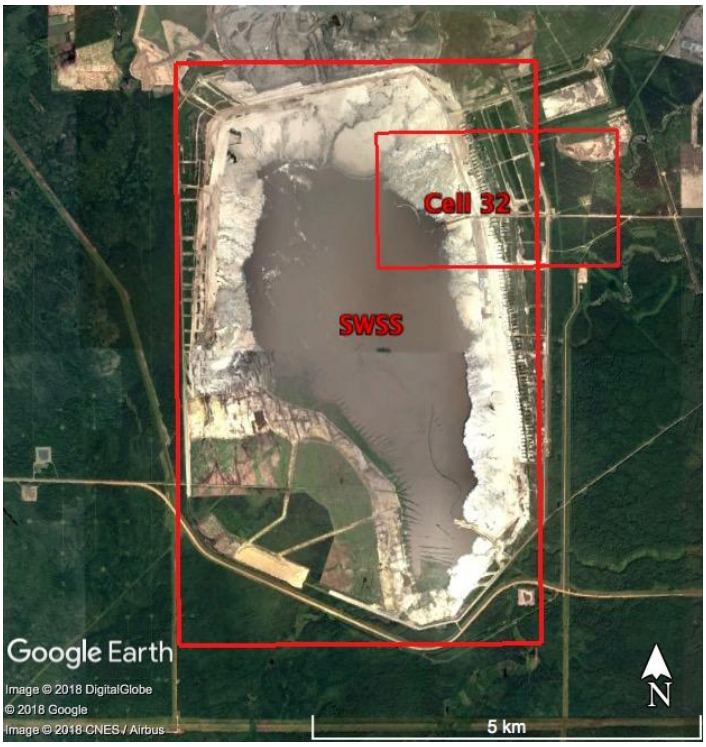

Figure 3.3 – SWSS (Google Earth)

Figure 3.4 – Cell 32 VWP Layout (Google Earth)

The top of the sand tailings dyke is to the west of BHLB07 and VP-12-32-02, and the toe of the dyke is just west of the road that runs NNW-SSE between VP-09-32-03 and BHLB03. The boreholes specifically drilled for this project are BHLB07, BHLB08 and BHLB03. The VWP stacks VP-12-32-02 and VP-09-32-03 were installed for geotechnical monitoring of the dyke.

No borehole logs were provided for VP12-32-02 and VP-09-32-03, however instrument details and installation depths were provided. All available installation details and borehole logs for SWSS can be found in Appendix A.

The VWP in Borehole BHLB07 was located at a depth of 45 m and the installation was in KC approximately 11.5 m below the tailing sands. BHLB08 was installed to a depth of 29.5 m in KC, approximately 13 m below the sand tailings. Table 3.2 shows installation depths and elevations.

Table 3.1- SWSS Installation depths

Hole ID	Surface Elevation (masl)	Depth drilled, (m)	Depth installed, (m)	Installation Elevation (masl)	Installed Formation Material
BHLB03	348.3	25.9	23.0	325.3	KC
BHLB07	389.1	50.3	45.4	343.7	KC
BHLB08	369.4	32.0	29.5	339.9	KC
VP-12-32-02-Lower Tip	388.5	66.8	55.1	333.4	KC
VP-09-32-03-Upper Tip	362.0	35.0	16.0	346.0	KC
VP-09-32-03-Middle Tip	362.0	35.0	22.2	339.8	KC
VP-09-32-03-Lower Tip	362.0	35.0	30.0	332.0	KC

BHLB03, at the natural site, was installed at a depth of 23.5 m in KC, approximately 15 m below the surficial fill materials (6 m in depth), till, clay, and into the Kc formation. The siting is relatively flat lying, and it is at the edge of a fenced compound that is occasionally used for material stockpiling.

BHLB07, BHLB08, and BHLB03 were initially installed with Geokon LC-2 dataloggers. Some monitoring of VP-12-32-02 and VP-09-32-03 was attempted using a Slope Indicator Quattro datalogger, however recorded datasets from VP-12-32-02 and VP-09-32-03 were not long and continuous enough for use.

In the spring of 2015, all the VWP dataloggers in the project were upgraded to new loggers by RST. This system is composed of "base" stations and remote single channel and multi-channel data loggers. The base stations are Campbell Scientific CR 1000 dataloggers in an automated collection system. The base station collects remote dataloggers over a wireless network. The remaining dataloggers were RST DT2011 for single channel sites and RST DT2055 for VP-09-32-03. This collection system collects all data for the SWSS loggers and transmits it over the internet to a computer at the University of Saskatchewan daily.

South Bison Hills (SBH)

South Bison hills is an overburden waste dump composed primarily of saline-sodic clay shales that have been either end-dumped or paddock dumped into the previously excavated West in Pit (WIP) (Chapman et al. 2006). The deep shale profile is generally unsaturated with deep, but rising, water levels as a result of filling of the adjacent end pit lake referred to as Base Mine Lake.

Two VWPs were installed at SBH: BHLB04, near the crest of the landform, and BHLB05 near the toe. This can be seen in Figure 3.5.

Figure 3.5 – South Bison Hills showing VWP installation (Google Earth)

BHLB04 was installed at a depth of 29.5 m at the bottom of the backfilled pit in order to target a small lens of intact KC above a lean oil sands deposit. BHLB05 was installed at a depth of 20.9 m in a thin silty clay member just above the interface of the Clearwater formation with underlying oil sands deposits. It is just below a fine sand lens. Full borehole logs can be found in Appendix A. Both boreholes were initially monitored using Geokon LC-2 single channel monitors. In the spring of 2015, these dataloggers were changed to a remote wireless collection system as described for SWSS above. In this case, BHLB04 was the designated "base" station using Campbell Scientific CR-1000 datalogger and BHLB05 was the remote station using a DT2011. Table 3.2 shows the completion elevations and depths.

Table 3.2 – SBH installation depths

Hole ID	Surface Elevation (masl)	Depth drilled, (m)	Depth installed, (m)	Installation Elevation (masl)	Installed Formation Material
BHLB04	348.5	50.0	29.5	319.0	Kc
BHLB05	315.1	21.5	20.5	294.6	Kc

W1/W2

W1 and W2 are both shale overburden dumps to the north of SWSS as shown in Figure 3.6. W1 was designed with a target height of 40 m (Personal correspondence with Dallas Heisler, SCL). The two sensors used for this project at the W1 site were installed for geotechnical monitoring. SIVP080046 is a 3-piezometer stack which began monitoring in Spring of 2015. All three tips are logged as being in KC at depths of 47, 59, and 62 mbgl. The overburden fill extends from ground surface to approximately 31 mbgl at that location. SIVP080069R is a 2-piezometer stack; however, only the upper piezometer, at a depth of 18.5 mbgl, in Pl material, was used for this study. The offset between the two sensors is approximately 14 m with SIVP080046 being uphill of SIVP080069R.

W2 is a shale overburden dump to the east of W1. No design details were available from SCL for this site. Two boreholes were drilled for the VWP installation. BHLB01 is near the crest of the dump while BHLB02 is midslope. BHLB01 was installed at 25 mbgl with a frac sand pack in KC. The drill log shows that the overburden fill begins at approximately 15 mbgl. BHLB02 was installed at 17.4 mbgl in frac sand. It was installed in KC with the overburden fill beginning at a depth of approximately 11 mbgl.

The W2 sensors were initially logged with Geokon LC-2 dataloggers, however in March of 2015 the dataloggers were changed, with BHLB01 becoming a base station with a Campbell Scientific CR-1000 datalogger and BHLB02 getting a RST DT2011. At the same time the W1 sites had a RST DT2055 installed on SIVP080046. SIVP080069R had a RST DT2011 installed on the upper channel. The W1 sensors use the BHLB01 as their base station. The installation depths and elevations are shown in Table 3.3.

Table 3.3 - W1/W2 installation depths

Hole ID	Surface Elevation (masl)	Depth drilled, m	Depth installed, m	Installation Elevation (masl)	Installed Formation Material
BHLB01	351.8	27.4	26.4	325.4	Kc
BHLB02	346.3	19.8	17.4	328.9	Kc
SIVP080046-Upper Tip	366.4	96.3	45.7	320.7	Kcc
SIVP080046-Middle Tip	366.4	96.3	57.9	308.5	Kcb
SIVP080046-Lower Tip	366.4	96.3	64.0	302.4	Kca
SIVP080069R-Upper Tip	354.6	28.6	18.3	336.3	Pl

Figure 3.6 – W1 and W2 showing instrument locations

3.6 Field Methods

Data was initially collected from the instrumentation every 2-6 months using a USB download from the Geokon LC-2 and Quattro dataloggers. The VWPs were read at 30-minute intervals over the course of the summer of 2013 from the VWP installation period to April 2015, when the RST system was installed. At the same time as the Geokon loggers were downloaded, the Solinst barologgers were also downloaded. Once the datalogger system was changed to the RST

system, the wireless network collected 10-minute interval readings and uploaded it to a host computer at the University of Saskatchewan daily.

Approximately 3 site visits were made each year. These visits occurred during the summer of 2013 through April of 2015 and were used to collect data from the various dataloggers and barologgers. Data was downloaded to a laptop. The sensors were initially set up to record every 30 minutes. This number of cycles per day (CPD) is a high frequency of data collection relative to the slow fluctuations commonly associated with barometric pressure. Even so, it would have been valuable to have set an even higher frequency; however, the internal memory capacity of the Geokon loggers would have filled sooner, necessitating more site visits. Once the RST loggers were installed in April 2015, there was no longer a restriction imposed by the logger data capacity, and so the frequency was set to 10-minute (144 CPD). After the April 2015 datalogger change, the RST network was downloaded daily onto a computer at the U of S. The data was downloaded as one large data file for each landform (SWSS, SBH, W1/W2). The large data file was separated using a custom MATLAB program that breaks the data up into files for each individual sensor.

3.7 Other instrumentation

Data from some previously installed VWPs at the site was also used in this study. This instrumentation included eddy covariance monitoring, barometric monitoring, and weather stations including near surface soil moisture sensors.

The primary weather station used for this project was installed near the BHLB08 site by O'Kane Consultants (OKC) in 2001. It is on the same bench as BHLB08, but approximately 200 m south. The station monitors temperature, solar radiation, relative humidity, wind speed and direction, and precipitation. The data collection and calibration of the weather station was performed by the OKC personnel. The instrumentation details have been provided in Appendix C (personal correspondence with Amy Heidman – OKC).

Barometric sensors were installed on BHLB07, BHLB01 and BHLB04. These were Solinst barologger model sensors. In early summer of 2015, a RST ELM0030A Vibrating wire barometer was wired into the DT2055 installed on VP-09-32-03. Prior to June 16, 2015, all barometric pressures were collected with a barologger co-located with BHLB07. On June 16, 2015, a pressure transducer was wired into the RST multi-channel datalogger at the VP-09-32-03 site and collected barometric data at the same interval and timing as the rest of the RST system. Other barologgers were available at BHLB01 and BHLB04 as a backup to the BHLB07 barologger.

An eddy covariance system was installed by personnel from the McMaster Watershed Hydrology group based in McMaster University. This system was installed near to the BHLB08 location, but approximately 60 m south. Data collection and processing for the eddy covariance system was performed by the McMaster university personnel. Details of the installation have been provided in Appendix B (Personal correspondence with Dr. Sean Carey).

4 METHODS OF ANALYSIS

This chapter summarizes the analytical methods used to evaluate the VWPs performance as GLs. This chapter briefly describes the link between pore pressure data and moisture loading (ML). The bulk of the remainder of this chapter describes taking the field data and building it into "moisture loading." After a description of the generation of ML estimates, there follows a description of the methodology of comparison of ML and other hydrological data from conventional monitoring is given.

The generation of ML is performed using Equation 2.7. The process to generate a ML is as follows (the individual steps will be expanded further in the following subsections):

1. The first term that exists in the pore pressure which may be clarified is the dissipation term. The β term is usually ignored for small timeframes (a few weeks); however, modeling could potentially be used be used to help characterize its impact. Limiting site selection to well confined (laterally and vertically) aquifers or aquitards will minimize the impact of this term. In this paper, the term was ignored due to selection of sites with a low hydraulic conductivity. For the purpose of interpretation, the GL dataset should show minimal dissipation within the timescale of days to a few weeks, but longer data sets may contain enough of the effect of dissipation to be in error.
2. The removal of p_a (barometric pressure) was performed during calibration. With the BRF term, by combining the BRF with the barometric pressure signal to produce a scaled and lagged input, which is then subtracted from the measured pore pressure. With the linear LE, the barometric pressure was multiplied by the LE and subtracted.
3. The removal of p_e (earth tides induced pore pressure changes) was a two-step process. Firstly, the pore pressure was checked using Fourier analysis to see if there was significant tidal energy. If cases had existed where there was a tidal effect, an artificial tidal signal was generated with the Tsoft tidal prediction software for the location and time and this tidal signal scaled and linearly subtracted from the pore pressure signal. No cases were found with noticeable effects of earth tides on the pore pressure signal once the barometric effects were removed. As such, no linear removal was performed.

At this point, the GL readings are referred to as MLs. The ML trends were:

1. Examined visually for visible hydrological influences and other influences.
    a. Those which show some effect of hydrological influences were further examined.
        i. They were examined both visually and statistically against other measurements of precipitation, and
        ii. they were compared to estimates of ET derived from Penman-Montieth and Eddy Covariance.
2. Finally, a simplified water balance was constructed from the hydrological monitoring and was compared to the ML for one of the sensors. The remainder of this chapter will describe the above processes in more detail.

4.1 Data Synthesis

The calibration of the VWPs was done by the manufacturers by comparing vibrating wire frequency to pressure standards, resulting in the "TI" or "ABC" parameters for converting the observed VW frequencies to pressure data. Field data from each VWP was converted to pressure values using the inverse process; field data was not corrected for barometric pressure changes during the initial conversion. The 'TI' calibration curve was used if available; however, for some sensors the "ABC" method was used as factory calibration sheets were not available. Provided conversion spreadsheets from SCL only had the "ABC" coefficients recorded from the factory calibrations. The conversion was performed in a spreadsheet (Excel, 2010) for the Geokon data; however, as the datasets became larger, especially after the RST installation, a custom script was created in MATLAB (MATLAB version R2013b, 2013) to convert the frequency data as it was imported from a large downloaded data file. The resulting pressure data is the raw piezometric time series data used in subsequent analyses.

The pressure datasets were then checked to ensure that readings existed at all times required to continuously fulfill the target frequency; that is to say every 10 or 30 minutes exactly. Occasionally one data point needed to be omitted or filled (by interpolation) between the datasets to maintain continuous data. If more than one consecutive point was missing or corrupted, no filling was done. The data were then stored as yearly sets. This was all done in using spreadsheet

software to limit the BRF process from removing too much data in cases where the sensor has an intermittent signal that misses a reading every few hours or days.

The yearly datasets of raw pore pressure data were first visually inspected to identify poor data sequences that could be excised before further processing of the data series. Some examples of poor data included: clearly erroneous readings (i.e. readings that show wild fluctuations with no corresponding hydrological process at the same time), no piezometer response readings, and data gaps. These data were excised where necessary.

4.2 Tidal Removal

Once the clearly erroneous data were removed, the data sets were examined for the presence of earth tides, and when found the tidal effects were removed. Solid earth tides were checked for using Fourier methods. The data set, and/or portions of that data set were imported into one of two software programs, MATLAB or TSoft, and a fast Fourier transform was performed. The transform was examined for significant spectral power at the characteristic tidal frequencies, as summarized in Table 2.1. If significant tidal influences were observed, they were removed by subtraction of a synthetic earth tide as generated by the TSoft software. This synthetic tide was scaled by an appropriate coefficient and subtracted from the data set. A subsequent Fourier transform would then check whether there was spectral power at tidal frequencies.

4.3 Linear calibration and barometric removal

Two methods of calculating γ were employed. The first was to compare the barometric pressure and pore pressure, and the second was to examine the change in barometric pressure against the change in pore pressure.

To use either method, firstly a system "calibration windows" was created at multiple times spaced evenly throughout the year (e.g. September, December, April, June). These calibration windows were an attempt to ensure that the loading efficiencies were stable and not changing due to well recovery or other effects. The calibration windows were limited to a month of data based on whatever continuous data set was available for that month. These windows were often

shortened to take advantage of continuous readings. This was performed visually to minimize the influence of pore-pressure trending and excess noise.

In the first method of calibration, a graph of δB vs δP (in this case the δ operator is used to indicate the change in value between two points, and not an infinitesimal change) was plotted for each calibration window and a linear best fit was performed on the results. In theory, this should yield a graph with a slope equal to γ; however, the plot can be susceptible to sensor noise (Tipman et al. 2017). Additionally, a full month of data processed at 48 or 144 CPD can contain enough data to be unworkable by spreadsheet. In these cases, the calibration window was shortened until the highest R^2 between the raw pore pressure and the barometric pressure scaled by the loading efficiency for that particular dataset was reached.

The second method of estimating γ was by cross-plotting B vs P. This plot differs from the plot of δB vs δP in that it is less susceptible to sensor noise and pressure changes not caused by barometric pressure loading changes (i.e. precipitation inputs). It has the disadvantage of being much more susceptible to long term trends in pore pressure such as drainage (Tipman et al. 2017). The barometric loading efficiency is evident in this plot by the overall slope of the plotted data while long-term trends in the pressure will cause the plot to shift up and down vertically. If vertical shifts in the plot are apparent, then the calibration window was shortened to find a smaller window that minimizes the drift. The slope of the diagonal movements represents γ in this case; as they are largely caused by barometric pressure fluctuations, and so it may be estimated through a regression line that matches the diagonal movement. It should be noted that directly estimating the slope is highly prone to capturing effects of pore pressure drift and should only be used as an estimate.

The two methods of estimating γ were applied on each calibration window for each sensor and the value of γ and the R^2 of the fit were recorded. Based on these initial estimates of γ, a value of γ was selected as a starting point for a visual analysis that was used to determine the final value of γ for the VWP. The visual analyses were performed by plotting the barometric pressure time series overlain on a plot of the pore pressure time series with γ times the barometric pressure removed from the pore pressure series. The value of γ was then varied until the influence of

barometric fluctuations on the corrected signal is minimized. Once a final gamma value was determined, the barometric transients were removed using the Smith et al. (2013) method of linear subtraction.

4.4 Time domain calibration and barometric removal

A BRF for each instrument was also calculated for each continuous dataset using the regression analysis and deconvolution method outlined by Toll and Rasmussen (2007). This was performed in MATLAB using a program designed to calculate the BRF and then deconvolute it. In this analysis, the length of the dataset being deconvoluted adds to the statistical rigor of the least squares regression that determines the BRF, so it is preferable to perform the process with larger data sets. Accordingly, the processing was done with the yearly datasets. The BRF and output pore pressure (with barometric transients removed) were examined after their calculation to ensure the deconvolution was successful. The window examined for maximum lag that was observed in deconvolution - an input requirement for the BRF algorithm as programmed - was initially set to a time lag exceeding any reasonable site parameter (e.g. 24 hours). The calibration window is shortened to match the "peak" of the output BRF. This process is iterated until the ultimate point is the final point in the BRF (occasionally the penultimate point was used). The BRF is then used by convoluting it with the barometric readings and removing it from the pore pressure readings. This process outputs the change in pore pressure without barometric effects.

A final comparison was made between the loading efficiency obtained using linear removal of barometric pressure from pore pressure, and those obtained with the time domain method of removing the barometric pressure from the pore pressure. This comparison was done visually. Typically, the two charts were very similar, but one would appear "cleaner" which is to say with less high frequency noise causing vertical banding of the data points. The "cleaner" chart and corresponding deconvolution method was then used for the further analysis of this project.

The determination of barometric loading efficiency/b-bar and its removal is a core concept of this work, and foundational to the derived moisture loading and other derivative outputs from

this process. An example of this technique, the calibration of the BHLB08 piezometer in 2014, is presented here. The linear technique is presented first. In this technique, the raw pore pressure is cross plotted with the barometric pressure and a residual pore pressure. The residual is generated by linearly subtracting a portion of the barometric pressure from the pore pressure. Figure 4.1 shows a linear calibration for the dataset with a γ coefficient of 0.9; this value was selected to be the best fit value after a manual optimization. The scales of barometric pressure and pore pressure/residual pressure are forced to the same range (20 kPa), so the variations are in proportion to one another.

The residual shows a fair amount of high frequency noise which may indicate incomplete removal of barometric pressure. To view it more clearly, Figure 4.2 shows just the month of April, 2014 with the same γ. Figure 4.2 shows visually that the removal of barometric transients from the pore pressure was likely complete.

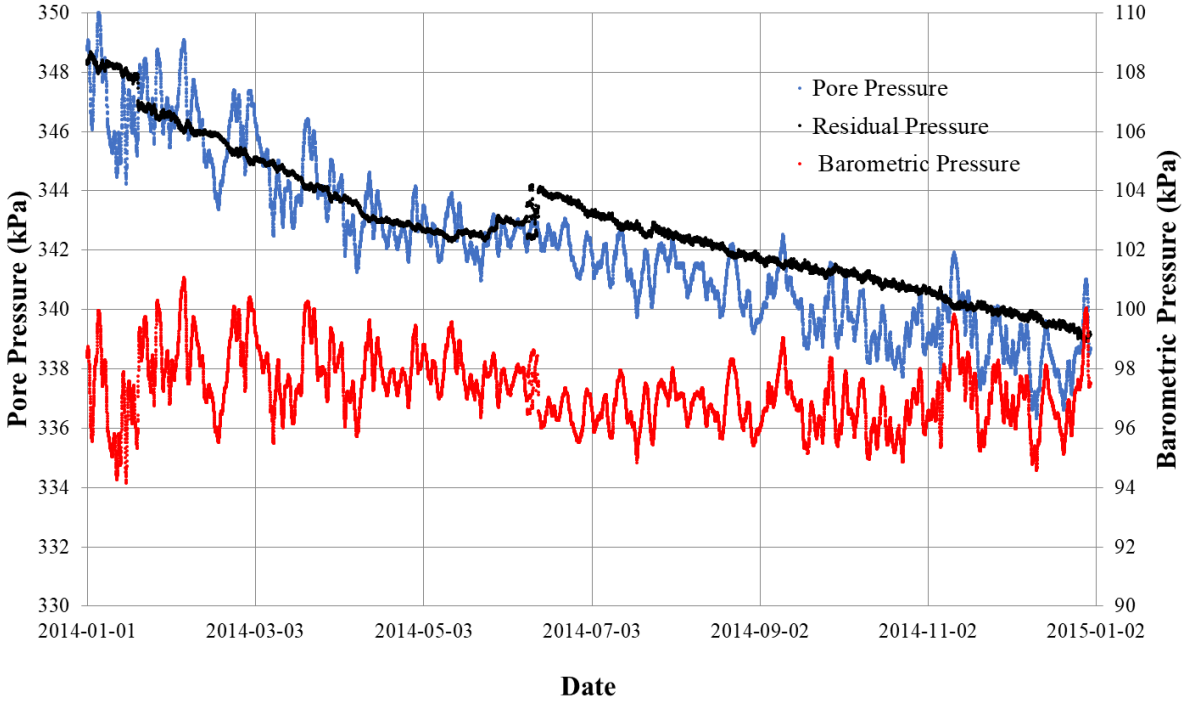

Figure 4.1 – Pore Pressure, Barometric Pressure and Residual pore pressure for BHLB08 during 2014

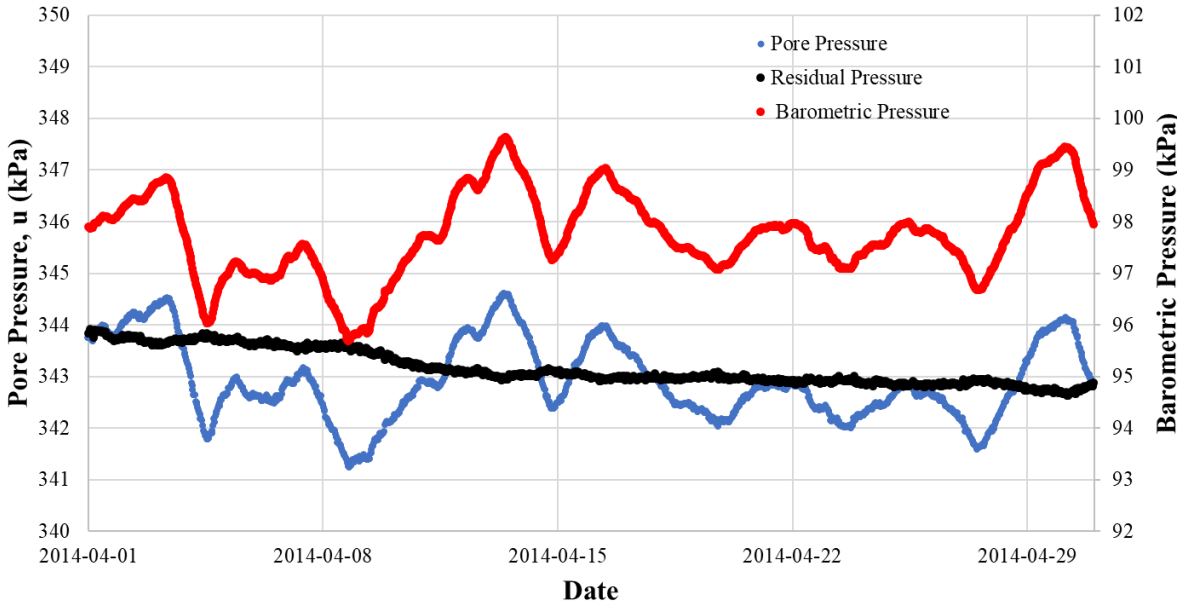

Figure 4.2 – Pore Pressure, Barometric Pressure and Residual pore pressure for BHLB08 in April 2014.

The BRF calibration was performed next. It was performed in computer using an algorithm as described earlier in the chapter. The BRF deconvolution is shown in Figure 4.3. A data gap is apparent in June of 2014. In the linear removal (Figure 4.1), there is no data gap, but in the barometric data some clearly visible erroneous data. That data is likely due to the severe thunderstorm causing a large pressure fluctuation. That particular data was having a large effect on the linear least squares averaging portion of the deconvolution process, and as such was excised. The results look similar to the linear removal, but the resultant line is smoother, with less variation. This is likely due to the small amount of lag that is accounted for by the BRF algorithm.

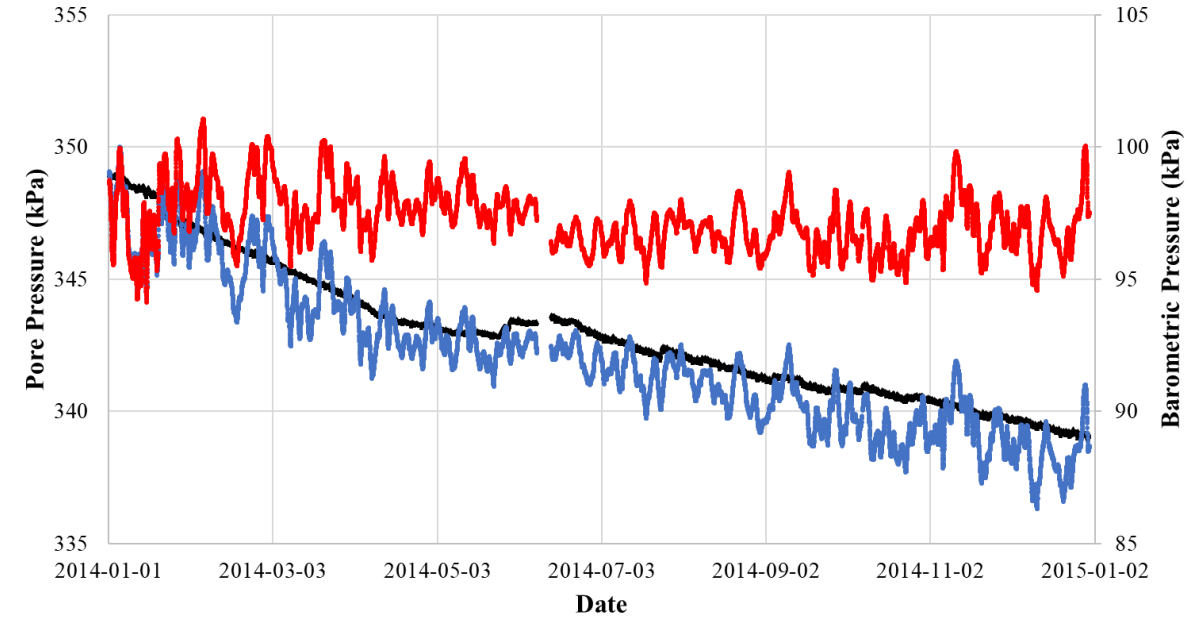

Figure 4.3 – Pore pressure, barometric pressure, and BRF deconvoluted pore pressure for BHLB08 in 2014

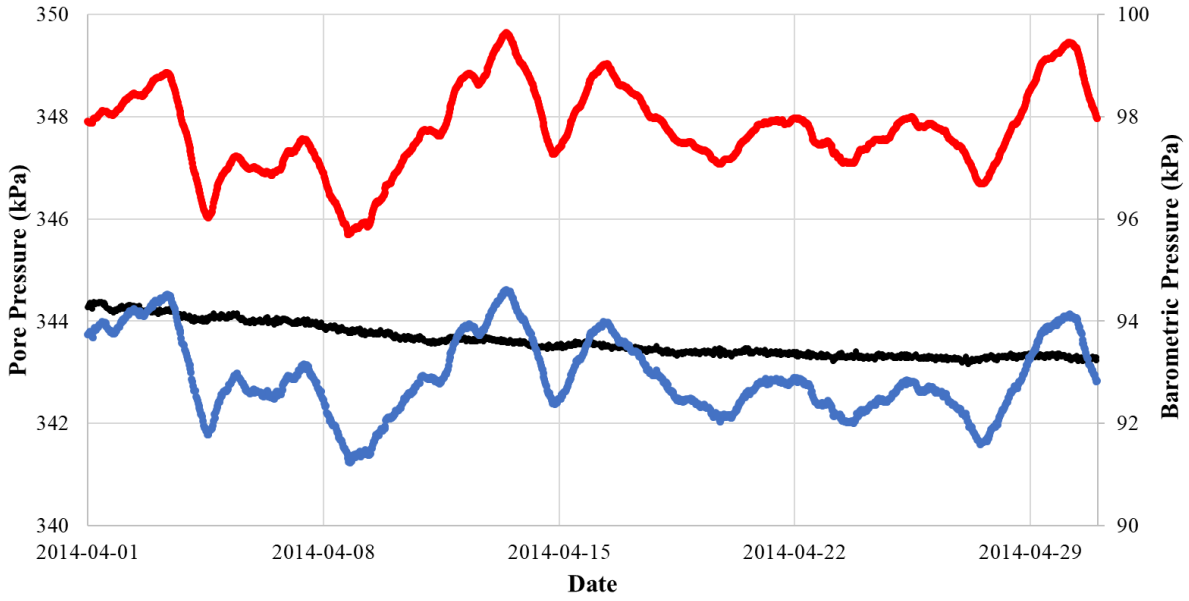

Figure 4.4 – Pore pressure, barometric pressure, and BRF deconvoluted pore pressure for BHLB08 in 2014

Once the linear and BRF removals are completed, the final step is to examine both by eye to see which has more completely removed the barometric pressure fluctuations in the pore pressure. The remaining pore pressure line shows some noise. This noise is consistent with the resolution of the instrument, in this case 8.9 mm of water or 0.1 kPa.

The resolution of the sensor is quantified as a percentage of full scale (0.025% for this installed instrument). It is defined as the change in the measured quantity that can be perceived by the sensor. This should be separated from the accuracy (how much the recorded value differs from the true value) and the sensitivity (what is the smallest change that can be recorded by the instrument). The 8.9 mm H2O (0.025% of a 350 kPa full scale value) is the resolution, and therefore a change in pore pressure of less than this value is not necessarily perceived. The accuracy of this sensor is 0.1 % of full scale, or 36 mm H2O. The use of these sensors as GLs allows the accuracy of the instrument, when compared to the scale of events to be measured, to be unimportant. The resolution is the value that shows what the sensor can clearly observe as a change in pore pressure. This effect shows up as scattering of the measured value around the true point and is described variously in this work as noise or banding depending on the context.

In this case, the BRF appears to have generated a slightly better result due to there being less of this vertically banded noise. As such, this dataset is used for 2014 going forward. With the current instrument set, a similar amount of noise can be expected in all instruments.

4.5 Comparison of ML to other hydrological instrumentation

4.5.1 Visual examination and assessment of the influence of hydrologic events

The ML, once generated, is first examined for signs of easily visible signs of hydraulic events. The presence of rainfall events in the time series is generally indicated by relatively short (>1 day) “jumps” in the moisture load. When a longer time series is viewed, these jumps appear almost as discontinuities in the time series as it is displaced vertically upwards. Secondly the presence of evapotranspiration is characterized by a slow decline in the moisture load. In a particularly clear ML with low amounts of noise, this may appear as a scalloped decline with a daily period as the evapotranspiration increases and decreases throughout the day. These trends

should be present during the summer high ET season, and be minimal or almost absent in winter. Another issue that can now be assessed is how thickly banded with noise the signals is. The more vertical scattering caused by noise, the harder it will be to examine smaller hydraulic events.

This examination will give an indication of how useful the sensor is for use as a GL. If a ML time series is composed entirely of sharp jumps up and slower declines down, without much vertical scattering from noise, it is likely to be very useful. Sensors that show other phenomena such as slow upwards trending or sudden drops in pore pressure are judged to be less useful for measuring near surface moisture loadings.

4.5.2 Comparison to precipitation data

Precipitation was assessed in two ways. The first was to compile the ML response to a series of known precipitation events (as measured by available rain gauges) and to evaluate the correlation statistically. The second approach was to examine the fidelity (magnitude and timing) of the observed ML signal with individual rainfall events.

To statistically assess the ML precipitation, the value of change shown in the moisture loading was required. This number was recorded from the plot of moisture loading at the times of precipitation as recorded by the rain gauge. The ML recorded precipitation values could then be compiled into a plot, where the rain gauge data was plotted against the corresponding ML reading. The chart was then assessed with a linear regression and a R^2.

For a single rainfall event, a time series of a large event was plotted overlapping with the ML readings and rain gauge readings. This plot can show the effects of the rainfall to the reading pore pressure formation. This should show the fidelity of a ML to the local weather station on an extremely short-term trend.

4.5.3 Comparison to evapotranspiration data

ET data for comparison to the ML loading data for this project has two sources. Firstly, from eddy covariance data generated by McMaster university personnel for the 2014 and 2015 high ET season as outlined in Chapter 3. It should be noted that no energy closure has been applied to that data, although in section 5.6 an energy closure value is estimated from the water balance data. A second source of ET data is estimation of the maximum potential evapotranspiration (PET) that might have occurred based on conventional weather station measurements. This estimation is performed using the Penman-Monteith (P-M) equation (e.g. Granger and Gray 1989, Allen et al. 1998, Kashyap and Panda 2001). For P-M estimation, the PET is always equal to or higher than the AET. As such, AET is often estimated as a fixed percentage of the calculated PET. The ML series is likely to reflect the AET, and therefore an estimation of the percentage of P-M PET used to estimate AET may be made from the ML.

4.6 Development of a partial water balance

There is potential application of the ML to establish a simplified water balance comparing P, ET, and ΔS at selected site locations. The method for this is, firstly, the ML has the precipitation subtracted and the evapotranspiration added to it. What remains is a combination of several factors. The net percolation of moisture that has seeped out of the domain on the subsurface is seen as a decline in pore pressure. Secondly, the runoff, if any is present, representing overland flow out of the sensor's domain is also seen as a declining pore pressure trend. Thirdly is the residual representing any under or over estimation of precipitation or evapotranspiration. For precipitation, this would likely come from rainfall over part of the sensors sensing area, but of a different intensity on other parts of the sensor's sensing area. For evapotranspiration, this may come from several things, but for EC estimations, it may be the result of the lack of an energy closure variable, while for P-M estimation, it may come from the difference between PET to AET.

5 RESULTS AND DISCUSSION

The loading efficiencies obtained from the piezometer data are summarized and discussed in this chapter. These loading efficiencies were then used to develop a moisture loading estimate for selected sites which were then compared to independent measurements of specific components of the water balance (i.e. precipitation and actual evapotranspiration). The application of this approach to develop a site-specific water balance is also illustrated. This chapter also includes a discussion of the limitations and failures of the instrumentation and the limitations in estimating hydrological measurements from these data sets.

The first thing is to check for sensors that have, in some aspect, failed. The presence of barometric transients in the pore pressure indicates that a sensor is able to detect total stress changes within the pore pressure. As such, moisture loadings should also be able to be detected. Of the moisture loadings which are visible in the pore pressure, the most distinctive are the short-term rainfall loadings.

The results presented in this section loosely follow the methodological chronology laid out in the previous chapter. First, the data collection approaches utilized in the study will be discussed along with the generated pore pressures data sets including the barometric calibration. The raw readings with the barometric transients removed will then be presented and discussed with respect to the hydrogeological setting of the VWPs. The corrected pore pressures are then presented and discussed as moisture loadings where they are compared to other independent hydrological measurements. Finally, a full annual cycle of change in stored water volume is then presented and discussed using only the data from the moisture loading trend which appears to be the closest to the actual hydraulic conditions. This annual cycle of storage changes is compared to the pattern of precipitation minus evapotranspiration.

5.1 Data collection and raw pore pressure

The raw VWP data was collected from the dataloggers and converted to pressure as outlined in the previous chapters. For all data sets, some data was useable (i.e. continuous for a significant length of time) and some was unusable for various reasons. What follows is a discussion of the portions of data that were determined to be unusable. The useable data is discussed in the sections following this one.

Due to site conditions, there are obvious breaks in the data record. One example of these breaks was the shutdown of the monitoring cycle during extreme cold (Winter of 2013 until spring of 2014) most likely due to loss of power (i.e. battery voltage drop due to extreme cold temperature). That specific failure was systemic, but there were many other data breaks for other reasons including: memory overrun, faults in sensor grounding, data collector failure, and other miscellaneous problems. These problems form general data gaps that will be seen in the resultant pore pressure time series readings.

There were several specific problems encountered with data collection. The barologger's internal clock was offset from the internal clock of the dataloggers early in the monitoring program (i.e. the two instruments were set to take readings at different times). The same intervals were maintained between the datasets, and therefore the datasets had to be linearly interpolated between readings to allow for time series analysis to be performed on the data. Once this error was understood, it was corrected by resetting the internal clocks for all instruments to the same timing.

The barometric record was also not continuous as outlined in Chapter 3. This change may have caused errors in the barometric correction since the elevation difference may have resulted in small differences in barometric pressure between the two sensors due to orographic pressure differentials. This was mitigated by not appending the VP-09-32-03 barometric data to the BHLB07 data, but rather running the analysis separately for each data set. Additionally, having an orographic offset between the barometric data sets is not fatal to the analysis as it relies on the change within the barometric set rather than its absolute values.

Estimation of loading efficiency was attempted on all the data collected from the research specific VWPs with subsequent removal of the barometric transients based on an estimate of the loading efficiency. There were very few data sets generated prior to the RST installation for the SCL geotechnical VWPs. Data that was collected on the geotechnical monitoring VWPs tended to be only a few days or weeks in duration with several months of intervening data gaps. Very little analysis could be done with this data and, as such, it is not used in the results. This limited the analysis of the SCL geotechnical VWPs to a time window from April 2015 to May 2016.

Two VWPs that could not be used were BHLB04 and BHLB05. During calibration, BHLB04 and BHLB05 were both found to be not responding as expected to the barometric inputs. The raw piezometric pressure for those VWPs, uncorrected for barometric fluctuations, is shown in Figure 5.1 to Figure 5.3. BHLB04, at the crest of the SBH landform, has intermittent disruptions and appears to be slowly declining from an initial high pressure (> 200 kPa) after installation towards zero. There is a large stretch where the sensor appears to be working correctly but with a reading of zero. These points have been left in Figure 5.1. Any attempt to correlate these pore pressure readings with barometric pressure readings do not show any influence of barometric pressure. This can be verified by eye in Figure 5.2 as the scale of barometric fluctuations is 5-10 kPa, and even after scaling the barometric signal by γ, no reasonable influence of barometric fluctuations can be seen in the raw pore pressure.

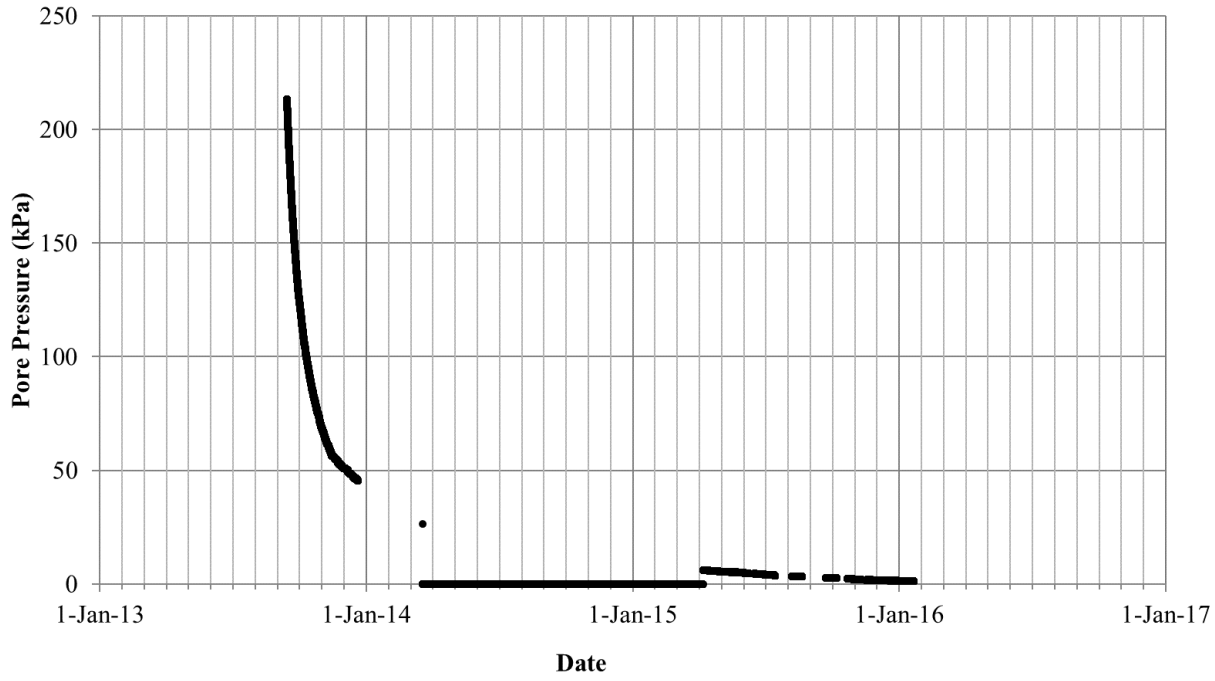

Figure 5.1 – BHLB04 raw pore pressure

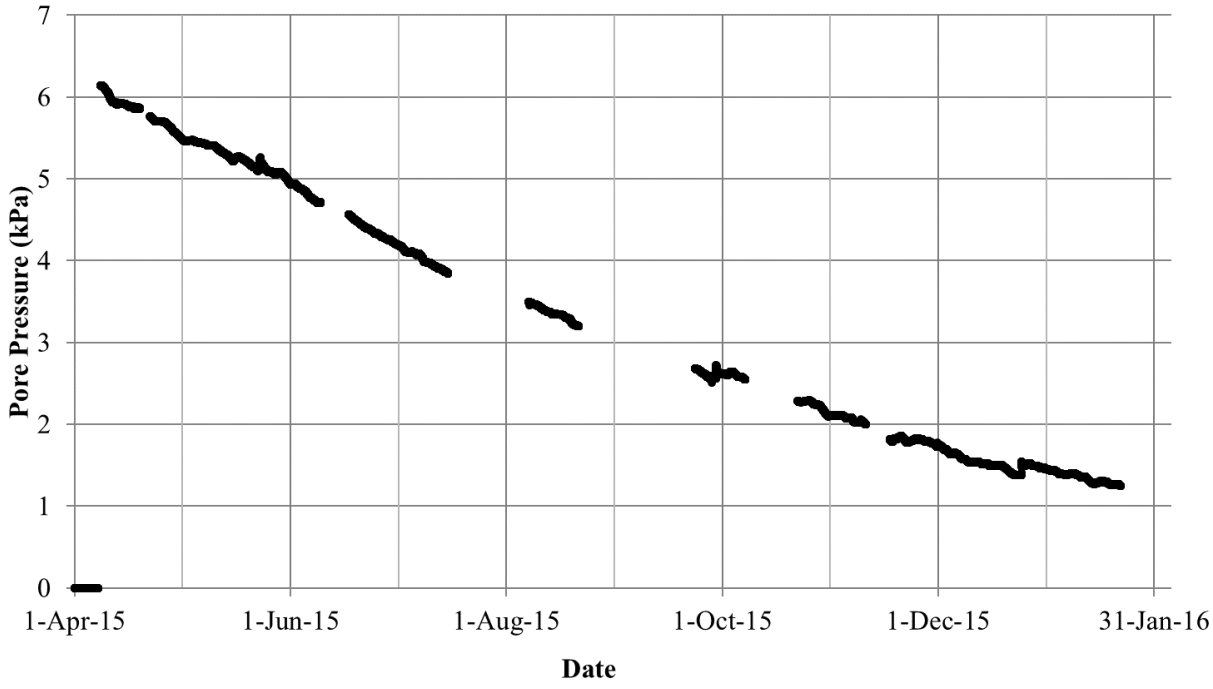

Figure 5.2 – BHLB04 raw pore pressure in 2015 to early 2016

BHLB05, located low on the SBH landform, also shows a declining pore pressure as shown in Figure 5.3. The pore pressure starts at 25 kPa and quickly declines to a negative pore pressure, which may indicate unsaturated conditions. There is a continuity break in April of 2015 where the datalogger is changed to the RST system and the subsequent pore pressure trend becomes less noisy. This is possibly due to the RST datalogger's internal design or better thermal shielding; however, these are just speculative guesses. This pore pressure time series has no correlation with the barometric pressure trend similar to BHLB04, therefore it cannot be calibrated to a loading efficiency, and moisture loadings cannot be seen. Neither BHLB04 nor BHLB05 will be used in the remainder of this analysis.

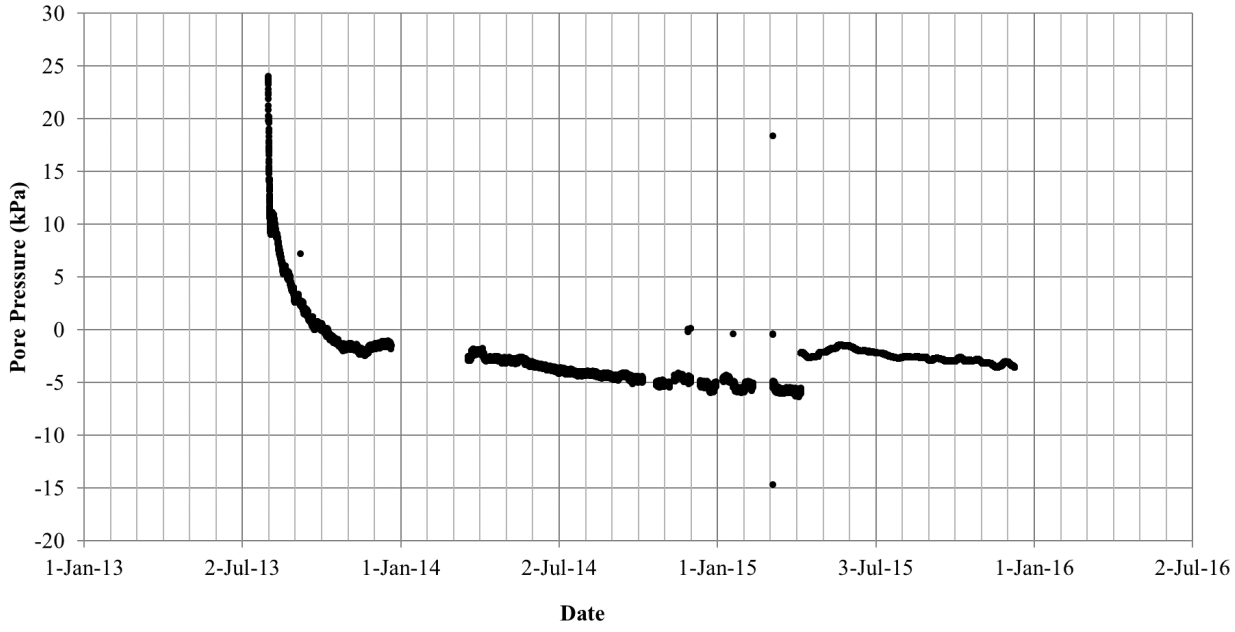

Figure 5.3 – BHLB05 raw pore pressure

5.2 Loading Efficiencies and Corrected Pore Pressure Records

Table 5.1 shows loading coefficients and the methods used to generate them. In all cases, the final judgement on LE/γ (LE is being used to indicate a BRF fit) was confirmed by a visual inspection as outlined in Section 4.3 based on the judgement that the fit should provide the most complete removal of barometric transients; and, that high frequency noise should be minimized.

In all cases where a substantial lag time was detected, the BRF method was found to be more suitable.

The installed sensors (BHLB01, 02, 03, 07, and 08) show a more compressible material (indicated by a higher γ/LE) that allows a larger portion of the barometric stress to be borne by the pore pressure. These sensors tend to cluster around a γ/LE of 0.9 - 0.95 with a high of 0.965 to a low of 0.800. They also show a time lag of around 1-1.5 hours, with a high of 5 hours and a low of either a small or non-detectable time lag. The geotechnical VWPs showed a much wider variety of responses, from a γ/LE of 1.0 to a low of 0.58. This low value indicates a somewhat stiffer material than was observed by the BHLB sensors. These time lags were generally very small, ranging from 0 to 20 minutes, with one outlier of 4 hours.

Table 5.1 – Calibration Parameters for all GWLs

Landform	Sensor	Calibration Method	γ / LE (-)	Time Lag (min)	Installation Formation Geology	Installation Elevation (masl)	Installation Depth (m)
SWSS	BHLB07	BRF	0.90	90	KC	343.7	45.4
SWSS	BHLB08	BRF	0.90	90	KC	339.9	29.5
Natural	BHLB03	BRF	0.96	600	KC	325.3	23.0
SWSS	VP-12-32-02 – Upper Tip	BRF	0.78	10	KC	332.0	55.1
SWSS	VP-09-32-03 – Upper Tip	Linear	1.00	-	KC	346.0	16.0
SWSS	VP-09-32-03 – Middle Tip	BRF	0.88	240	KC	339.8	22.2
SWSS	VP-09-32-03 – Lower Tip	BRF	0.85	20	KC	333.4	30
W2	BHLB01	Linear	0.97	-	KC	325.4	26.4
W2	BHLB02	BRF	0.80	120	KC	328.9	17.4
W1	SIVP080046 – Upper Tip	Linear	1.00	-	KC	320.7	45.7
W1	SIVP080046 – Middle Tip	Linear	0.83	-	KC	308.5	57.9
W1	SIVP080046 – Lower Tip	BRF	0.70	< 10	KC	302.4	64.0
W1	SIVP080069R – Upper Tip	BRF	0.58	< 10	PL	336.3	18.3

It was noted that the time lag characteristics of BHLB08 appears to change after the datalogger was swapped out, with the 2015-2016 data having almost no time lag. There are several possible sources for this error:

- there may have been some error due to swap of the piezometer to the RST logger system, or the barologger to the RST system. This may be caused by differences in the wiring between the two systems, differences in the internal electronics or shielding of the data loggers, or other physical characteristics that differ between the two dataloggers,
- it may be that the earlier time series has enough noise or other transient events causing scatter in the data to be causing a poorer fit in the regression analysis,
- in the RST system all the logger timing events are controlled by a central timing setting, while the Solinst barologger and Geokon datalogger had to be individually set to the time of the logging computer, and,
- the readings could potentially have drifted over time with temperature and voltage problems.

For the rest of this discussion, the data for BHLB08 was calibrated with a 90-min time lag, except for the data from 2016. The 2016 data are calibrated with no time lag. The LE value for BHLB08 does not vary between these two different data sets.

5.3 Correct Pore Pressure examined by Sensor and Landform

Once the calibrations were completed, the pore pressure data sets were corrected for barometric transients based on a selected loading efficiency. The corrected pore pressure was examined to determine if any hydrogeological influences due to siting were visible in the corrected pore pressure, and to check for any readily identifiable hydrological events.

Ideal sites for moisture loading analysis have a relatively uncomplicated hydrogeological setting and would generally show a pore pressure trend that undergoes limited but gradual changes. The expected annual range of change associated with moisture loading would be on the order of 0 - 5 kPa (~0 - 500 mm H_2O). Large or rapid fluctuations in the pore pressure due to the hydrogeological system make interpretation of the hydrological events using the VWP more difficult, particularly in the case of the small daily changes in pore pressure associated with evapotranspiration.

The trends observed in the various VWPs are grouped by landform and the geologic formation into which they are completed. The only sensor that is not on a specific closure landform was installed at the background site (BHLB03), which is close to the SWSS sand dyke and forms part of a cross section past the toe of the dyke. BHLB03 is, accordingly, included with the SWSS analysis.

5.3.1 SWSS

SWSS is the most instrumented closure landform involved in this project. There were 2 VWPs installed on the landform (BHLB07 and BHLB08) and one VWP installed past the toe of the dyke (BHLB03). An additional 4 sensors installed as geotechnical monitoring were also assessed using GWL methodology: a stack of 3 VWP's on a lower bench of SWSS (VP-09-32-03) and the upper tip of a stack of 2 VWPs installed on the upper dyke (VP-12-32-02). The three sensors that were installed specifically as part of this project are considered first. A cross section of SWSS is presented in Appendix D. This cross section is perpendicular to the crest of SWSS through from BHLB07 to BHLB08 and shifted to the south at the toe of the slope to pass through BHLB03; the points can be seen in Figure 3.4.

BHLB07

The VWP for BHLB07 is on a high terrace on the dyke, but not at the crest, and is installed into a KC horizon below the sand tailings. The corrected raw pore pressure is shown in Figure 5.4. The sensor was monitored from mid-2013 to mid-2016 with some data breaks due to datalogger problems and the datalogger swap in April of 2015. In some cases, there is a relatively instantaneous changes in pore pressure which could not be correlated to a possible cause. It was assumed therefore that these instantaneous discontinuities were caused by errors in the dataset or some other error.

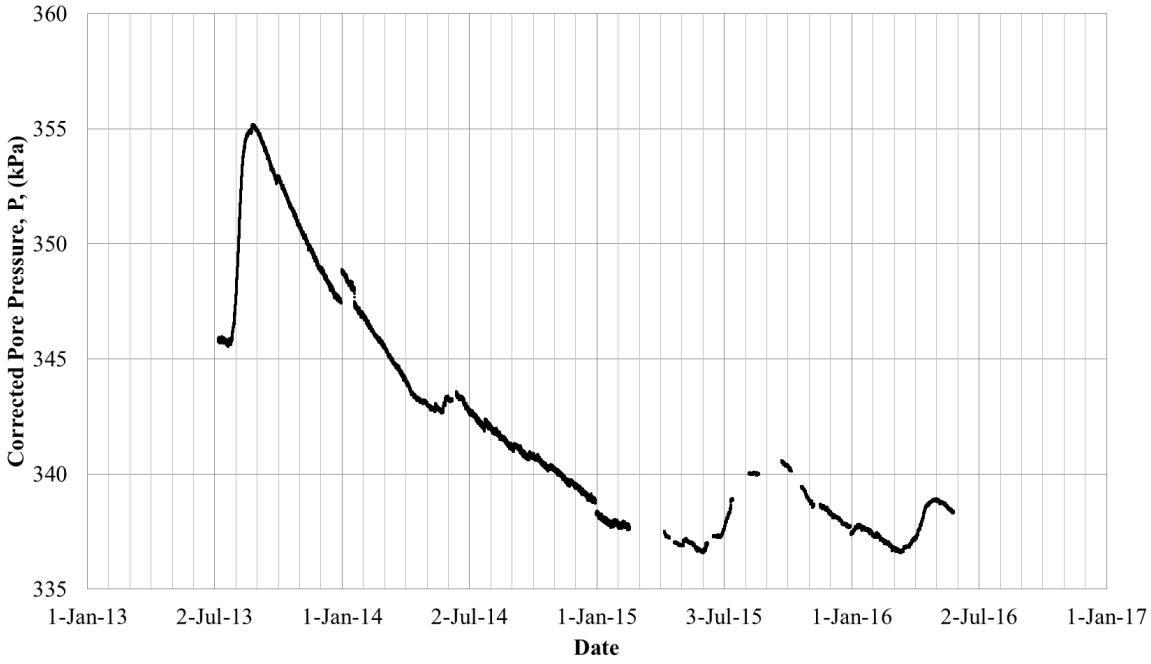

Figure 5.4 – BHLB07 Pore Pressure

There is an initial rise in pore pressure of approximately 10 kPa and then a nearly continual decline over the following year and a half. The first portion of this decline is likely attributable to well recovery from drilling, but at some point, likely in early 2014, it transitions to a different mechanism. It may be that this large decrease in pore pressure has an underlying hydrogeological cause. From June until September of 2015 there seems to be a 3 kPa (~ 300 mm) rise and subsequent fall which possibly reflects the influence of freshet; however, freshet should have started before July. A second similar 2 kPa (~200 mm) rise and fall occurs in early 2016. This appears too early in the year to be freshet. It seems probable that both events may have been caused by some other hydrogeological influence. Hydrological trends are evident in 2014, and can be seen in the sharp rises in pore pressure, interspersed with slow declines. This indicates that for some time periods, moisture loading and especially precipitation can be seen. The unexplained rises and falls, however, indicate that evapotranspiration trends are likely to be superimposed with the hydrogeological influences. It is possible that those influences could be removed if their source can be found and quantified.

A possible mechanism for the cyclic rises and falls apparent in the BHLB07 record is lateral stress transfer from the changes in the SWSS pond freeboard. A rise in the SWSS pond level would act as a surcharge on the SWSS dyke and underlying foundation as well as initiating an excess pore pressure which would dissipate through the adjacent soil layers as a dampened transient pulse.

The large recovery fluctuation early in the BHLB07 dataset will eventually dissipate out of the excess pore pressure of the formation as the excess undrained pore pressure transitions to drained pore pressure. After recovery and as on an ongoing basis, this pore pressure record may become increasingly useful as a data set for examination as a ML.

The pore pressure for BHLB07, groundwater table readings from a nearby (~10 m away) surficial standpipe piezometer, and SWSS freeboard levels were all cross plotted with the same scale to attempt to see if this mechanism can be found, shown in Figure 5.5. The freeboard shows a steady rise throughout the time series, while the ground water table starts out stable and then rises ~ 4 kPa. There is no clear correlation between the three series. Lateral stress transfer from the SWSS freeboard should influence the pore pressure, and at the same time, while changes in the ground water table should be lagged due to pressure propagation through the KC layer. The effect of the various inputs should result in one of two scenarios: that a loading is instantaneous or that it is transient, and as such exhibits lag. There is no evidence of instantaneous loading in Figure 5.5, therefore any effect of the GWT and SWSS reservoir level must be lagged. To attempt to remove these hydrogeological influences from the pore pressure would require extensive numerical modeling.

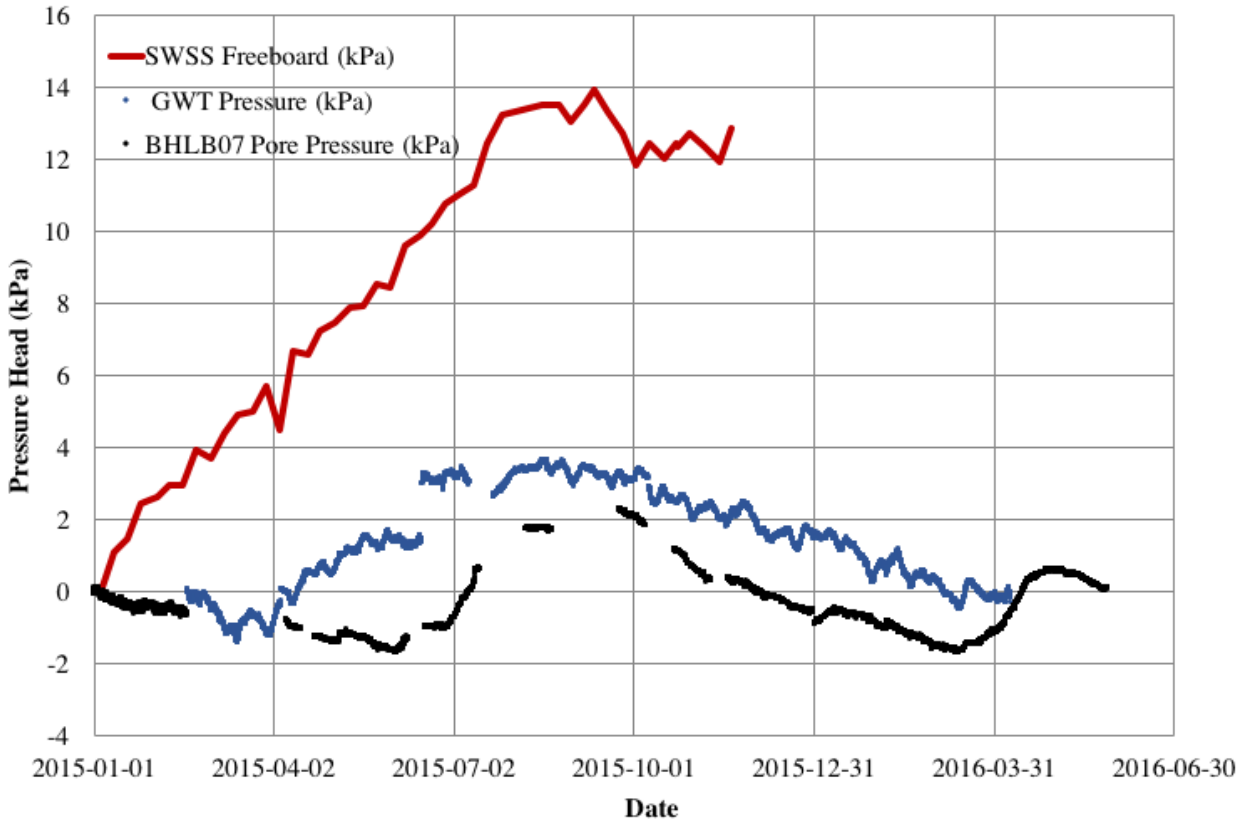

Figure 5.5 – BHLB07 pore pressure indexed with changes in local GWT and SWSS freeboard

BHLB08

The pore pressure record in BHLB08 spans from the summer of 2013 to the end of spring 2016. The pore pressure record is shown in Figure 5.6. The pore pressure trend doesn't show the same type of recovery as was seen in BHLB07. It shows an increase throughout the summer of 2013 and then it begins a decline in fall of 2013 to January of 2015. It is interspersed with sharp rises in pore pressure which are likely due to precipitation events, this assumption is examined further in the thesis with a statistical comparison to rainfall records. From the beginning of 2015 to 2016 it shows an increase to a peak in July of 2015 and then declines again until the end of the data track in Spring of 2016. The gradual declining pore pressure may represent decreases in water storage which may also be due to a drainage of the dyke or water losses from the surface. Since the decline appears to continue throughout the winter in 2013 (assumed), 2014 and 2015 it suggests that drainage or sublimation may be the causal mechanism. The connection at the data break in June of 2015 may be offset by a small amount due to changing barometric datasets.

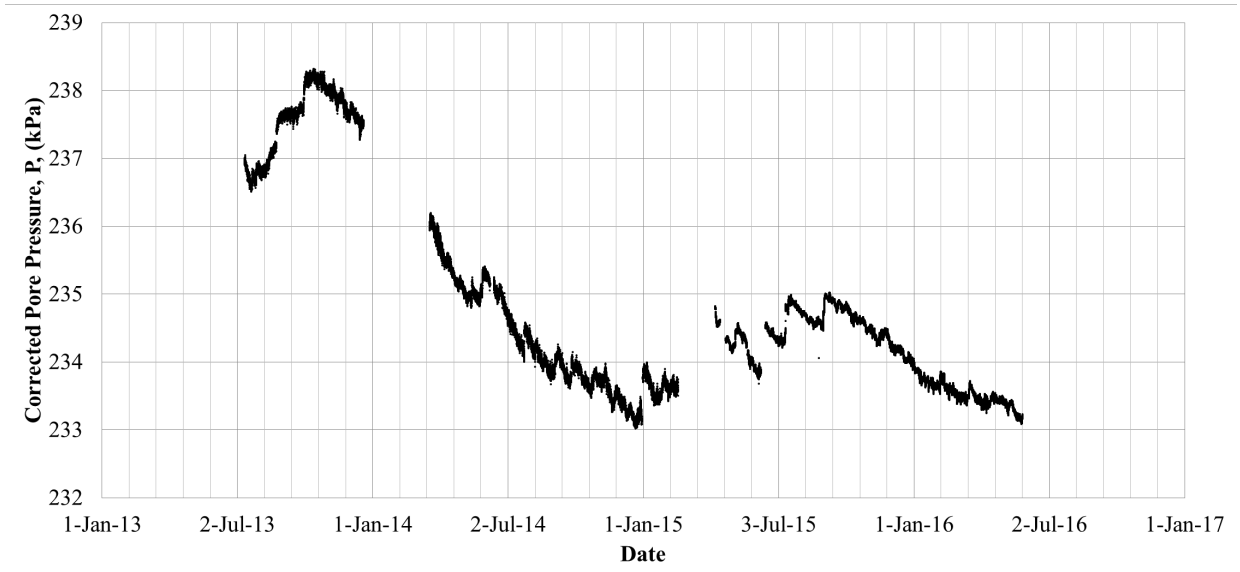

Figure 5.6 – BHLB08 Pore Pressure

BHLB03

The corrected pore pressure record for BHLB03 is shown in Figure 5.7. This trend shows recovery in the last half of 2013. The sensor then goes offline throughout winter 2013-2014 and when it comes back online there is some unreliable data. The sensor shows a large jump at the end of spring 2014. This large jump may be due to a large rainfall (30 - 40 mm) at the end of May that is seen in both SWSS and SBH weather stations. Through late summer and into fall of 2014 the pressure increases, but not generally in jumps commonly associated with rainfall (one rainfall event may have been recorded in late September 2014). Rather, it has a linear trend up until the data gap through to 2015. This trending implies some non-hydrological explanation for the change in pore pressure. The datalogger was replaced in March of 2015, with the first data from the sensor being unreliable for some reason, and as such is omitted until May. The data trend from April through to the fall of 2015 shows reasonable results, with large jumps indicating rainfall events. There is then an increasing trend through to Spring of 2016, which is similar to the one from the fall of 2014, however at a much smaller slope. The increasing trends through fall and winter indicate mass increase, perhaps from snowpack accumulation. It is possible that this rise is associated with a general rise in water levels as drainage from the SWSS dyke enters local groundwater slowly over the winter. During spring there is a mass loss with may be due to

runoff, especially as ditches near the lay down yard that this sensor is installed into conveys off meltwater.

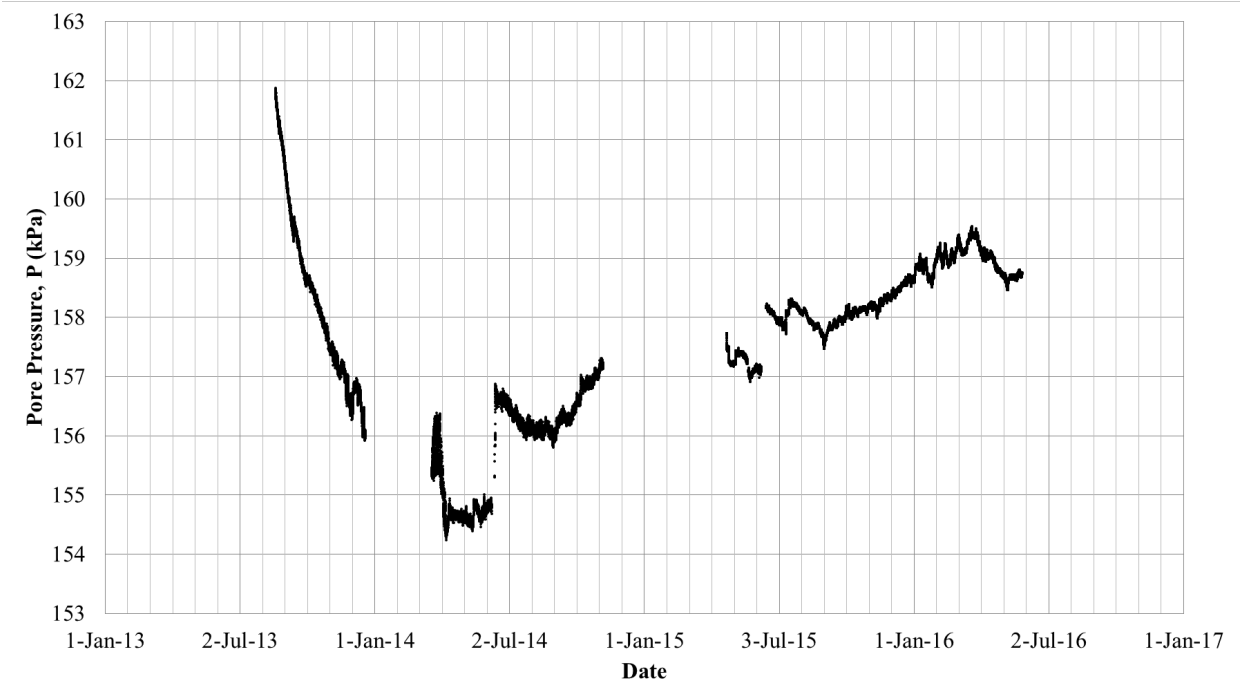

Figure 5.7 – BHLB03 pore pressure trend

SWSS Cross Section Sensors

The three SWSS sensors are indexed and compared in Figure 5.8. BHLB07 and BHLB08 show similar trending, but with differing slopes in 2014. This may possibly be due to a 'hinge' effect of hillslope drainage where upper sites will drain more quickly than lower sites. The beginning of the year shows a small bump up at the same time, perhaps due to spring rainfalls. They then decline at differing rates as noted above. At the early portion of 2015, all three records look similar; however, later into the spring and summer, BHLB03 and BHLB08 now show a correlation while BHLB07 begins its strange rise. BHLB08 alone seems to be responding to moisture loading changes at the end of 2015 and into 2016.

The ML at the SWSS cross section sensors have the potential to be influenced by pore pressure changes resulting from changes in the SWSS ponding level. A cross section in Appendix D

shows the relationship between these sensors and the SWSS pond. A positive change in pond elevation should result in an increase of pore pressure. This trend is not seen for BHLB07 and BHLB08. BHLB03, which does show some positive pore trending across a similar time frame as the pond elevation is increasing, is far enough from the pond that it seems unlikely that an effect could be seen. Any effect that is seen in BHLB03 should also be noticeable in BHLB08 and BHLB08.

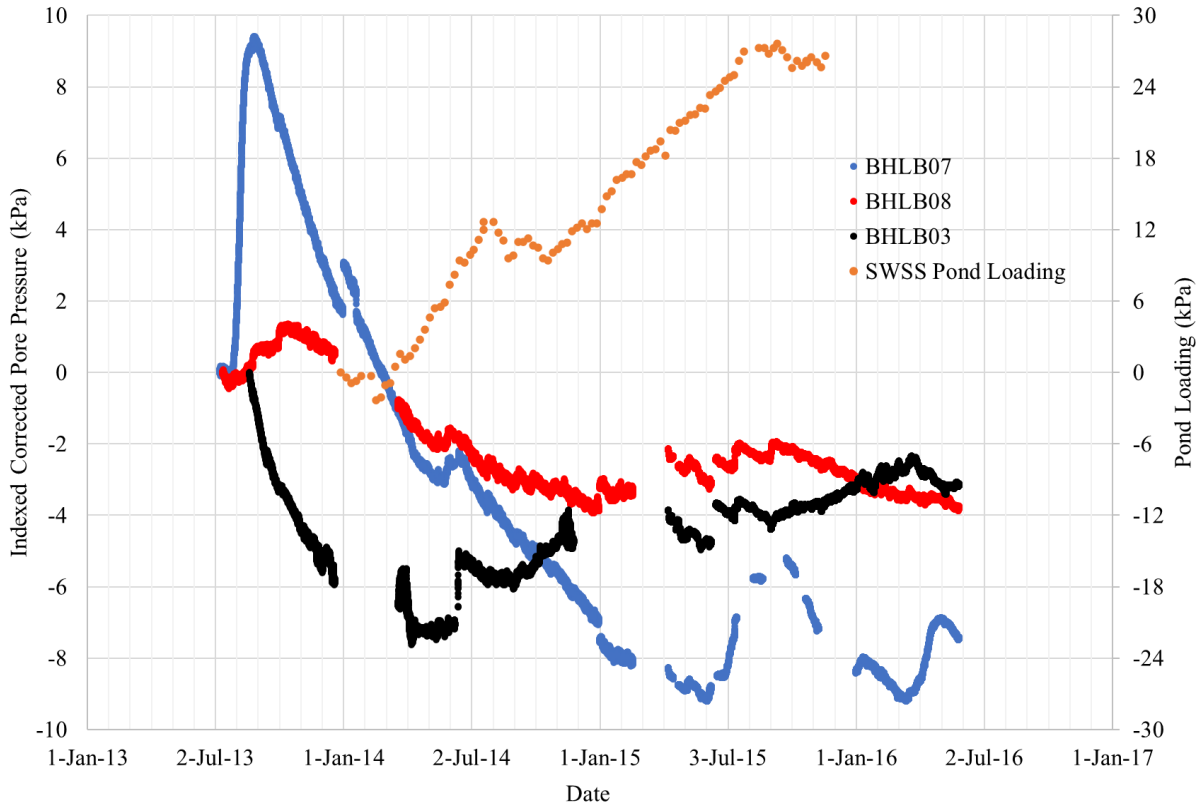

Figure 5.8 – Comparison of SWSS ML trends and SWSS pond level

SCL Geotechnical Sensors on SWSS

There are 4 SCL sensors on the landform: the triple stack at VP-09-32-03 and a single monitored sensor at VP 12-32-02. The 09-32-03 sensors are shown indexed against one another in Figure 5.9. The upper tip has an intermittent signal, leading to the fragmented signal seen in that figure. The pore pressure increases through the fall and declines in winter into spring, where

the signal levels out again. The intermittent signal makes it difficult to analyze the signal coming from the upper layer. The middle tip shows a steady signal through fall and then declines into winter, before beginning to rise again in the next spring. This seems reasonable; however, the scattering of the signal appears to be nearly 1 kPa, or in hydrological terms, approximately100 mm of water, making it very difficult to analyze except as a trend. The lower tip shows a clearly defined trend declining in fall, rising in winter, and beginning to decline again in spring. This is the clearest trend, but it also shows a noise band of about 0.75 – 1 kPa. The lower tip also shows many data breaks which, perhaps, are due to an intermittent fault in the sensor ground. This will make it difficult to interpret any precipitation signals from it. The long-term trends might be useful to analyze evapotranspiration in all cases.

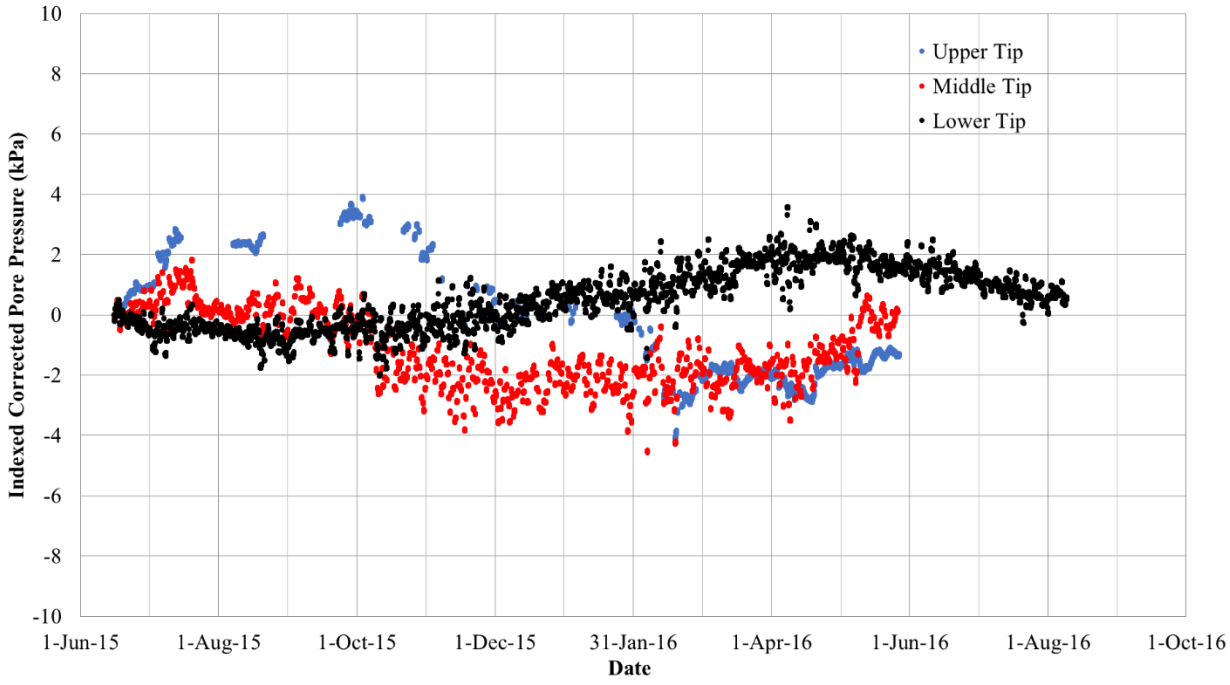

Figure 5.9 – 09-32-03 sensor stack corrected and indexed

VP-12-32-02 is shown in Figure 5.10. The pore pressure fluctuates ~6 kPa over the course of the year. There is some sensor error which shows up in the trending that makes analysis for individual moisture loading events almost impossible. No potential rainfall events can be seen in this trending. Evapotranspiration has the potential to be seen, with a rise through summer of 2015 and a decline through fall and winter, with a rise beginning again in spring of 2016. There

are also some sensor faults of unknown origin in this data trend which is characterized by vertical bands.

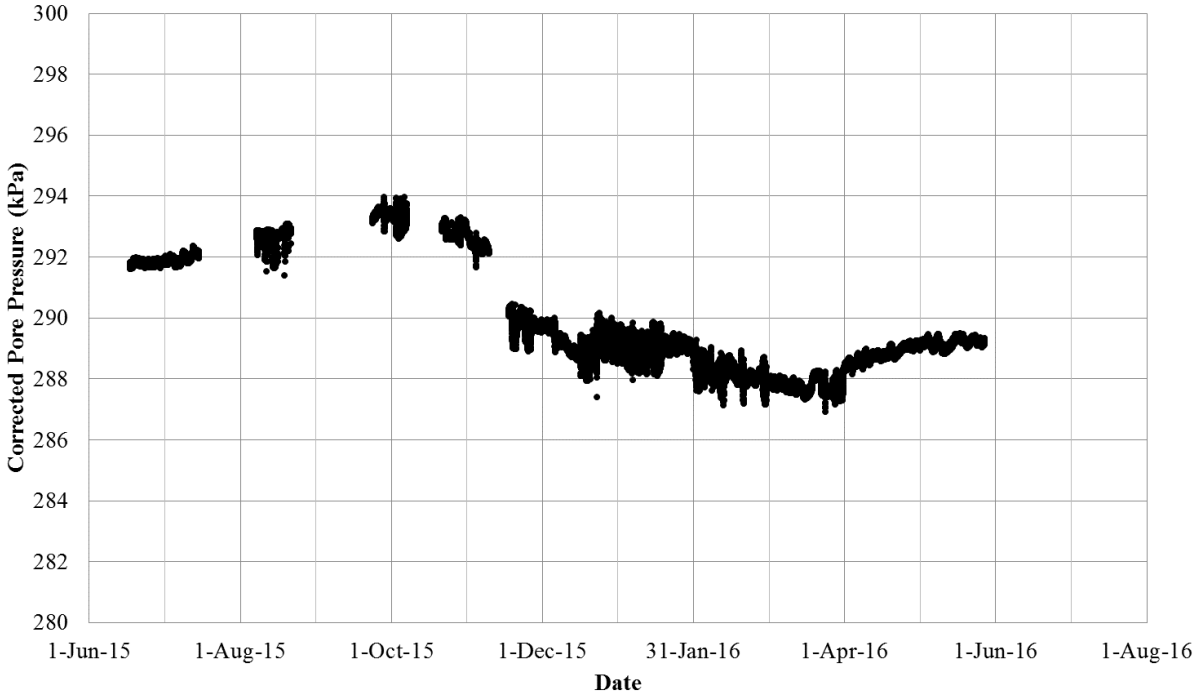

Figure 5.10 – Pore pressure for VP-12-32-02

5.3.2 W1

W1 has 4 monitored VWPs at 2 sites. The uppermost site has a sensor stack (SIVP080046) that contains 3 sensors. The lower site also has a sensor stack (SIVP080069R) that contains 2 sensors, of which only one is monitored. The data set for these begins in March of 2015 when an RST datalogger was installed after the upgrade. Some data exists from before 2015; however, the data has numerous discontinuities that will not all it to be processed as described in Chapter 4.

The lower site pore pressure, shown in Figure 5.11, shows some remaining influence of barometric pressure, or other influence. This influence, viewed as a band, is about 0.3 kPa in width, which is large compared to the hydrologic events that should be seen in the corrected pore

pressure. The pore pressure drops about 1.5 kPa over the course of the summer of 2015 to early 2016, where it begins to stabilize. This sensor does not appear to correlate to any hydrological events.

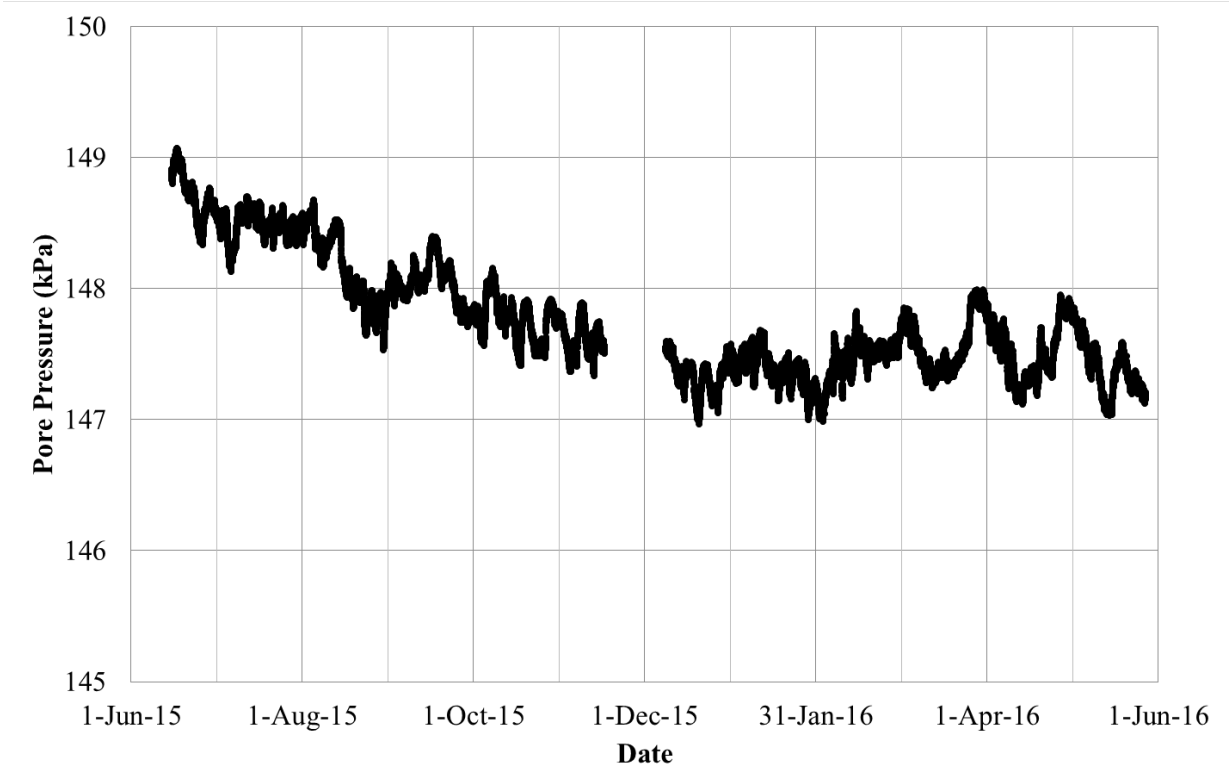

Figure 5.11 – W1 lower site (upper tip) sensor pore pressure

The upper site has data from all three sensors, shown in Figure 5.12; however, the upper tip provided an inconsistent signal, and would drop to 0, and then come back up over a series of readings. This prevented it from being calibrated properly with either a linear method or an automated BRF calculation without a large amount of excision of data. The small trace that is remaining does correlate well to the middle tip's data over the same period. The middle tip reflects a gradual decline in pore pressure of just over 2 kPa over the year of monitoring. These trends match the effects of the lower site as; however, it stabilizes slightly earlier and begins to decline again in spring of 2016. There is about 0.5 kPa band over which the sensor operates. The lower tip shows wild variation. This may be due to some loadings from adjacent aquifers, the general trend is draining.

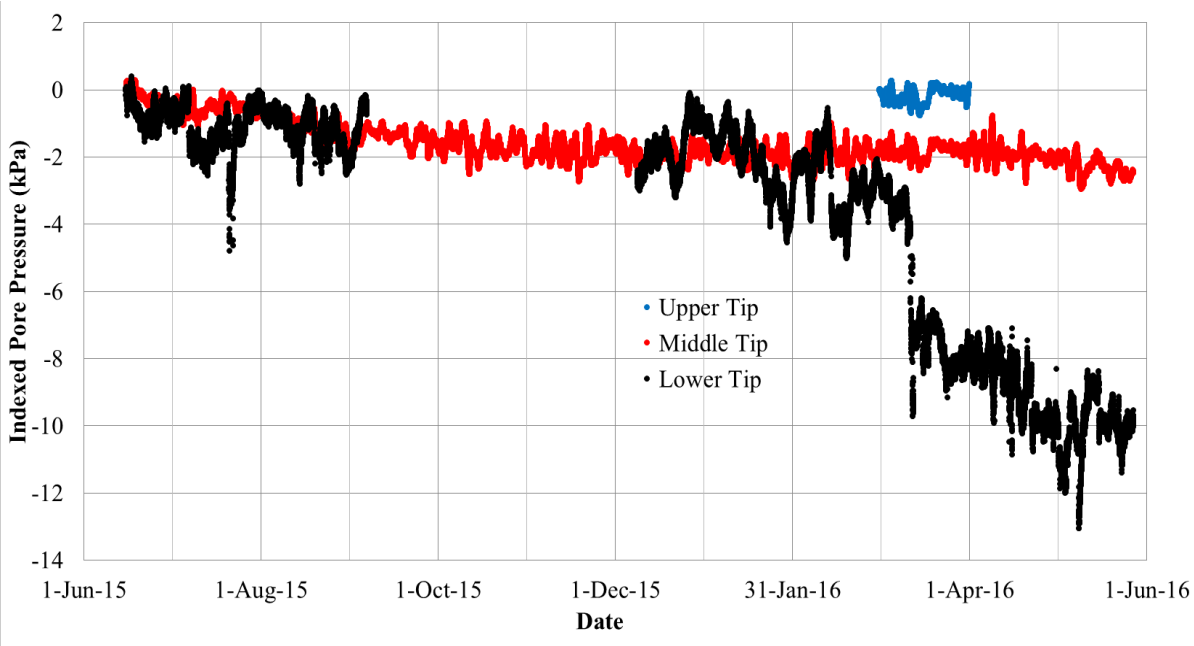

Figure 5.12 – W1 upper site pore pressure indexed to 0

5.3.3 W2

The W2 landform has 2 VWPs; BHLB01 near the crest and BHLB02 midslope. Some data from the early portion of this project was found, however there is a suspected shielding error on BHLB01 which interfered with data collection. Once the RST system was installed in 2015, data collection was much more consistent.

The pore pressure for BHLB01 (Figure 5.13) begins with a rapid decline of pore pressure as the sensor recovers from installation. Then the data interrupts (BHLB01 showed consistent problems interacting with the Geokon loggers) and is only brought online for a short period in late 2014. When the RST system is installed in 2015, it begins to show pore pressure readings that may correlate to a moisture loading trend, with rainfall "jumps" followed by declines; however, there is some error in early fall of 2015. The appearance of the jumps is somewhat atypical because at the beginning of every large rainfall the pressure would undergo a large drop and then recover just post rainfall to a point above the assumed rainfall. That is to say: if the ML is measured from a few hours prior to the rainfall against a few hours post rainfall you get an assumed rainfall loading. If you measure from the readings just prior to the rainfall to just after,

then the reading is much larger. There is a large drop in moisture load near the start of the rainfall, which then stops and swings upwards and overshoots the assumed rainfall load. This may be a barometric pressure fluctuation but should have been removed with the rest of the barometric pressure readings. It stabilizes after the rainfall into the post rainfall ML level. This large oscillation masked the magnitude of the rainfall, and as such was excised from the data. Additionally, this sensor was affected by the RST base station overwriting its data on several occasions throughout the summer, which contributed to the fragmentation of the time series. The sensor continues to decline into 2016 which is reasonable if the landform is undergoing a slow change in stored water volume change over the winter. This is at a much shallower negative slope than the summertime trends which may be consistent with less evapotranspiration (possibly due to ablation) and other losses during the winter.

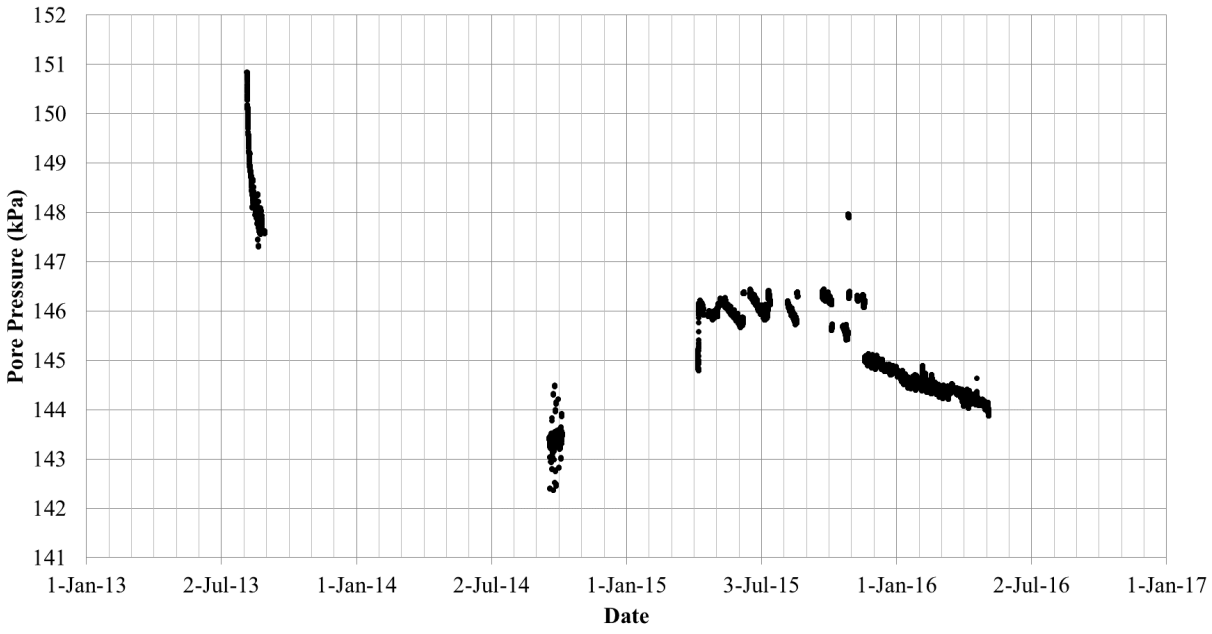

Figure 5.13 – Pore Pressure of BHLB01

The pore pressure lower down in the W2 landform at BHLB02 is shown in Figure 5.14. This pore pressure shows a continual almost linear decrease throughout the collection window. It decreases until spring freshet and then regresses back to an underlying value during the late summer and early fall period. There are some events in spring-summer 2015 that may be rainfall events. There is no evidence to decide if the flat portions in spring and summer of 2014 and

2015 are some sort of error or actual phenomenon that effects the data trend. The summer of 2015 seems to be reasonably influenced by hydrological trends except for its increase in March of 2015 and decline in September 2015.

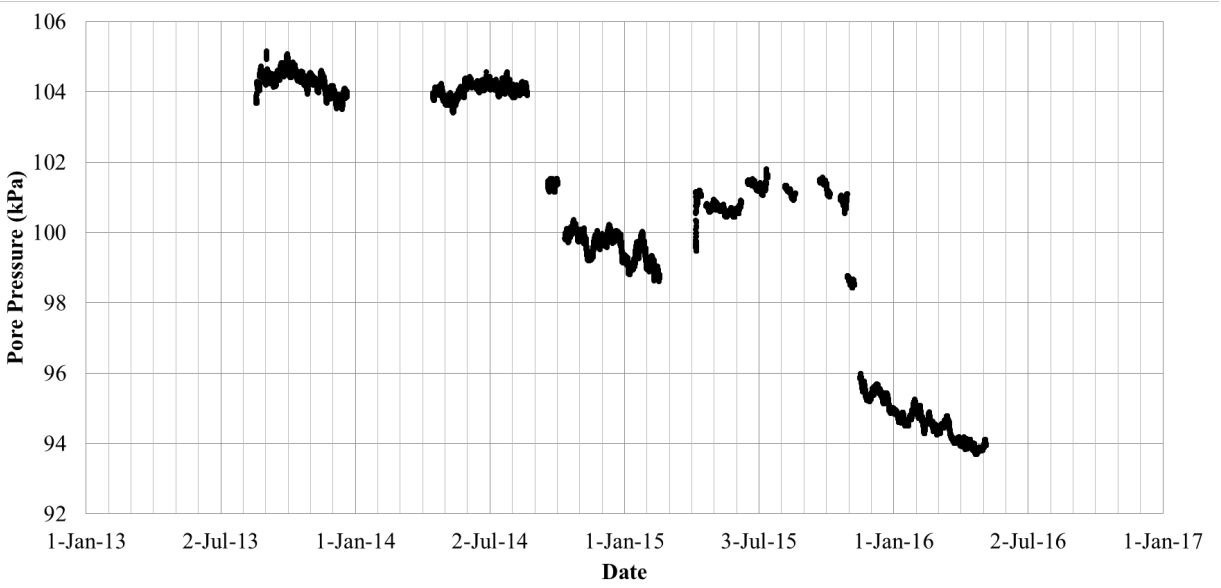

Figure 5.14 – Pore pressure of BHLB02

5.4 Moisture loading and comparison to hydrologic readings

A smaller subset of the instruments were selected to evaluate for moisture loading signals following examination of the loading efficiencies, pore-pressure dynamics, and pore-pressure trends for the data sets. This will be done by first examining how the ML trends can be interpreted for precipitation events and evapotranspiration. An annual cycle of moisture loading based on the data from one of the instruments will be also presented as an illustrative example.

5.4.1 Precipitation

Precipitation events are discernible in some of the pore-pressure records as discrete events. They show a nearly instantaneous (on at yearly or monthly scale) upticks in the moisture loading trend. GLs that appeared to show correlation to these hydrological events were used in an analysis that compared the timing and magnitude of apparent events to independent measurements of

precipitation. For those sensors found on or near SWSS, the weather station there is used. For those in the W1/W2 region, the meteorological data from the W1 landform is used. The distance from each of the VWPs to the associated meteorological station is shown in Table 5.2.

Table 5.2 – Distance between VWP's and Meteorological Stations

VWP	Distance from SWSS Meteorological Station (m)		VWP	Distance from W1 Meteorological Station (m)
BHLB07	410		BHLB01	990
BHLB08	150		BHLB02	1090
BHLB03	1070			
VP-09-32-03	280			
VP-12-32-02	650			

To compare the two phenomena, the daily rainfall data from the meteorological station was used. The ML was viewed for that day and any sharp rises from the perceived general trending of the ML were recorded. In some cases, it became very difficult to interpret any change in ML as being distinguishable from the general noise in the ML, in which case the rainfall was recorded as 0. The results are cross plotted to try to evaluate the relationship between the two measurements of precipitation.

BHLB07

The comparison of the precipitation loading response as detected at BHLB07 with the SWSS meteorological station is shown in Figures 5.15 and 5.16. Figure 5.15 shows the entire record and Figure 5.16 is for only those GL readings above the instrument's resolution limit (8.9 mm or higher). Different instruments and instrumentation setups will have different resolution limits. This instrument is operating at the factory settings which suggest that the limit is 8.9 mm; however, the resolution may vary with the installation and analysis and in some places appears to be much lower. Data averaging may improve this data if performed at higher frequency and averaged to the frequency required for the analysis (i.e. averaging 1 Hz data and downscaling it

for 10-minute resolution. That was not done on this data due to hardware constraints. The data are presented as a raw correlation and with the values below the resolution limit removed to see the impact of the low value scatter on the correlation between the rain gauge and the ML.

There is clearly a general agreement between the GL readings and the recorded precipitation. This agreement shows validates that surficial loading translates to changes in pore pressure, and that such readings in the moisture loading trend can be labelled as hydrological events. Errors in these readings, whether seen as scatter in the data, or incorrect slopes, can be interpreted in the context of sensor noise, pore pressure transients that serve to mask the rainfall events, and variation in the loading coefficient used for barometric removal.

At low rainfall values, the GL readings are higher than those measured with the rain gauge. This may be because the typical precipitation event also involves a change in barometric pressure and temperature. There may also be a undercatch at the rain gauge at low rainfall values. Undercatch can vary according to the wind speed and can be up to 20% depending on site conditions. The rainfall may not be perfectly even over the sensing area, leading for more reported rainfall than is seen at the gauge, but this is speculative.

Agreement between the GL readings and the rain gauge is much improved for larger precipitation events. Figure 5.16 highlights the good agreement (slope of 1.05 and a R^2 of 0.70) between the GL and rain gauge readings for GL responses greater than 8.9 mm. Even with this filter there is more scatter at smaller rainfall values, likely due to there being more numerous small events. The possibility that this is due to inaccuracies in the rain gauge measurements themselves cannot be entirely ruled out for these lower values. The precipitation gauge readings are likely very accurate and increasingly dependent on the rain gauge location relative to a small rainfall event.

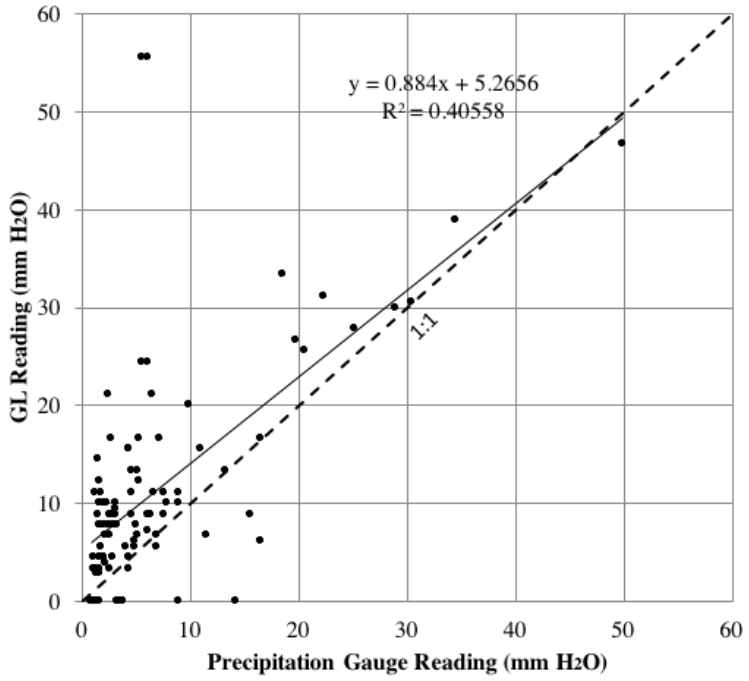

Figure 5.15 – BHLB07 readings correlation with SWSS meteorological station

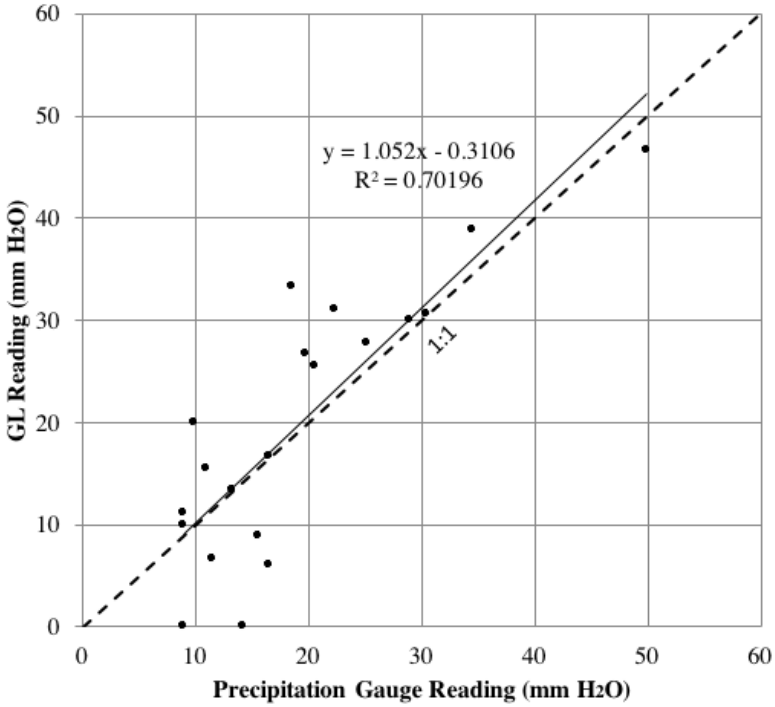

Figure 5.16 – Precipitation correlation between BHLB07 and SWSS meteorological station for all readings above the resolution limit

BHLB08

BHLB08 is located closer to the meteorological station than BHLB07 was and therefore should have better fidelity to the loadings than BHLB07 did. Figure 5.17 shows the correlation of all rainfall gauge readings to the associated moisture loading changes.

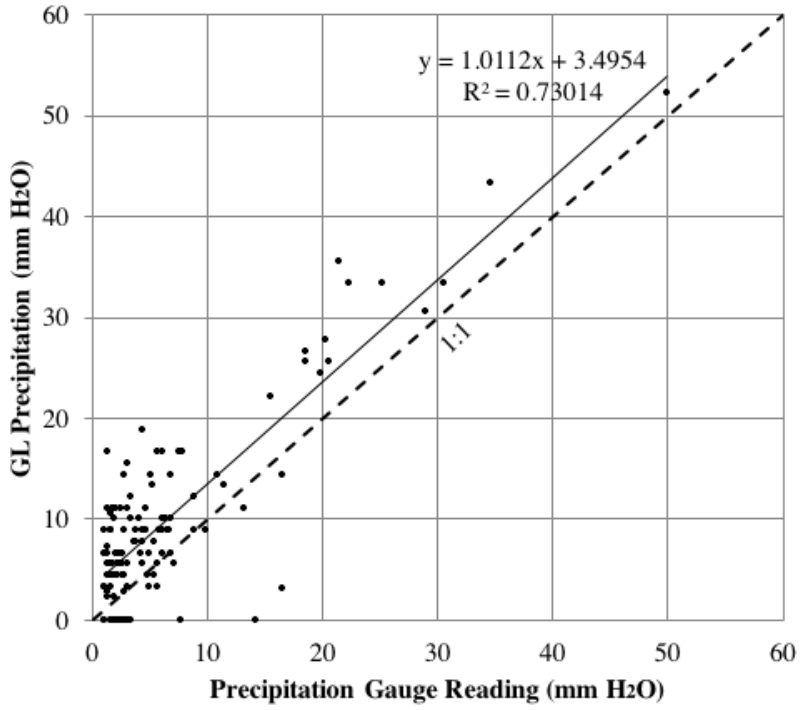

Figure 5.17 – BHLB08 readings correlation with SWSS meteorological station

Once again, the correlation between the GL and the rain gauge readings are good (slope of 1.01 and a R^2 of 0.73). It is interesting to note the presence of a clear intercept in the correlation with the best fit line offset by approximately 3.5 mm with the readings from the GL being higher than those from the rain gauge. It cannot be determined if this is because the point reading at the rainfall gauge and the areally averaged value of the GL are systemically different, or perhaps because of some other factor like the barometric pressure and temperature changes associated with rainfall skewing the GL results upward.

Figure 5.18 shows the same data with the results below the resolution limit (8.9 mm) removed. This shows a slope that is diverging from the 1:1 line. The divergence is due in part to two rainfall events recorded by the rain gauge that were not observed in the GL. The R^2 remains at

0.75. There is a relatively low number of rainfall events above the 8.9 mm cut off, giving a statistical n value of 4.

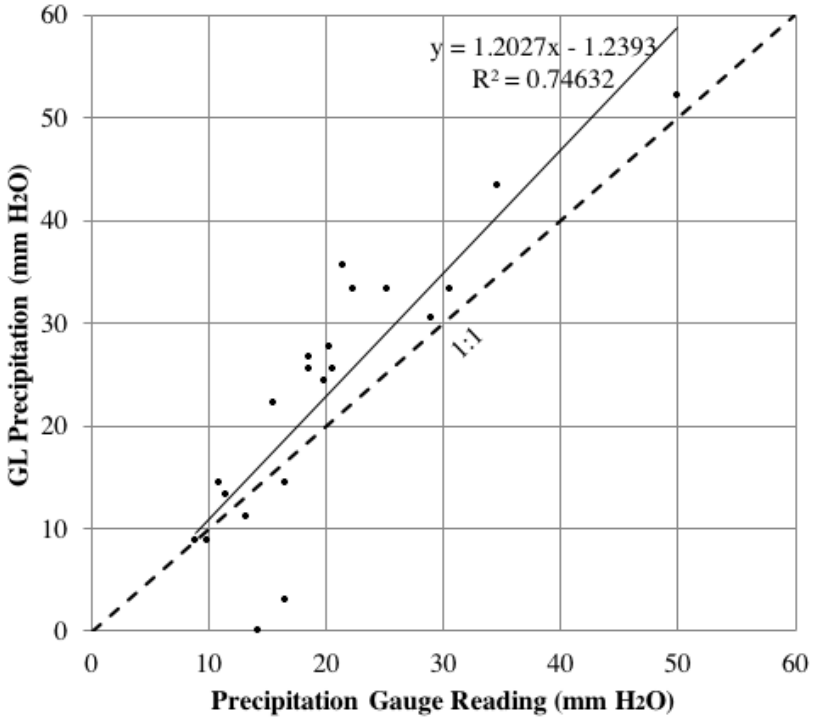

Figure 5.18 – Precipitation correlation between BHLB08 and SWSS meteorological station for all readings above the resolution limit

BHLB03

BHLB03 is the sensor that is located the farthest from the SWSS meteorological station at ~1 km. As such there should be more scatter to the results. The comparisons for entire data set as well as the events greater than the resolution limit are shown in Figures 5.19 and 5.20, respectively. The fit between a 1:1 line and the best fit line for the scatter plot is not good. The slope of the best fit is 0.55 for all data and 0.61 for those measurements above the sensor resolution. For larger events, most events fell below the 1:1 line, indicating that either there was less rain in the BHLB03 site. The increased scatter in this data is not unexpected given the distance between the VWP location and the meteorological station.

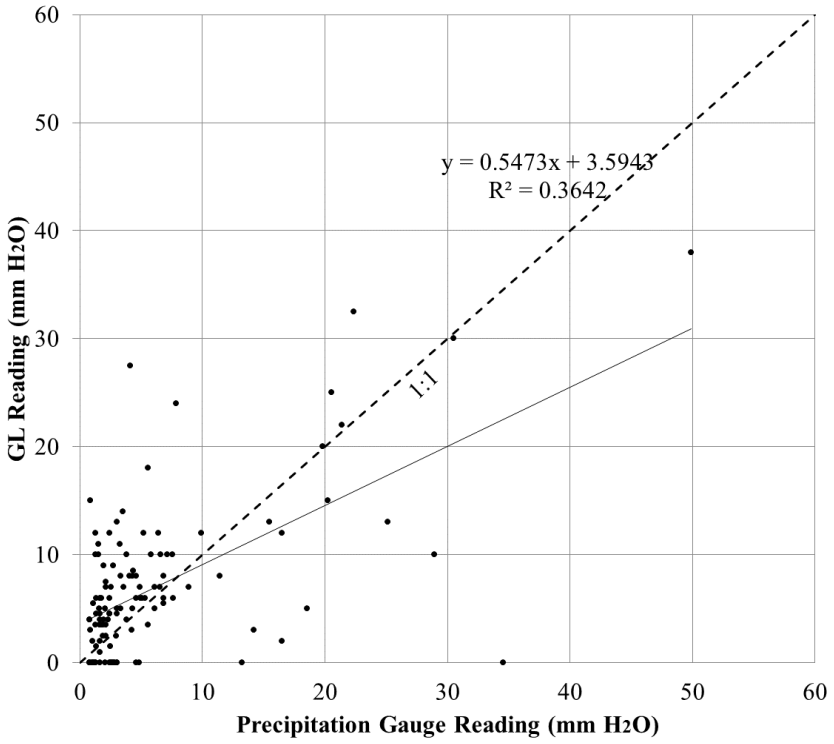

Figure 5.19 – BHLB03 readings correlation with SWSS meteorological station

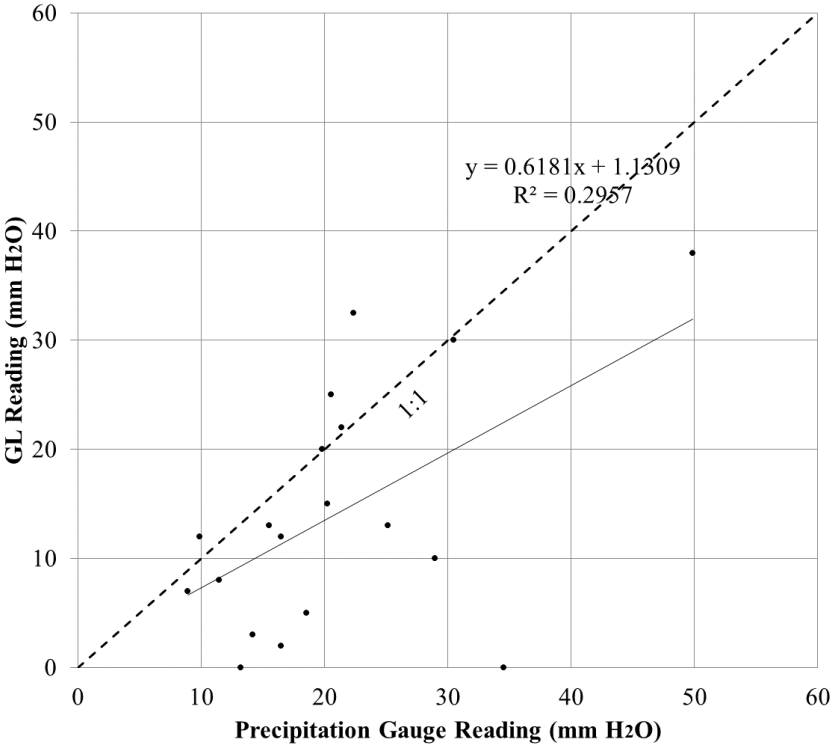

Figure 5.20 – Precipitation correlation between BHLB03 and SWSS meteorological station for all readings above the resolution limit

VP-12-32-02 and VP-09-32-03

The correlation between VP-12-32-02 and the SWSS meteorological station can be seen in Figure 5.21 below. The location for VP-12-32-02 is on SWSS at approximately the same elevation as BHLB07; as such their correlation should be similar. Only data after the RST data logger install (summer of 2015 until 2016) is shown. There are almost no inferences that can be drawn from this graph. Only 2 data points exist after above the resolution limit. The only inference that can reliably be made is that some larger rainfalls can be seen in the ML data.

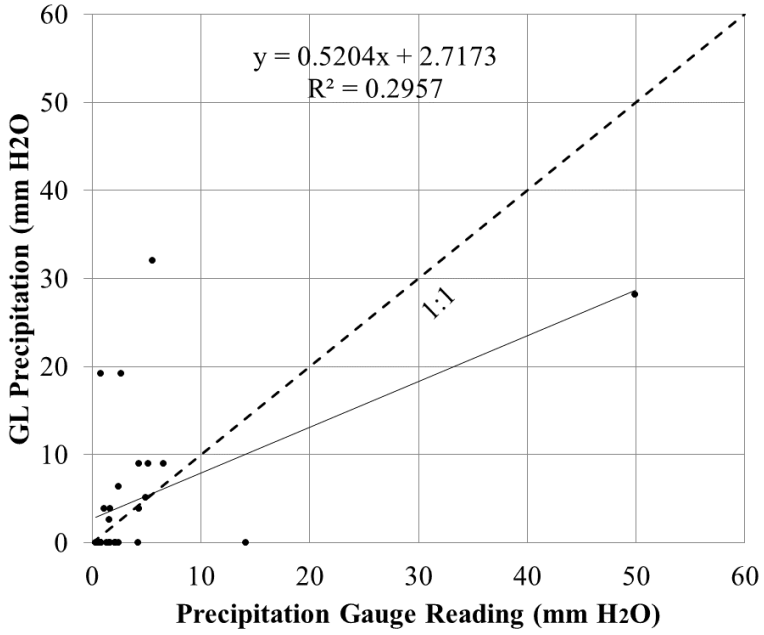

Figure 5.21 – VP-12-32-02 readings correlation with SWSS meteorological station

The correlation between VP-09-32-03 and the SWSS weather station is shown in Figure 5.22 below. This graph is largely similar to Figure 5.21. Again, there is only one data point recorded above the resolution limit. That data point is close to the 1:1 line which indicates that there might be good association there. More data is required to make any more inferences later.

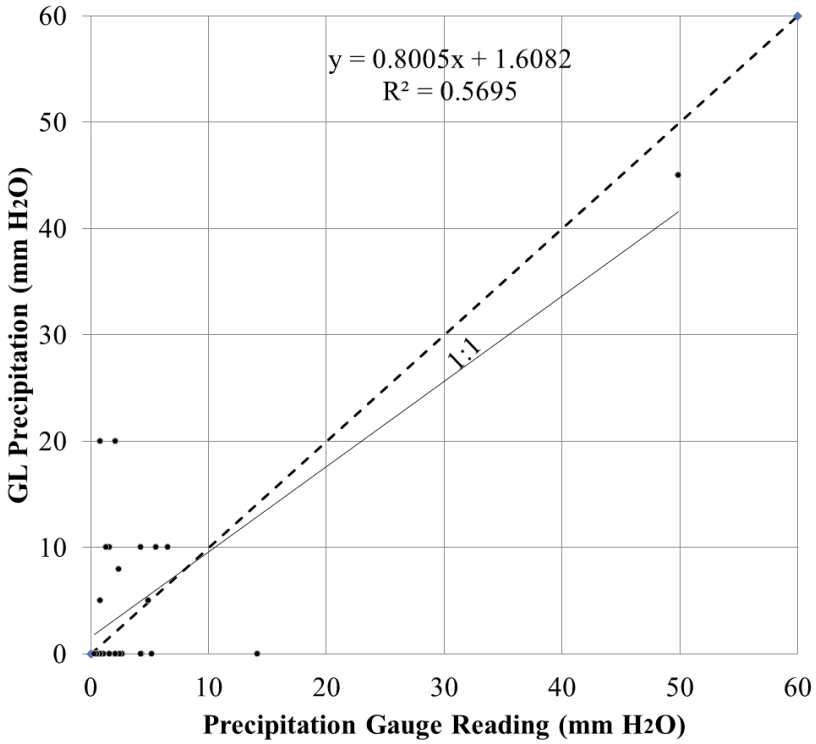

Figure 5.22 – VP-09-32-03 readings correlation with SWSS meteorological station

BHLB01

BHLB01's correlation to the W1 meteorological station is shown in Figure 5.23 and Figure 5.24 below. The correlations show only a few points which are over the resolution limit. These points have a good slope; however, they are consistently 15 mm under the 1:1 line. Once again, the statistical n of this site is hampered by the lack of data. There are clearly some readings that can be seen by BHLB01.

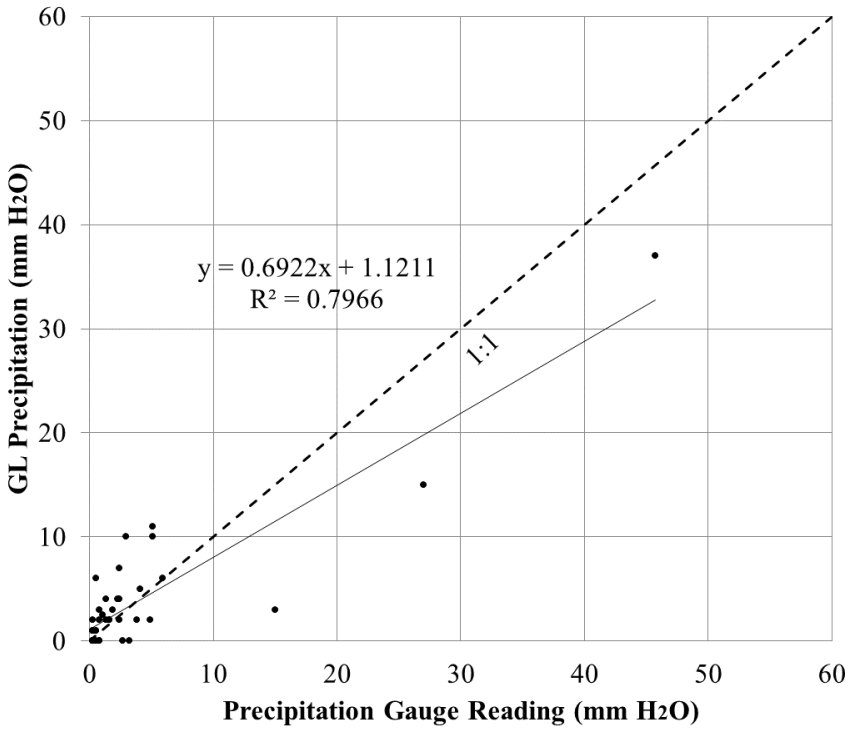

Figure 5.23 – BHLB01 readings correlation with W1 meteorological station

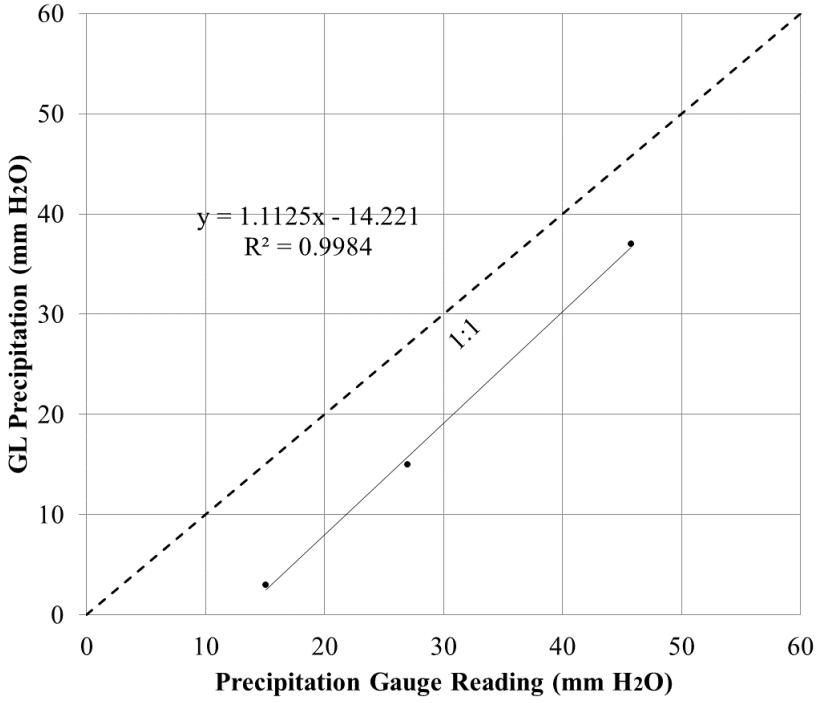

Figure 5.24 – Precipitation correlation between BHLB01 and W1 Meteorological station for all readings above the resolution limit

BHLB02

BHLB02, shown in Figures 5.25 and 5.26 below, shows more data than BHLB01. There is a lot of scatter and there are several 10-20 mm precipitation events (as recorded by the meteorological station) which are not seen by the BHLB02 VWP. This may be due to the distance, or it may be due to noise in the sensor, or the complicated hydrogeological setting. Without the readings below the sensor resolution limit, the slope looks good; however, it is being skewed downwards by the under reported BHLB02 readings. Several of the readings are on the 1:1 line, but none are above. The scatter in this graph is similar to Figures 5.19 and 5.20 for BHLB03. The exception is that there is only 1 reading above the 1:1 line.

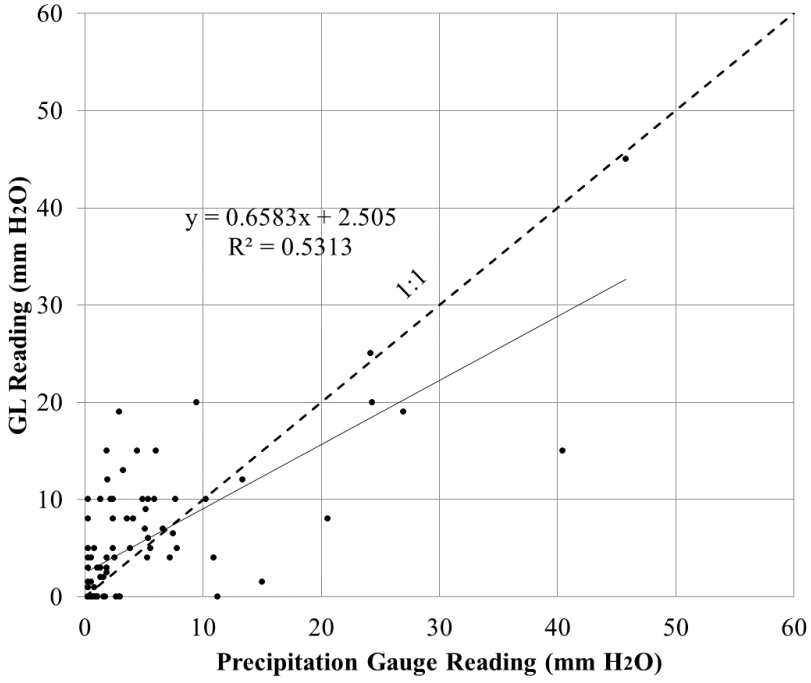

Figure 5.25 – BHLB02 readings correlation with W1 meteorological station

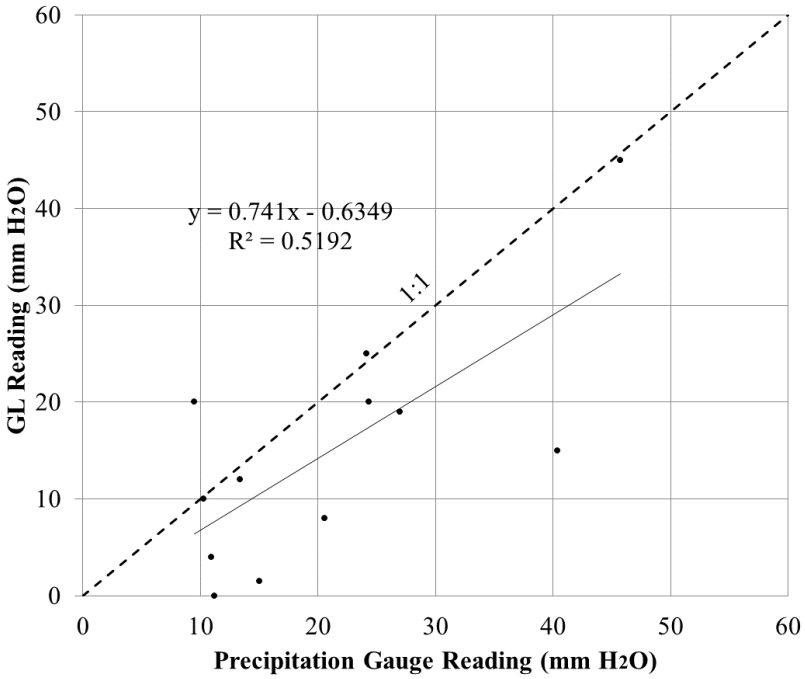

Figure 5.26 – Precipitation correlation between BHLB02 and W1 Meteorological station for all readings above the resolution limit

5.4.2 High Frequency Precipitation

The previous comparison between the GL readings and the rain gauge was focused on the magnitude of daily rainfall. In this section, the timing and pattern of a selected rainfall events is compared to the GL measurements of moisture loading. To view the high frequency response of the ML to a rainfall event, a single moisture loading event was compared with 60-minute data from the precipitation gauge and 10-minute data for BHLB08, BHLB07, and BHLB03 moisture loading, shown in Figure 5.27. The time dependent response of both sets of instrumentation is highly correlated including storm duration and magnitude, with BHLB03 showing some reduction in cumulative rainfall.

To attempt to understand the fidelity of the sensor to the tipping bucket rain gauge, the specific records for impulse (dP) are compared for this rainfall event in Figure 5.28. The ML data is downscaled to 60-minute frequency to match the rain gauge data. During the rainfall the hour by hour rainfall records match well.

These comparisons demonstrate the theoretical correlation to the rain gauge records. The cumulative loading specifically matches very well. The loading impulse graph shows an oscillating reading on a 10-minute scale. This could likely be smoothed out with some averaging; however, it was left without averaging to show both the accuracy of the GL in reading single impulses and the banding effect seen by the 8.9 mm resolution limit of the VWP that the data trend is taken from.

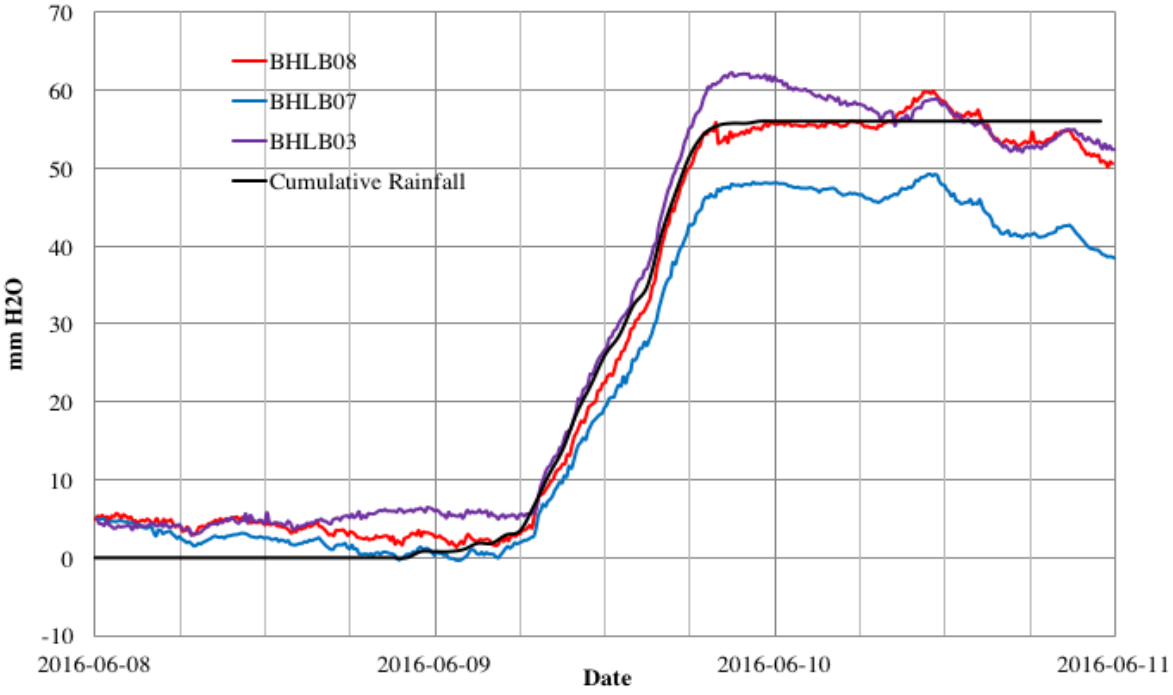

Figure 5.27 – Time series of a rainfall event captured with a GWL ML and cumulative rainfall gauge

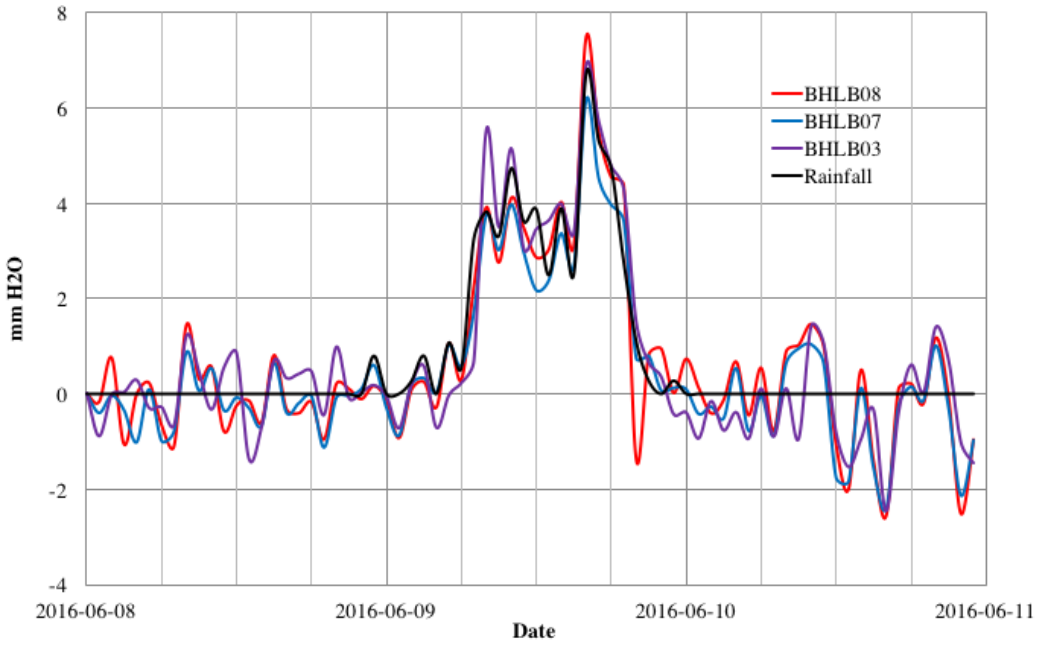

Figure 5.28 – Rainfall event time series captured by ML loading change and rainfall gauge

5.5 Evapotranspiration

To investigate for the presence of ET within the ML, a simple visual method is used; viewing the ML and compare it to various estimates or measurements of AET. Trends of combined precipitation and AET data will be created, and then compared to the actual ML trend.

5.5.1 Creation of ET time series

Two methods of determining ET were used for this project. During the 2014 and 2015 seasons, the SWSS landform was monitored with both eddy covariance and P-M estimations from the local weather station. Additionally, the landform had a weather station which produced data for a P-M estimation of ET Trends for the years investigated by this project shown in. The EC measurements are a measure of AET while the P-M method calculates the PET. The EC data was only measured from late spring to early fall. The P-M method is available for a continuous daily estimate of PET. As such, to generate a working estimate of AET estimate, the P-M data is linearly reduced to approximate the eddy covariance data. This estimate of AET is then used to evaluate the Moisture loading Data. Figure 5.29 shows the P-M data for 2014-2016. Figures

5.30 and 5.31show the linear correlation of the P-M data to the EC data for 2014 and 2015, respectively.

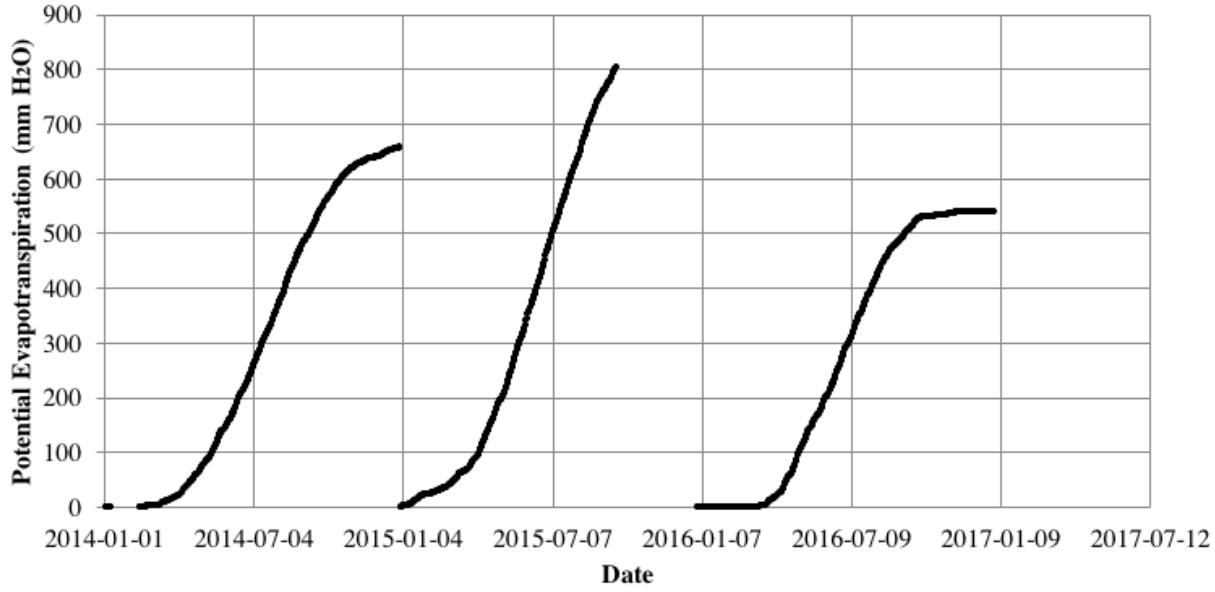

Figure 5.29 – Penman-Monteith PET estimates for 2014 to 2016

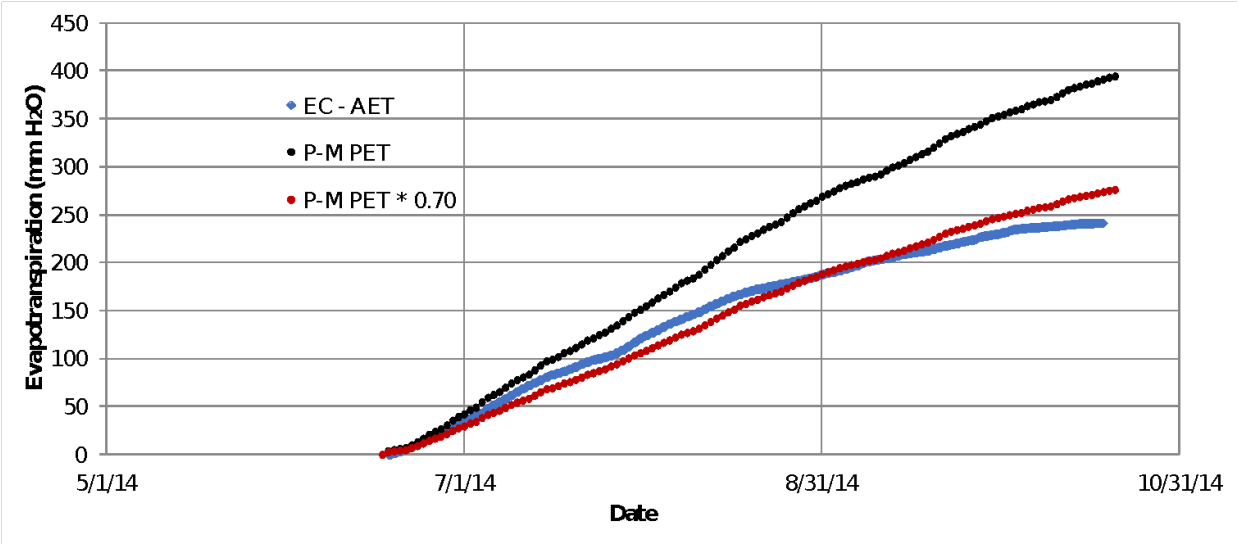

Figure 5.30 – All 2014 ET estimates indexed to the start of EC data

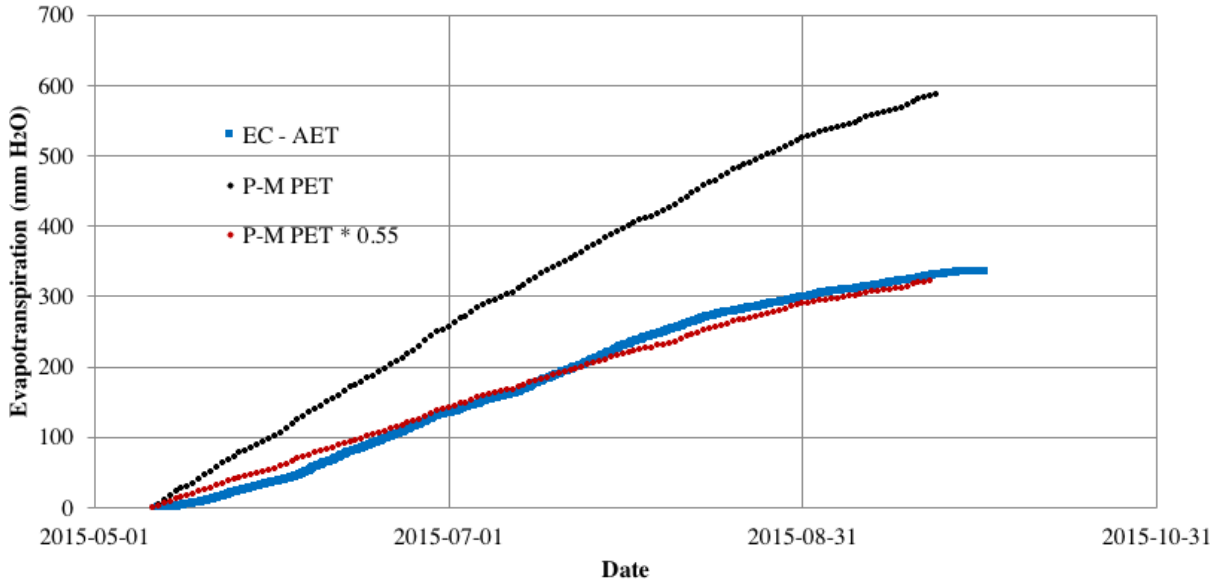

Figure 5.31 – All 2015 ET estimates indexed to the start of the EC data

The coefficients seen on Figures 5.30 and 5.31 were used to scale the entire series of P-M data for 2014 and 2015. The 2016 AET data was scaled by 0.625, that being the average of the 2014 and 2015 scaling coefficients. The scaled P-M data is shown in Figure 5.32 compared to the unscaled data. This data is then used to evaluate the ML Data. To make the form of the data closer to the ML as seen by the GL, the precipitation data is combined into the PM data such that the precipitation shows an increase in moisture loading while the AET reduces it.

There is no energy closure coefficient applied to the EC data, and as such it is likely 20% lower than actual evapotranspiration. The amount of energy closure is hard to estimate as the EC tower is located on a terrace in SWSS, near the bottom of one slope with low, grassy vegetation and shrubs. The terrace contains grassy vegetation with some short trees. To the east is a second slope which is well vegetated with mature trees. Both of the slopes and the terrace are linear features, consistent for approximately 1 km to the north and 4 km to the south. As such, the EC data is used without an energy closure coefficient. In Section 5.6, the BHLB08 2018 water balance is used to visually estimate what the energy closure might be if the ML data is regarded as accurate, with no transients such as runoff or percolation be considered. This closure coefficient was estimate at 28%.

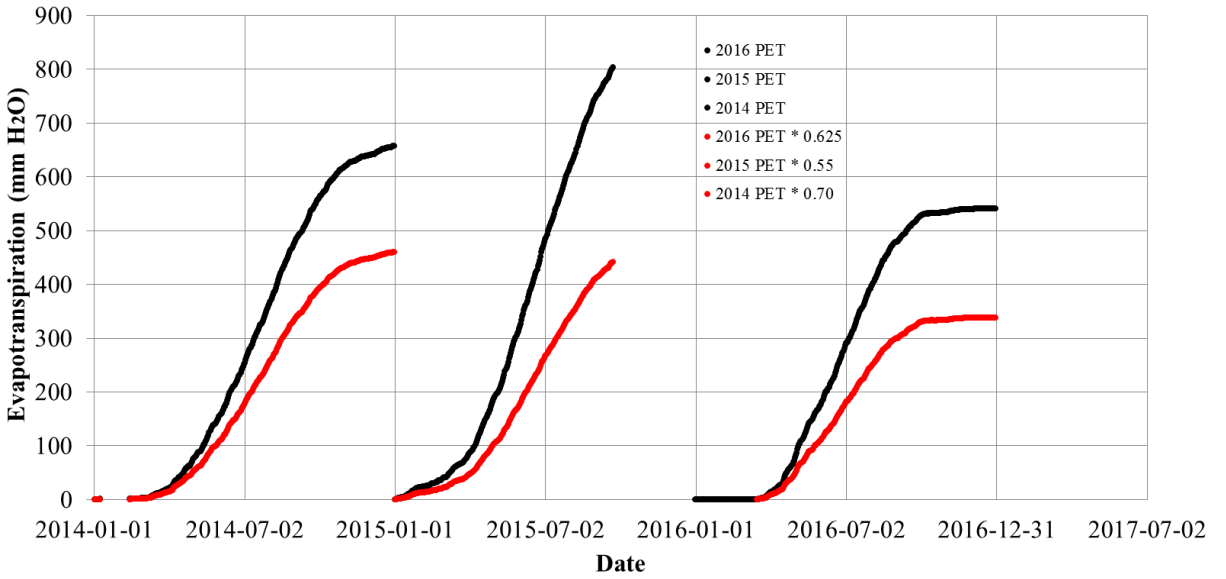

Figure 5.32 – P-M PET and scaled PET for 2014 – 2016

5.5.2 Visual comparison of ET to the data series

The seasonal pattern of AET and precipitation, calculated in the previous section, are compared to the patterns of ML obtained from the GLs. The focus of this comparison is on timeframes of a few days or more in which there was little recorded precipitation, and therefore can be seen where vertical jumps are not recorded. The AET generated by scaling the P-M to match the EC data are used in these charts.

Similar patterns of water loss will be generated from the GL time series from BHLB02 and BHLB08. Figures 5.33 and 5.34shows the comparison between BHLB08 and the P-ET estimates for 2014 and 2015, respectively. BHLB01 is also shown for 2015, after the RST install. The P-ET trend is shown from March 16 to October 31, as the solid precipitation data is not consistent throughout the winter. These sensors show some potential for ET results. BHLB07 and BHLB03 show other influences on their pore pressure as discussed in previous sections, and as such are not suitable to evaluate ET against.

The time frames in which the P-AET data and the ML data for BHLB08 overlap show good correlation. The precipitation events seem to happen in the same places in 2014, and the dry periods between the precipitation jumps occur in a manner consistent with expected ET trends. The slopes do not match throughout the estimate, with the ML showing more assumed moisture loss over the course of the year than the scaled PM data indicates. Towards the end of the year, the slopes become closer, but there is some additional noise in the ML in the fall that is not accounted for in the P-AET line. It is unknown what mechanism causes this difference in moisture loss. It could be due to some instrumentation error, an error in the calibration, or moisture loss out of the landform.

In 2015, the fit between the P-AET and the ML is much better, with the ML showing less ET in July and August compared to the P-AET trend. Overall, the slopes match more but it appears that the precipitation magnitude recorded at the weather station is generally less than the GL sees. There appears to be a large rainfall in early June, in particular, which is quite small in the P-AET data but quite large in the ML data. A point of interest in both the 2014 and 2015 data is that the EC records a slower rate of moisture loss in spring than the ML does, but the end of the year the slopes of the ML has changed to be a better fit for the rate of loss shown by the AET. This changing slope can be better seen in the 2014 data, but it is present in the 2015 data.

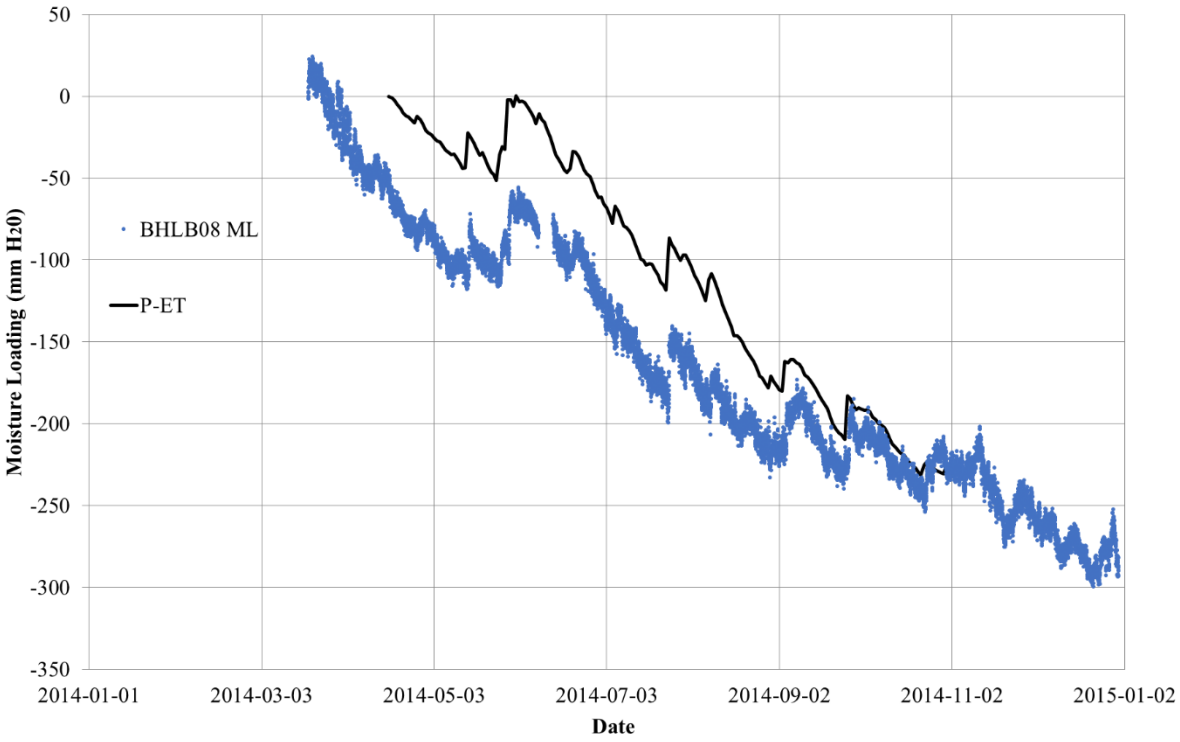

Figure 5.33 – Comparison of change in moisture loading storage at BHLB08 for 2014

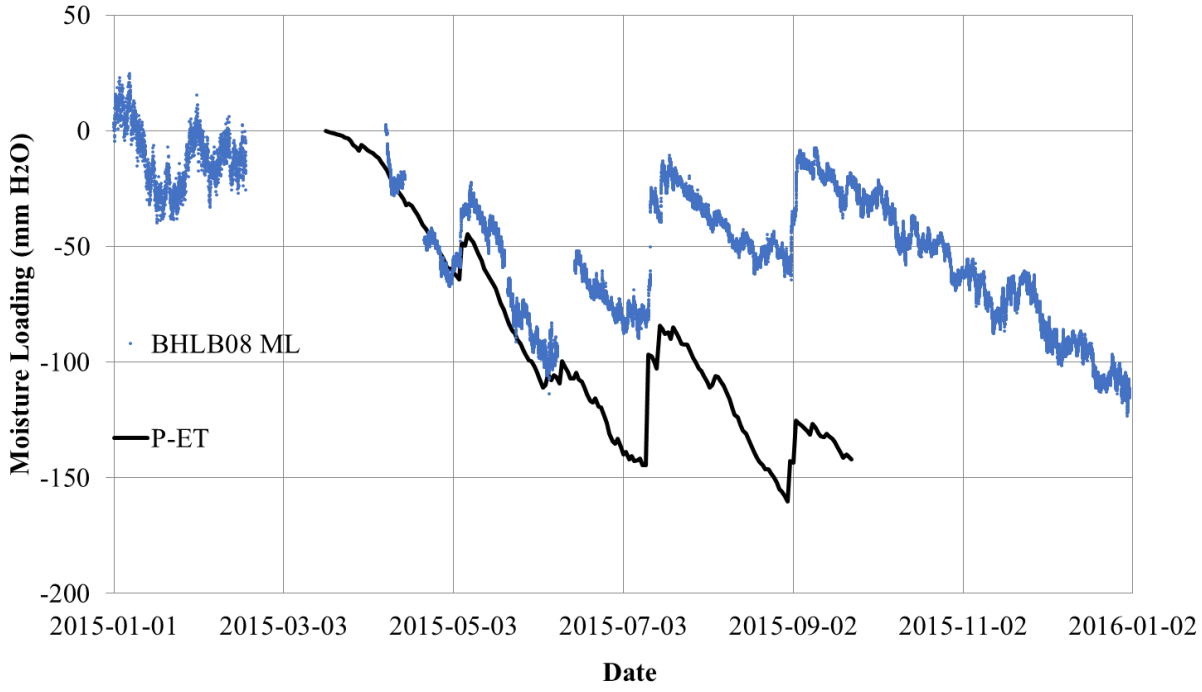

Figure 5.34 – Comparison of change in moisture loading storage at BHLB08 for 2015

The BHLB02 comparison of ML to the P-ET estimates is shown in Figures 5.35 and 5.36. The ML from BHLB02 does not correlate well to the P-AET estimates in 2014 but the correlations improve in 2015. A possible precipitation event is shown in June of 2015 which does not correlate to the moisture loading trend, but later precipitation events are seen. In fall, there is a large change in the ML signal, and even though there is no ET data with which to compare this change, it does not seem likely that it is ET is the cause of this ML given the time of year and the amount of decline (~600 mm in less than a month). Some portions of the ML slope in summer do match to the EC line.

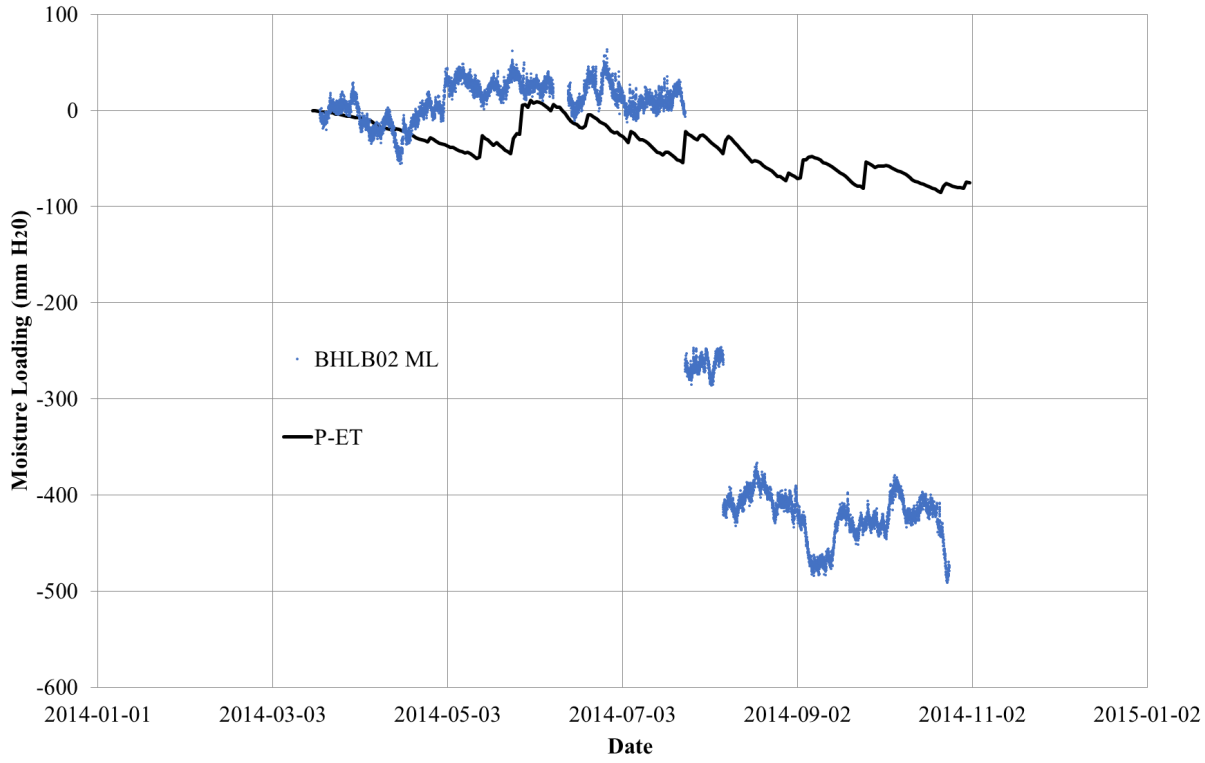

Figure 5.35 – Comparison of change in moisture loading storage at BHLB02 for 2014

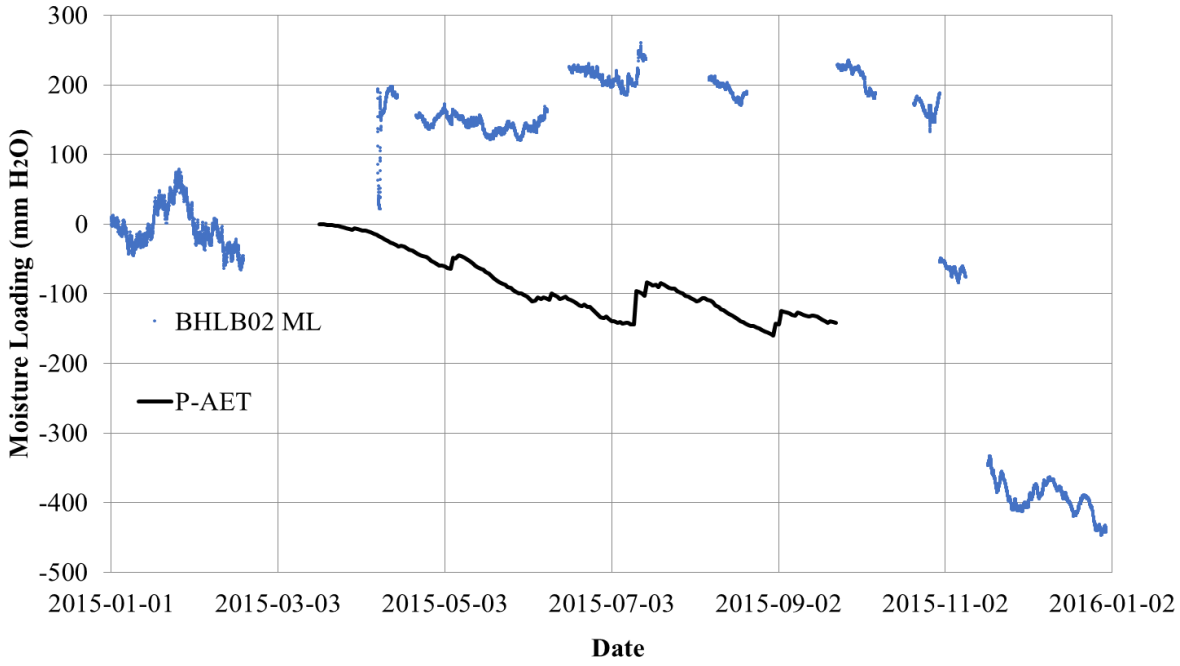

Figure 5.36 – Comparison of change in moisture loading storage at BHLB02 for 2015

BHLB01 is also shown compared to the ML trend for 2015 in Figure 5.37 below. This shows a reasonable correlation. In the fall the moisture load levels out nicely. The precipitation events are not well defined in BHLB01, with the sensor failing to show the events well. The ML appears to line up with the precipitation event shown in the weather station record. As with BHLB02 there is an additional event in early June 2015 which was not seen on the SWSS precipitation gauge. The periods of consistent ET shown in BHLB01 show a reversal to BHLB08 where the slopes align better in the early parts of the year but then get much steeper later in the year than the P-AET data. If the data for this sensor had less interruptions, then it would likely be very good.

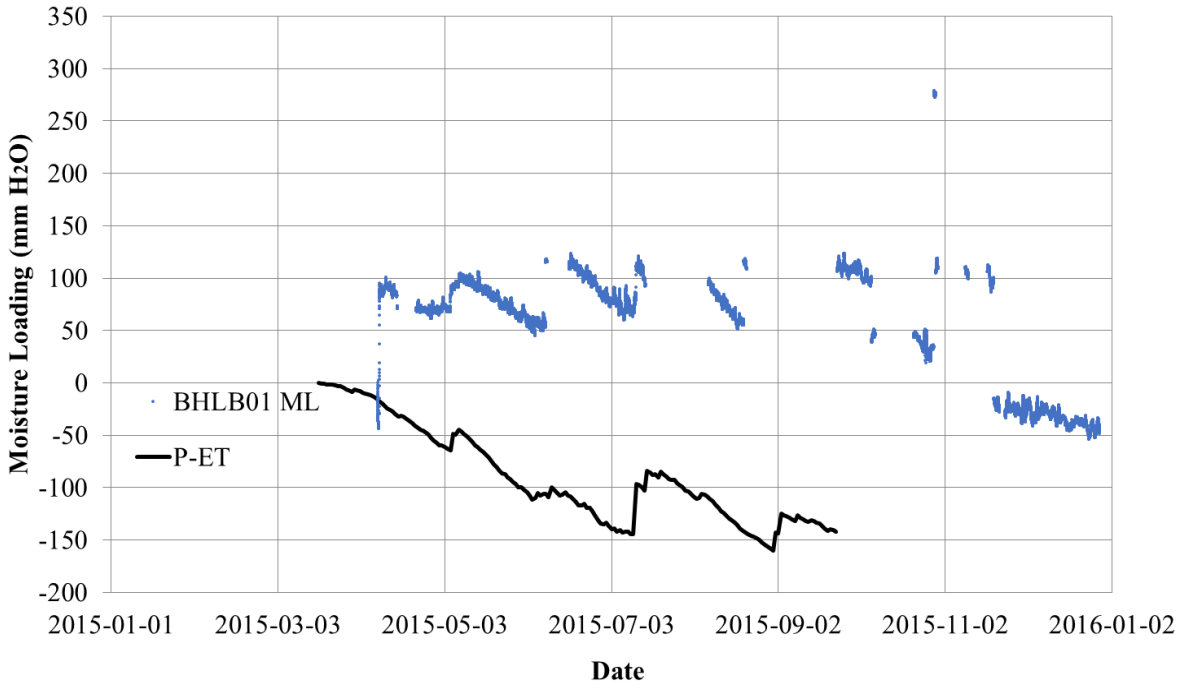

Figure 5.37 – Comparison of change in moisture loading storage at BHLB01 for 2015

5.6 Simple water balance for BHLB08

The water balance for a soil profile can be calculated based on the following equation:

$$dS = P\text{-}AET\text{-}R\text{-}NP \quad (5.1)$$

where dS is the change in stored water volume (mm), P is precipitation (mm), AET is actual evapotranspiration (mm), R is runoff (mm) and NP is net percolation (i.e. surface water that moves down and joins the saturated zone associated with the GWT) (mm).

A water balance was attempted using the ML from BHLB08. BHLB08 provided the ML trend most likely to provide a ML trend with good fidelity for 2016. The ML is compared to a water balance estimated based on monitored data.

To estimate the ET, the P-M method was calculated from the meteorological data, which was collected in SWSS Cell 32 near BHLB08. This estimate provides the PET, and as performed in

the previous sections, the PET was scaled to estimate AET. As no EC data was available to scale this data, the data was scaled by the average of the two previous years, 0.625. The raw P-M PET data and the scaled AET data are shown on Figure 5.38. Precipitation and ET records are not calculated for times where the predominant precipitation is snow, due to no consistent snow records being kept. As such, the P and ET records are presented from March 16 to October 31.

The precipitation records were obtained from the rain gauge near BHLB08. The combined precipitation and evapotranspiration (P-AET) was calculated from April 15, and was subtracted from the moisture loading record leaving an estimate of the change in storage. This change of storage is compared to the ML, which is being treated as an estimate of dS. All of these data are shown in Figure 5.38.

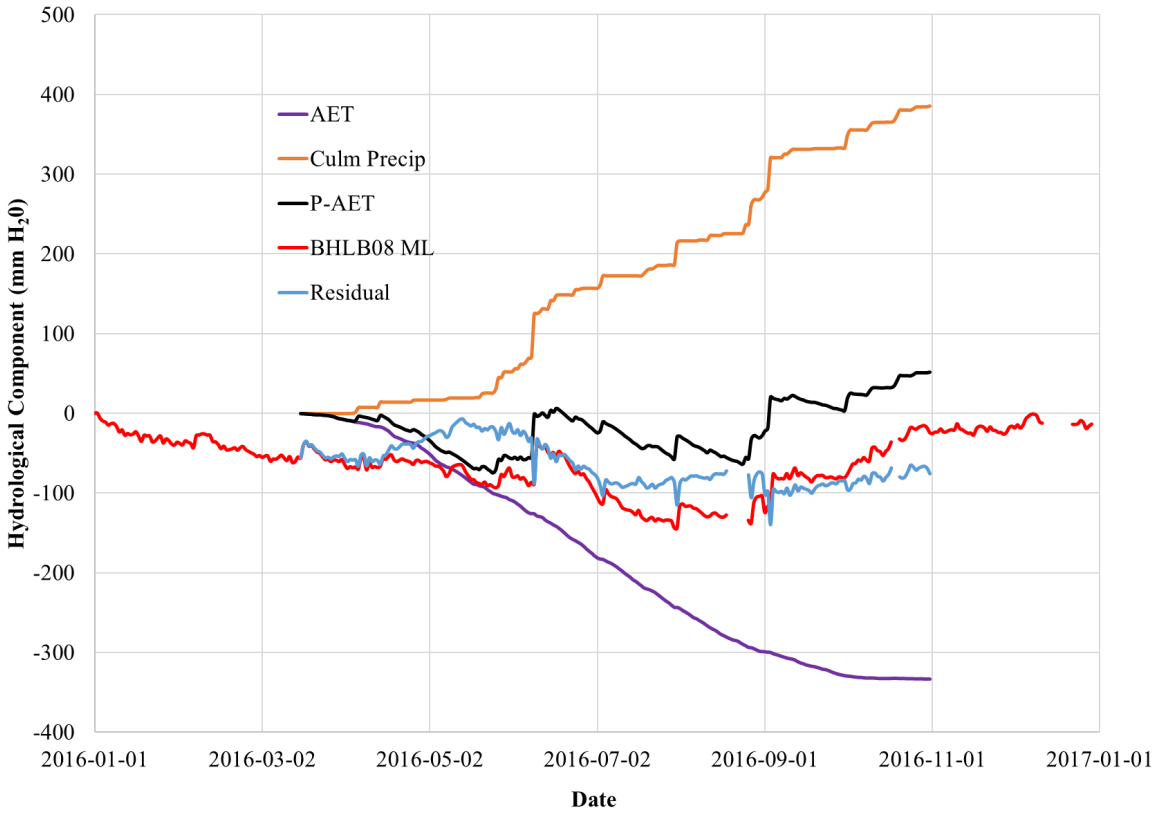

Figure 5.38 – All hydrological data for BHLB08 in 2016 with a correction of 0.625

The combined graph shows how the water balance (P-AET) compares to the ML for BHLB08. A residual is also calculated (ML-(P-AET)) which shows an estimate of hydrologic fluxes that

might be seen in the (P-AET) and not in the ML. This residual line begins at the point that all hydrological data is available. From January until approximately the beginning of April, the ML trends downwards, likely due to a continuing but lessening long-term downward trend in the pore pressure, which shows more clearly for 2014. Two mechanistic explanations for the declining trend in early 2016 are that it may be due to either drainage of the local groundwater (which may be considered NP), or consistent ablation of snow.

It is also possible that this decline is due to vertical dissipation of the excess pore pressure into surrounding formations. Research by Smith et al. (2013) indicates that such pressure transients may last up to a year or more in shale formations. Over the course of the year, the transient will gradually dissipate and lose its fidelity to the specific loading. This allows for reasonable expectation of minor pressure dissipation in the short-term (days to weeks) but over the course of months and years this mechanism will gradually induce error. This error is on the order of the previous pressure fluctuations recorded in the ML. They will dissipate proportionally to the amount of excess pore pressure in the formation at any particular point in time and the conductivity of the formation. For our SWSS sites, this provides confidence in the short-term fluctuations, but less confidence about the overall trend of the ML as the time frame examined increases. Because the change in ML is both positive and negative the overall direction of the dissipation is not specifically unidirectional. Instead it is in the direction of the drained pore pressure. For saturated formations at depth, a large unloading event may cause the undrained pore pressure to be lower than the drained pore pressure and therefore have to increase in pressure to equalize.

The residual line follows the ML line until late March, and then an increase back towards zero during April and early May as AET estimates increase while the moisture load continues at approximately the same rate as it had from the beginning of the year. The residual then decreases again from late May until mid-July, after which it remains more stable for the rest of the year. The mechanisms that explain this change may be due to the way the ML ET slopes varied against the AET slope. As these change throughout the year in relation to each other, the residual would vary accordingly. Over the year, the ML shows a change in storage of -15 mm

throughout the year, compared with an input (calculated with other instrumentation) change in storage of 50 mm.

In June, rainfall begins to be seen in the ML trend, and the P-AET estimate shows the best correlation to the ML. The PET estimate from June through the beginning of August seems to be less than the ML record indicates, which is shown by the residual line increasing again. Once again, this is likely attributable to the difference in PET to AET. Finally, from August to the end of December the ML and P-PET match up quite well, shown by the residual having almost no slope.

Direct measurements of R+NP (net surface and subsurface flow of water out of the tailings) are not available for this site; however it is interesting to note that previous estimates of these from water balance modeling (Huang et al. 2015, Alam et al. 2017) are in the order of 50-60 mm. The scaling coefficient (0.625) that was applied to the P-PET to calibrate the P–M data into an estimate of AET was varied to match an assumption that no error, and no hydrological phenomena needed to be accounted for except rainfall and ET. The best coefficient was found to be 0.80, which is similar to the 0.7 found for 2014 but further from the 0.55 found for 2015. This would represent an approximate 28% energy closure on the Eddy Covariance measurements, should all the error in the datasets be attributable to that single component. The data has been replotted showing this correction in Figure 5.39. This estimate, however, cannot be relied upon as there are several unknowns operating in this scenario which are not considered. Some unknown effects on the ML readings are: the assumption of no dissipation of pore pressure over the examined period, the effect of changes in mechanical loading from the saturated zone, any NP or R, and other pore pressure transients. Depending on the size of these unknowns and how they interact, the reliance on energy closure as a factor that can explain all of the variance between the ML and P-AET is unwarranted. As the time-line of this water balance is approximately 9.5 months, some dissipation effects and loading effects from the upper saturated zone are likely influencing the ML.

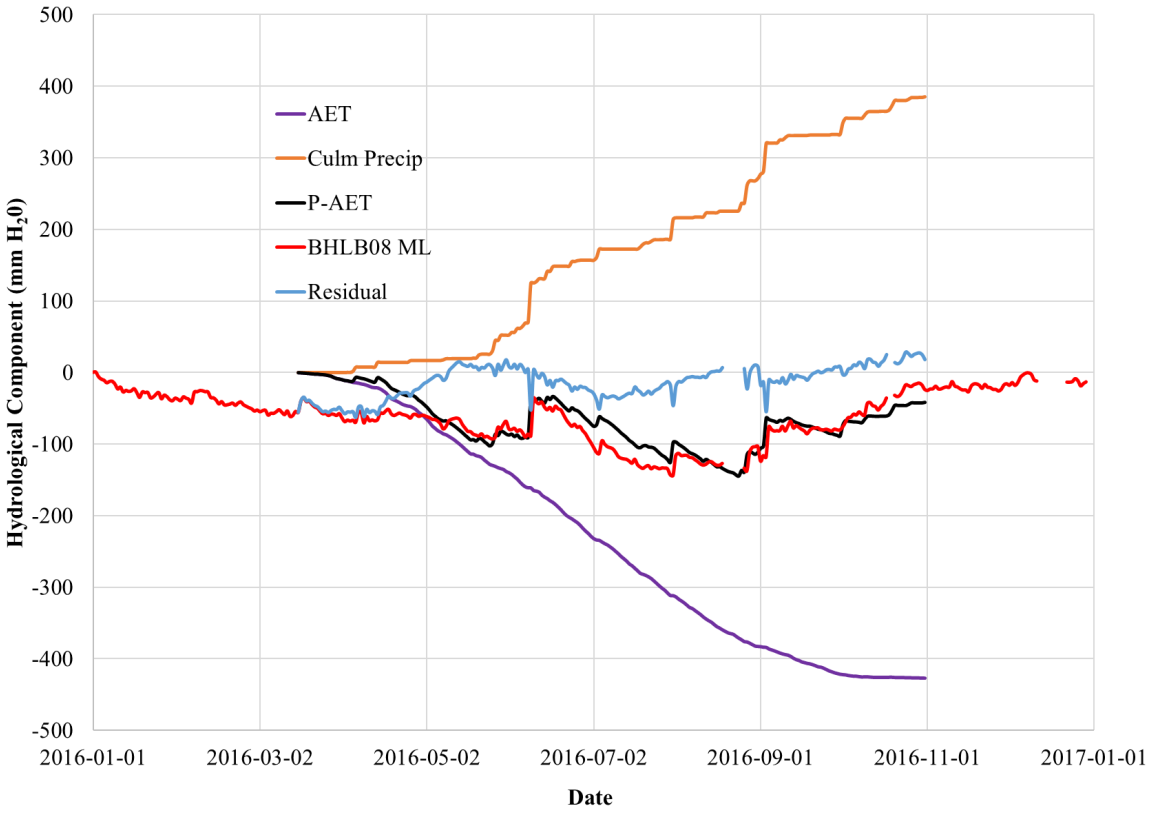

Figure 5.39 – All hydrological data for BHLB08 in 2016 with a PET – AET correction of 0.80

Seasonal cycles in water levels near to BHLB08 within the sand tailings may show recharge and drainage cycles which may be influencing changes in moisture loading detected by the GL. The standpipe well hydraulic head change is shown in Figure 5.40 for a 15 mbgl depth, installed in the tailing sands. This well is located within 5 m of BHLB08 on the same bench.

The standpipe installed in the tailings sand shows a loss of approximately 150-200 mm of head over the course of the year, in a steady decline. This may indicate a drainage phenomenon within the slope. As the tailings level lowers, the stress induced in the pore pressure reduces. The change in weight is the specific yield (Sy) times the decline in water level. In this case, for a change in water table of 200 mm, and specific yield of the tailings sand assumed at 0.20, the change in induced load would be 40 mm (ML change).

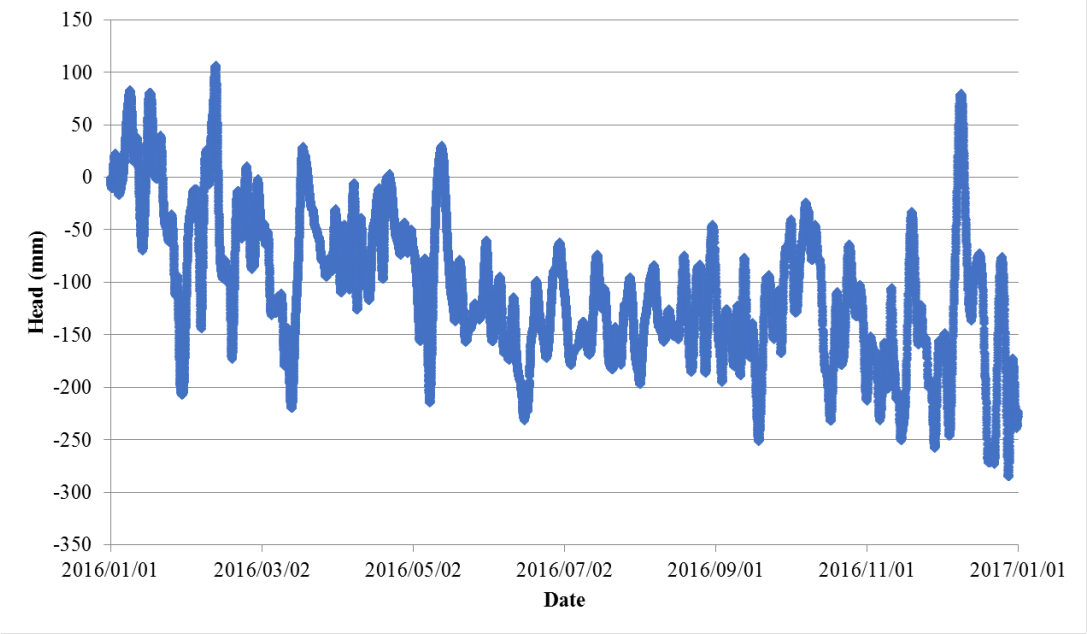

Figure 5.40 – Standpipe well near BHLB08 with 15 mbgl depth installed in tailings sand

There is also a soil monitoring station located in the vicinity of BHLB08 which tracks soil water content and suction of the near surface soils. The volumetric water content, measured at the SWSS weather station, is shown in Figure 5.41and the matric suction at the same locations and depths is shown in Figure 5.42. For the early portion of the year the soil is frozen, and so the measurements should be discounted, however following spring thaw in March the volumetric water content rises to around 0.30 - 0.33 cm^3/cm^3 during freshet. The 5 and 10 cm till measurements show a trend that is very similar to the BHLB08 trend in Figure 5.38. The 40 cm till measurement is more muted, while the tailings sand shows big swings in saturation. In the middle of summer, from July to September, the near surface soils are unsaturated, which may be the cause of the change in the BHLB08 moisture load change due to EVT. The near surface volumetric water content sensors show a good correlation to the BHLB08.

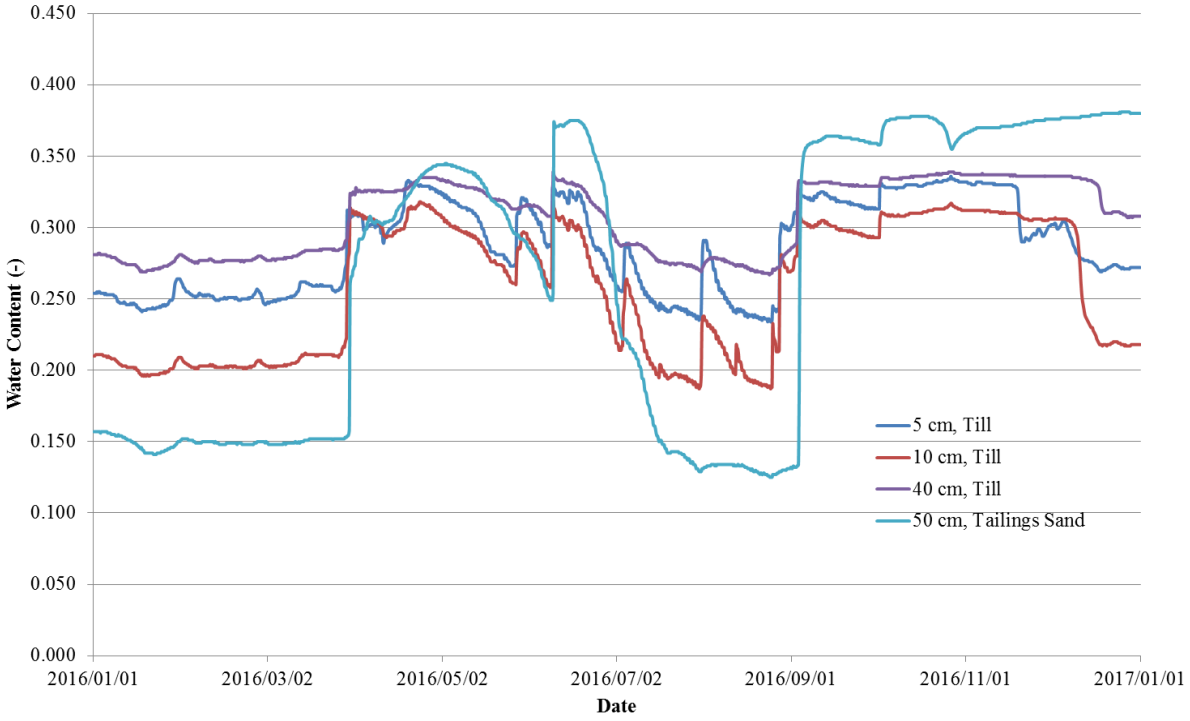

Figure 5.41 – Volumetric water content at SWSS weather station for 2016

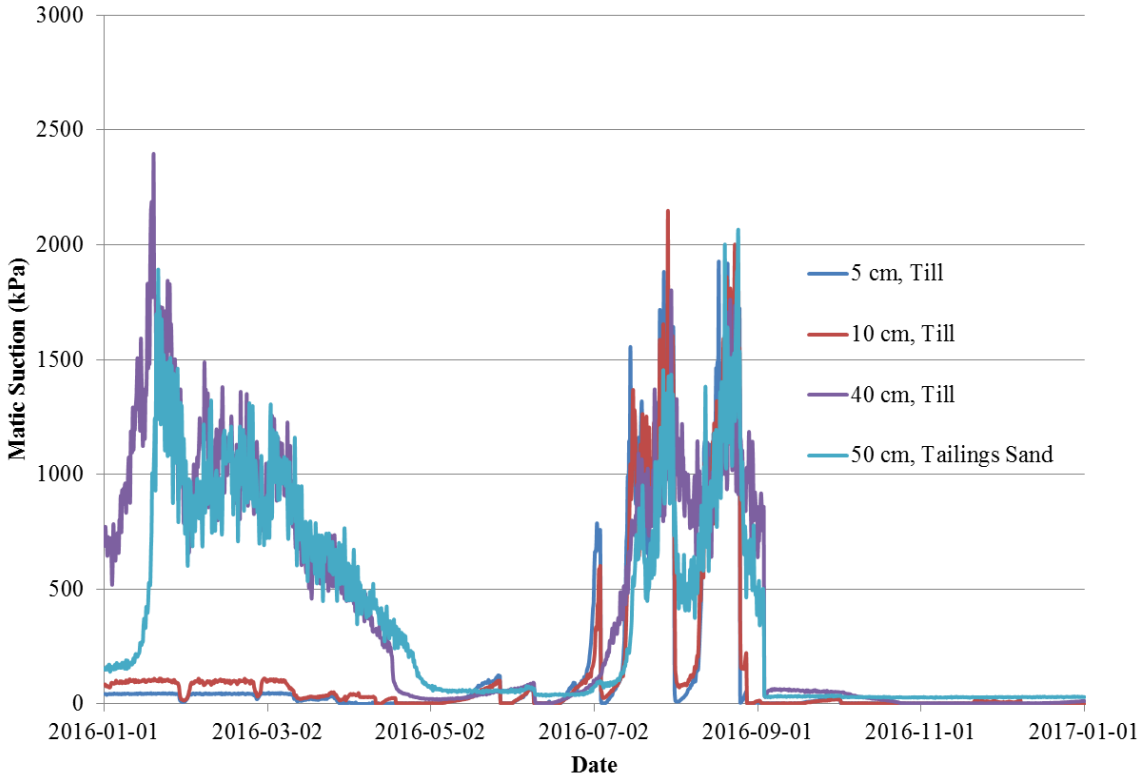

Figure 5.42 – Matic suction at SWSS weather station for 2016

6 CONCLUSIONS AND RECOMMENDATIONS

The results section discussed the results, finding what the best-case scenarios were for the implementation of GLs into closure landforms specifically, and other potential industry implications in general. It also investigated the potential failure modes that could be seen in the project. What follows are the key findings of the project, lessons learned from the project, and recommendations.

6.1 Key Findings

The moisture loading effects were seen in most of the sensors, and the theory shows that loading effects should be seen in all pore pressure records from saturated conditions. The potential of this method is most clearly seen in the BHLB08 results. This sensor showed a ML trend that closely matched the results from EC data, precipitation data, and ET data generated from a nearby weather station. It showed high fidelity to the rain gauge for a single loading event. It showed a small difference (~50 mm H2O) over the course of the year between it and more traditional methods that could be attributable to net percolation, error in PET-AET comparisons, vertical dissipation, or other sources. This type of hydrological monitor has the potential to add a great deal of nuance to hydrological and hydrogeological estimates of landform performance. The output from moisture loading estimates should be taken into account in any numerical simulations of coupled stress and flow at locations in mine sites. Doing so would allow the incorporation of moisture storage effects into those simulations.

Other sensors had potential such as BHLB07, BHLB01 and BHLB03 but show influence from other hydrological events or had sensor errors which limited their usefulness. Most of the SCL geotechnical VWPs were not useable for these analysis.

The potential of the GL method is that these sensors can either stand alone as a monitoring of the general hydrological loading, they can be used as an additional check on the hydrological balance to help determine other hydrological factors such as NP, and they can be used as inputs to modeling scenarios. In particular: its potential to verify point readings from other instrumentation to averaged surficial loadings is quite promising.

6.2 Lessons learned

The overall goal of this project was to evaluate whether methods and techniques which have been previously verified from an academic perspective might be applied in an operational industrial setting. A number of the key issues which occur and will have to be addressed to make this transition in future will be highlighted in this section. The major lessons revolve around sensor and site selection as well as calibration issues.

The first thing to discuss is the sensor and datalogger system. Both manual and automatic downloading of data have been problematic. The manual method showed shutdowns and data collection problems due to cold weather, sensor/datalogger incompatibility, shielding errors, instrument timing errors, and memory overwriting. While not all of these errors are unique to the GL method - in fact none of them are - the GL method works best with more continuous datasets and more accurate individual readings. For example, in one case the sensor was unplugged by site personnel to take a reading and was not then reconnected.

The automatic system was, in general, more successful in obtaining the required data records although it still suffered from memory overrun issues when the automatic downloading failed. This occurred at the Base station locations (BHLB07 and BHLB04). This specific error may be limited to the RST system, but it may be safely assumed that similar issues would exist in any automated system.

The issues related to different instruments generating their own timestamps have the potential to induce error in the calibration, either from having to interpolate one set of readings to match the timing of the other, or by inducing extra lags into the system. These lags may be resolvable using the BRF method but solving the timing issues using BRF methods may lead to incorrect assumptions about the interaction of the wellpack and formation if they are unknown at the time of calibration. This error is reflected in the calibration changes in BHLB08 pre to post RST install.

Sensor selection is a key issue. The actual pore water conditions should be assessed and the sensor with the maximum (full scale) pressure rating that most closely matches the expected conditions should be used. In this case, the sensor resolution is linked to the maximum pressure of that sensor. BHLB03 was installed with a 350 kPa sensor which gives a resolution of 8.9 mm. The actual pore pressure at BHLB03 was ~165 kPa. If a sensor with half the maximum pressure had been used, then the resolution should have decreased to < 5 mm. As seen in the rainfall correlations, the resolution limit has an effect in the smallest detectible rainfall limits. While this was a problem within the project installed VWPs, it was even more noticeable in the sensors that were loaned to the project from the SCL geotechnical monitoring program. This was especially seen in the VP-09-32-03 data where the data was quite a large "banding" effect which is assumed to reflect the sensor resolution.

Averaging is another consideration. Data can be averaged during collection (i.e. averaging a large number of readings as one monitoring point) or post collection. In this study, only post collection data averaging was possible; however, this was not used because an averaging window long enough to smooth out the dry periods would also severely affect the precipitation events from being clear and distinct. The goal of this project was to determine how best to set up the site sensors. For ET monitoring, and other events that occur over a longer time frame, averaging can be assist in showing long term data trends; however, for the monitoring of rainfall data and other short-term mass changes the averaging may miss the peaks and lead to underestimation of the size of the rainfall.

In general, it is not expected that averaging post data collection (effectively downscaling the results) would have "helped" the data enough to make it to the quality of some high-end research papers in this field. Some dataloggers that are used for very fine pore pressure readings have been set to collect data at an appropriate interval (10-60 min); however, average the data within the data logger at a much higher frequency (e.g. 1 Hz) (Correspondence with Garth van der Kamp). This form of averaging might have helped with data clarity. This method was considered for the project midway through but could not be implemented due to the programming restrictions of the RST dataloggers.

Site selection is also important. The comparison between BHLB08 and BHLB02 is an example of site selection effects. BHLB08 shows a good agreement with the local moisture loading while BHLB02 has a distinct rise for the summer months, and then little change during the summer, with a sharp drop off in the fall. The piezometers at VP-09-32-03 show some gentle variations, but no clear rainfall events. While it is difficult to predict the hydrogeological conditions of installation, locations that are hydrogeologically stable (or those that will become stable) should be preferred. BHLB07 is a particularly important example, with a very strange pore pressure fluctuation in 2015 that could not be related to hydrological events.

Calibration is the next factor for discussion. A large portion of effort in this project was spent investigating calibration routines in the hope that some calibration method might remove barometric effects completely leaving a smooth and ideal pore pressure. As such it was determined that for each sensor an investigation into both the linear coefficient and time domain regression is important for each variable to choose the most appropriate γ/LE and time lag. While this relationship should not change over time, it should be rechecked at several time periods to ensure that a proper loading value is chosen. The selection of a BRF calibration method requires that some data is lost at the beginning of each continuous portion of the datasets. If a time lag of 12 hours was found, then each break in the data, even of 1 data point, would require either filling by some method, or the loss of the next 12 hours of data for the BRF method to have enough history of barometric fluctuation to be able to calibrate then following points. All sensors were also investigated using Fourier techniques to see if any of the noise was removable by filtering or attributable to earth tide effects. Any tidal effects observed were minimal, and most of the residual noise was high frequency noise that was not attributable to any frequency dependent phenomena.

Geotechnical sensors that were later used as GLs in all cases for this project did not work well enough to be used. One thing that may be contributing is the “stacked” nature of all these sensors which may be causing interference within the pore signals in the stack. Additionally, the geotechnical VWPs in general had much larger resolutions than the project specific VWPs. In the inverse, all the sensors that were installed to be used as GLs could be used as geotechnical VWPs due to the much lower precision generally required for that role (0.1 kPa vs. 0.005 kPa).

Finally, the installation nature of some sensors being attached to the outside of slope indicator casings and grouted into place may have caused issues.

The characteristics of the datalogger should be considered as part of equipment selection. Some notes from the sensors used in this project are that the Geokon loggers generally performed well; however, required manual downloads several times a year. Additionally, there was no way to tell if the logger had failed at some point during the year until the next field visit. The timing of all the Geokon sensors was performed in each individual unit and could only be checked by verifying it against the timing of the logging computer when downloads were happing. It was found to occasionally drift, presumably due to ambient temperature variation and voltage differences in the batteries within the logger. Cases of the Geokon logger not recognizing the sensor due to shielding errors, grounding errors or other problems also occurred. Finally, the Geokon loggers were stand-alone which required nearby barologgers to be used, which had the same difficulties in timing as the geokon sensors.

The RST loggers performed better with respect to timing and shielding errors. They also gave the ability to be checked from an office every day. This potentially mitigates the error induced by the sensors failing in between field visits. These sensors performed well in general. Some drawbacks that they had was no ability to make readings at a higher frequency than the recording rate and logging the average value as discussed above; instead each sensor is “plucked” once at the reading interval and the result is the recorded value. Another problem encountered is that if the downloads do not happen as scheduled, the “base” stations may overwrite their memory. Additionally, to recover any data from the remote loggers in this case a site visit is required for the download.

All of the dataloggers had some difficulties assumed to be due to ambient temperature changes. In the case of BHLB03 and BHLB08, some data from the very beginning of the RST data had to be excised for this reason.

6.3 Recommendations

Many errors occurred during this project, hopefully informing future projects. In general, the most mitigation of errors can be achieved through more careful planning and site assessment. The following recommendations should be considered when planning and setting up a GL program.

1. Site Selection: Sites should be selected with an eye towards hydrogeological stability. This means that ideal sites should be away from bodies of water with fluctuating head levels, areas with fluctuating water tables, and also places with significant loading which has yet to dissipate. These phenomena will mask hydrologic loadings. Alternatively, such loadings should be monitored to be able to remove from the GL trends, or the GL trends should be treated as only able to be accurate over very short time periods (i.e. good for precipitation estimation but not ET estimation).
2. Sensor selection: Sensors to be selected should have the lowest resolution limit possible for the siting. This is usually a function of the full scale of the sensor, and as such, the sensor with the lowest pressure rating that can manage site conditions should be selected.
3. Installation: Sensors should be installed in aquitards or confined aquifers that have a response to pore pressures induced by surface loading. Aquitards should generally have a lower rate of dissipation of loadings which may be preferable. All sensors in this project were installed using a "fully grouted" methodology to which no failures were attributed. As with all VWP installations, care should be taken to ensure no damage to the sensor or wire during installation.
4. Surface equipment: The datalogger should be able to take readings at a higher frequency than the recording interval. The recording intervals can be set on the order of 10-60 minutes. As the transition from the Geokon intervals of 30 minutes to the RST intervals of 10 minutes shows, once the readings are faster than the hydraulic dissipation and, in the case of BRF calibration, fast enough to appropriate the BRF curve, little is gained in the output. That said, averaging within the instrumentation to determine the recorded point may serve to filter out noise below the resolution limit. Additionally, the surface equipment should be thermally buffered. The datalogger may be placed in a shady spot

in an insulated box, or a small cavity may be dug for it, which is covered by an insulated lid (provided no water will collect in the cavity).

5. Supporting equipment: Barologgers do not need to be on the same site as the VWPs, although best practice would be to have them directly over top of the VWP installation. Care should be taken in setting up the timing to ensure that the readings are at the same time and interval as the VWP readings. They should also be thermally buffered, a suggested implementation of which is installing in a vented standpipe, just below ground level. It may be advantageous to have 2 barologgers at the same position in case one fails, as opposed to 2 at different locations, due to orographic pressure differences. Additionally, it will be useful to have water table records nearby to each GL, which may be collected through standard methods.
6. Data Collection: Care should be taken to ensure the smallest number of data gaps in the sensor data. This can be achieved through automatic collection or scheduled regular downloads.
7. Calibration: The VWP should be calibrated using both linear and BRF techniques. The resultant ML trends can be examined visually to see if there's any difference between the two. Additionally, they should be subjected to a Fourier analysis to see if any tidal effects exist that might be removable. This calibration should be rechecked periodically, and especially after any equipment changes to ensure that the ML readings remain accurate.
8. Verification of the GLs hydrological readings: During the first part of the program the ML readings should be checked against local instrumentation such as a rain gauge and ET data from PM estimates or EC data. This will help to determine the fidelity of the GL's reading to other instrumentation and also help to show if any other effects are observable in the residual pore pressure after rain and ET removal.

BIBLIOGRAPHY

Alam, M.S., Barbour, S.L., Elshorbagy, A., and Huang, M. 2017. The Impact of Climate Change on the Performance of Oil Sands Reclamation Covers: A Comparison of Multiple General Circulation Models and Representative Concentration Pathways. *Proceedings of 70th Canadian Geotechnical Society Conference, GeoOttawa 2017, Ottawa, Ontario, October 2-4*.

Allen, R.G., Pereira, L., Raes, D., and Smith, M. 1998. Crop evapotranspiration - Guidelines for computing crop water requirements - FAO Irrigation and drainage paper 56. *In* FAO - Food and Agriculture Organization of the United Nations. Rome. pp. 1–15.

Anochikwa, C.I., van der Kamp, G., and Barbour, S.L. 2012. Interpreting pore-water pressure changes induced by water table fluctuations and mechanical loading due to soil moisture changes. *Canadian Geotechnical Journal*, 49(3): 357–366.

Bardsley, W., and Campbell, D. 2000. Natural geological weighing lysimeters: calibration tools for satellite and ground surface gravity monitoring of subsurface water-mass change. *Natural Resources Research*, 9(2): 147–156. Available from http://www.springerlink.com/index/v8180201172412u8.pdf.

Bardsley, W.E., and Campbell, D.I. 1994. A new method for measuring near-surface moisture budgets in hydrological systems. *Journal of Hydrology*, 154(1–4): 245–254.

Bardsley, W.E.E., and Campbell, D.I.I. 2007. An expression for land surface water storage monitoring using a two-formation geological weighing lysimeter. *Journal of Hydrology*, 335(3–4): 240–246.

Barr, A.G., Kamp, G. Van Der, Schmidt, R., Black, T.A.A., van der Kamp, G., Schmidt, R., and Black, T.A.A. 2000. Monitoring the moisture balance of a boreal aspen forest using a deep groundwater piezometer. *Agricultural and Forest Meteorology*, 102(1): 13–24.

Biot, M.A. 1941. General Theory of Three-Dimensional Consolidation. *Journal of Applied Physics*, 12(2): 155–164.

Bishop, A.W. 1954. The Use of Pore-Pressure Coefficients in Practice. *Géotechnique*, 4(1953): 148–152.

Box, G.E.P., and Jenkins, G.M. 1976. Time Series Analysis: Forecasting and Control. *In* Revised. Holden-Day, University of Michigan.

Chapman, D., Barbour, S.L., and O'Kane, M. a. 2006. Hydrogeology of South Bison Hill. 7th International Conference on Acid Rock Drainage 2006, ICARD - Also Serves as the 23rd Annual Meetings of the American Society of Mining and Reclamation, 1: 336–343.

Ferris, J.G., Knowles, D.B., Brown, R.H., and Stallman, R.W. 1962. Theory of aquifer tests. *Geological Survey Water-Supply Paper 1536-E*, (WSP 1536-E): 69–174. Available from http://www.usgs.gov/default.asp.

Granger, R.J., and Gray, D.M. 1989. Evaporation from natural nonsaturated surfaces. *Journal of Hydrology*, 111(1–4): 21–29.

Huang, M., Barbour, S.L., and Carey, S.K. 2015. The impact of reclamation cover depth on the performance of reclaimed shale overburden at an oil sands mine in Northern Alberta, Canada. *Hydrological Processes*, 29(12): 2840–2854.

Hvorslev, M.J. 1951. Time Lag and Soil Permeability in Ground-Water Observations. *Bulletin n. 36*, (36): 53.

Jacob, C. 1940. On the flow of water in an elastic artesian aquifer. *Transactions - American Geophysical Union*, 21(2): 574–586.

van der Kamp, G. 2001. Methods for determining the in situ hydraulic conductivity of shallow aquitards - an overview. *Hydrogeology Journal*, 9(1): 5–16.

van der Kamp, G., and Gale, J.E. 1983. Theory of earth tide and barometric effects in porous formations with compressible grains. *Water Resources Research*, 19(2): 538–544.

van der Kamp, G., and Maathuis, H. 1991. Annual fluctuations of groundwater levels as a result of loading by surface moisture. *Journal of Hydrology*, 127(1–4): 137–152.

van der Kamp, G. and R. Schmidt, 2017. Review: moisture loading – the hidden information in groundwater observation well records. *Hydrogeology Journal, 25, 2225-2233, DOI 10.1007/s10040-017-1631-z.*

van der Kamp, G., and Schmidt, R. 1997. Monitoring of total soil moisture on a scale of hectares using groundwater piezometers. *Geophysical Research Letters*, 24(6): 719.

Kashyap, P.S., and Panda, R.K. 2001. Evaluation of evapotranspiration estimation methods and development of crop-coefficients for potato crop in a sub-humid region. *Agricultural Water Management*, 50(2001): 9–25.

Lambert, A., Huang, J., van der Kamp, G., Henton, J., Mazzotti, S., James, T.S., Courtier, N., and Barr, A.G. 2013. Measuring water accumulation rates using GRACE data in areas experiencing glacial isostatic adjustment: The Nelson River basin. *Geophysical Research Letters*, 40(23): 6118–6122.

Marefat, V., Duhaime, F., and Chapuis, R.P. 2015. Pore pressure response to barometric pressure change in Champlain clay: Prediction of the clay elastic properties. *Engineering Geology*, 198: 16–29. Elsevier B.V.

MATLAB and Statistics Toolbox Release 2013b, The MathWorks, Inc., Natick, Massachusetts, United States.

Melchior, P. 1978. The Tides of the Planet Earth, Pergamon, New York. Pergamon Press, New York.

Merritt, M.L. 2004. Estimating Hydraulic Properties of the Floridan Aquifer System by Analysis of Effects , Collier and Hendry Counties , Florida. *Secretary*,: 70.

Microsoft Excel, 2010. Microsoft Corporation

Morgenstern, N.R. 2012. Oil sands mine closure - the end game: An update. *Proceedings of the Third International Oil Sands Tailings Conference*, (December).

Nur, A., and Byerlee, J.D. 1971. An exact effective stress law for elastic deformation of rock with fluids. *Journal of Geophysical Research*, 76(26): 6414–6419.

Province of Alberta. 1993. Conservation and Reclamation Regulation. *In* Environmental Protection and Enhancement Act: Conservation and Reclamation Regulation. Available from http://www.qp.alberta.ca/documents/Regs/1993_115.pdf.

Province of Alberta. 2017. ENVIRONMENTAL PROTECTION AND ENHANCEMENTS ACT.

Rasmussen, T.C., and Crawford, L.A. 1997. Identifying and Removing Barometric Pressure Effects in Confined and Unconfined Aquifers. *Ground Water*, 35(3): 502–511.

Rice, J.R., and Cleary, M.P. 1976. Some basic stress diffusion solutions for fluid-saturated elastic porous media with compressible constituents. *Reviews of Geophysics*, 14(2): 227.

Rojstaczer, S., and Agnew, D.C. 1989. The influence of formation material properties on the response of water levels in wells to Earth tides and atmospheric loading. *Journal of Geophysical Research*, 94(B9): 12403.

Smith, C., van der Kamp, G., L. Arnold, R. Schmidt 2017. Measuring precipitation with a geolysimeter. *Hydrology and Earth system Science Special Issue: The World Meteorological Organization Solid Precipitation InterComparison Experiment (WMO-SPICE) and its applications (AMT/ESSD/HESS/TC inter-journal SI); Hydrol. Earth Syst. Sci.*21,5263-5272, doi:10.5194/hess-21-5263-2017.

Skempton, A.W. 1954. The Pore-Pressure Coefficients A and B. *Géotechnique*, 4(4): 143–147.
Smith, L. a., van der Kamp, G., and Jim Hendry, M. 2013. A new technique for obtaining high-resolution pore pressure records in thick claystone aquitards and its use to determine in situ compressibility. *Water Resources Research*, 49(2): 732–743.

Sophocleous, M., Bardsley, E., and Healey, J. 2006. A rainfall loading response recorded at 300 meters depth: Implications for geological weighing lysimeters. *Journal of Hydrology*, 319(1–4): 237–244.

Terzaghi, K. 1943. Theoretical Soil Mechanics. John Wiley & Sons, New York.

Tipman, J., Barbour, L., and van der Kamp, G. 2017. An Evaluation of Methods to Remove Barometric Effects from Pore Pressure Data. *In* GeoOttawa. Canadian Geotechnical Society, Ottawa, Canada. p. 8.

Toll, N.J., and Rasmussen, T.C. 2007. Removal of barometric pressure effects and earth tides from observed water levels. *Ground Water*, 45(1): 101–105.

TSoft, version 2.2.0, 2013. Van Kamp, Michael. Royal Observatory of Belgium, Belgium

APPENDIX A - BOREHOLE LOGS AND SUMMARY

Name	Landform	Type of Installation	Depth	North	East	Elevation	Make	Model	S/N	Resolution	Resolution	Accuracy	Maximum Pressure
BHLB03	Natural	VWP	23.0 m	46619.992/ 456548	44480.884/ 6316520	348.252	Geokon	4500S	1237492	.025% FS	0.0875 kPa/ 8.9 mm	.1% F.S.	350 kPa
BHLB07	SWSS	VWP	45.0 m	6316967	455489	389.11	Geokon	4500S	1237493	.025% FS	0.0875 kPa/ 8.9 mm	.1% F.S.	350 kPa
BHLB08	SWSS	VWP	29.5 m	6316964	455488	369.393	Geokon	4500S	1237495	.025% FS	0.0875 kPa/ 8.9 mm	.1% F.S.	350 kPa
VP-09-32-03	SWSS	3 x VWP	16	6316675	455758		Slope Indicater	52611030	09-1880	.025% FS	0.17 kPa/17.5 mm	.1% F.S.	100 Psi (690 kPa)
			22	6316675	455758		Slope Indicater	52611030	09-1885	.025% FS	0.17 kPa/17.5 mm	.1% F.S.	100 Psi (690 kPa)
			30	6316675	455758		Slope Indicater	52611030	09-1887	.025% FS	0.17 kPa/17.5 mm	.1% F.S.	100 Psi (690 kPa)
VP-12-32-02	SWSS	2 x VWP	32	6316211	455308		Slope Indicater	52611030	12-5987	.025% FS	0.17 kPa/17.5 mm	.1% F.S.	100 Psi (690 kPa)
			61	6316211	455308		Slope Indicater	52611030	11-3686	.025% FS	0.17 kPa/17.5 mm	.1% F.S.	100 Psi (690 kPa)

LOGGED BY: B. Kafle/A. Park
LEAD SAMPLER: D. Pratt

STARTED: August 3, 2013
COMPLETED: August 8, 2013

RIG TYPE: Sonic
RIG No.: 89

INSTER INSTALL: VWP
INSTER DEPTH (ft): 82

GW ELEV. (ft): No GW
HOLE DIA. (in): 6

BACKFILLED (Y/N): Y

BOREHOLE: BHLB-01 LOCATION: W2 DUMP

HOLE COORDINATES
LAT: 57.009004 LONG: -111.701403

SURFACE ELEV. (ft): 1154
HOLE DEPTH (ft): 92

ISOTOPE COMPOSITION
- δO^{18} (slope adjusted)
- δ^2H

ATTERBERG LIMITS
- Liquid Limit (%)
- Plastic Limit (%)
- Plasticity Index (%)
- Non-plastic soil

CATIONS
- % Na (mEq/L)
- % Mg (mEq/L)
- % Ca (mEq/L)
- % K (mEq/L)

ANIONS
- % Cl (mEq/L)
- % SO_4 (mEq/L)

GRAIN SIZE
- % Gravel
- % Sand
- % Silt
- % Clay

LOGGED BY: B. Kafle/A. Park
LEAD SAMPLER: D. Pratt

STARTED: August 2, 2013
COMPLETED: August 2, 2013

RIG TYPE: Sonic
RIG No.: 89

INSTER INSTALL: VWP
INSTER DEPTH (ft): 57.1

GW ELEV. (ft): No GW
HOLE DIA. (in): 6

BACKFILLED (Y/N): Y

BOREHOLE: BHLB-02 LOCATION: W2 DUMP

HOLE COORDINATES
LAT: 57.00829 LONG: -111.700566

SURFACE ELEV. (ft): 1136
HOLE DEPTH (ft): 65

ISOTOPE COMPOSITION
- δO^{18} (slope adjusted)
- $\delta^2 H$

ATTERBERG LIMITS
- Liquid Limit (%)
- Plastic Limit (%)
- Plasticity Index (%)
- Non-plastic soil

CATIONS
- % Na (meEq/L)
- % Mg (meEq/L)
- % Ca (meEq/L)
- % K (meEq/L)

ANIONS
- % Cl (meEq/L)
- % SO_4 (meEq/L)

GRAIN SIZE
- % Gravel
- % Sand
- % Silt
- % Clay

LOGGED BY: B. Kafle/A. Park | STARTED: June 29, 2013 | RIG TYPE: Sonic | INSTER INSTALL.: VWP | GW ELEV. (ft): No GW | BACKFILLED (Y/N): Y

LEAD SAMPLER: D. Pratt | COMPLETED: July 5, 2013 | RIG No.: 78 | INSTER DEPTH (ft): 75.4 | HOLE DIA. (in): 6

BOREHOLE: BHLB-03 LOCATION: Magazine storage

HOLE COORDINATES: LAT: 56.990133 LONG: -111.716568 | SURFACE ELEV. (ft): 1143 | HOLE DEPTH (ft): 85

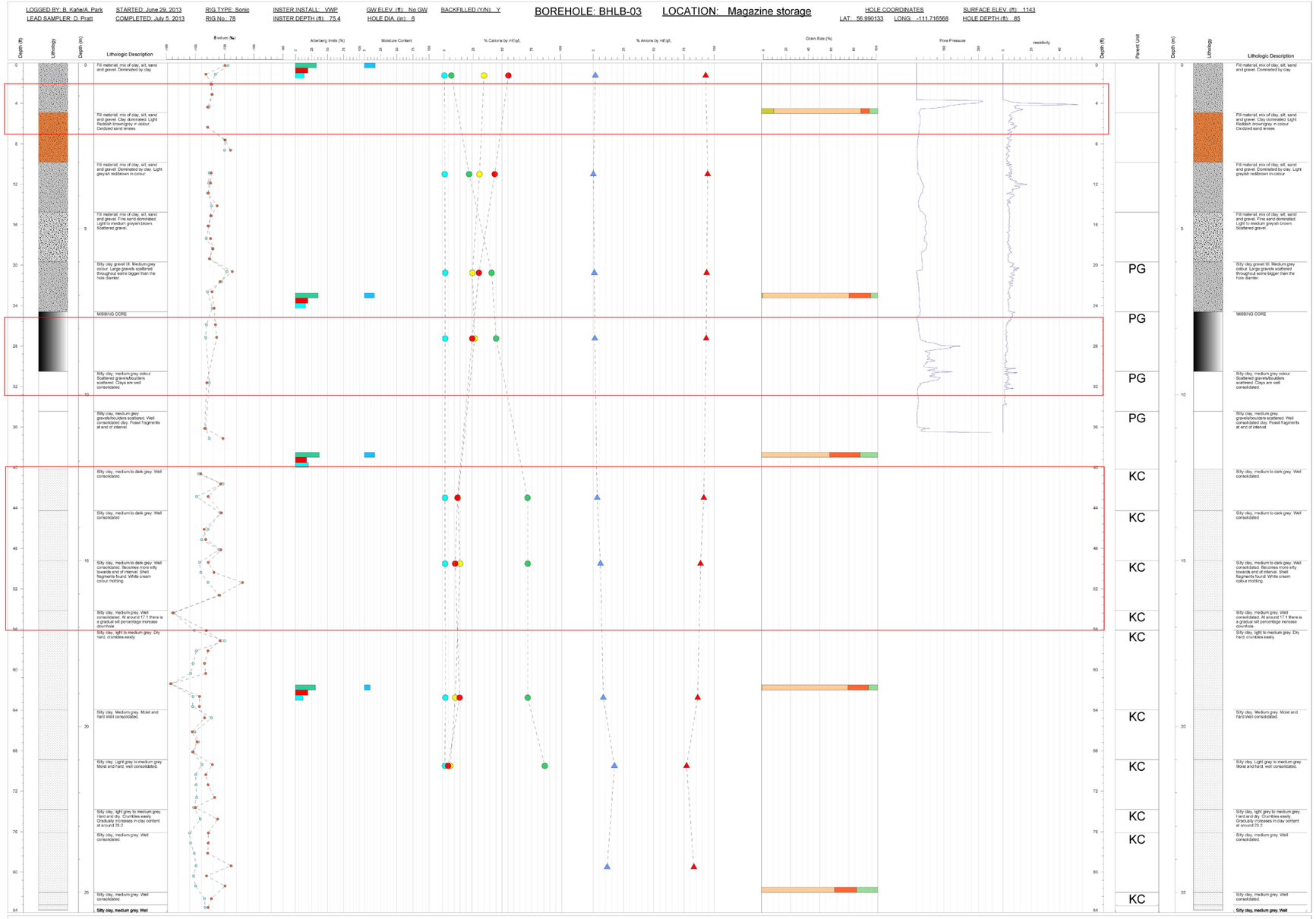

ISOTOPE COMPOSITION
- δO^{18} (slope adjusted)
- $\delta^2 H$

ATTERBERG LIMITS
- Liquid Limit (%)
- Plastic Limit (%)
- Plasticity Index (%)
- Non-plastic soil

CATIONS
- % Na (mEq/L)
- % Mg (mEq/L)
- % Ca (mEq/L)
- % K (mEq/L)

ANIONS
- % Cl (mEq/L)
- % SO_4 (mEq/L)

GRAIN SIZE
- % Gravel
- % Sand
- % Silt
- % Clay

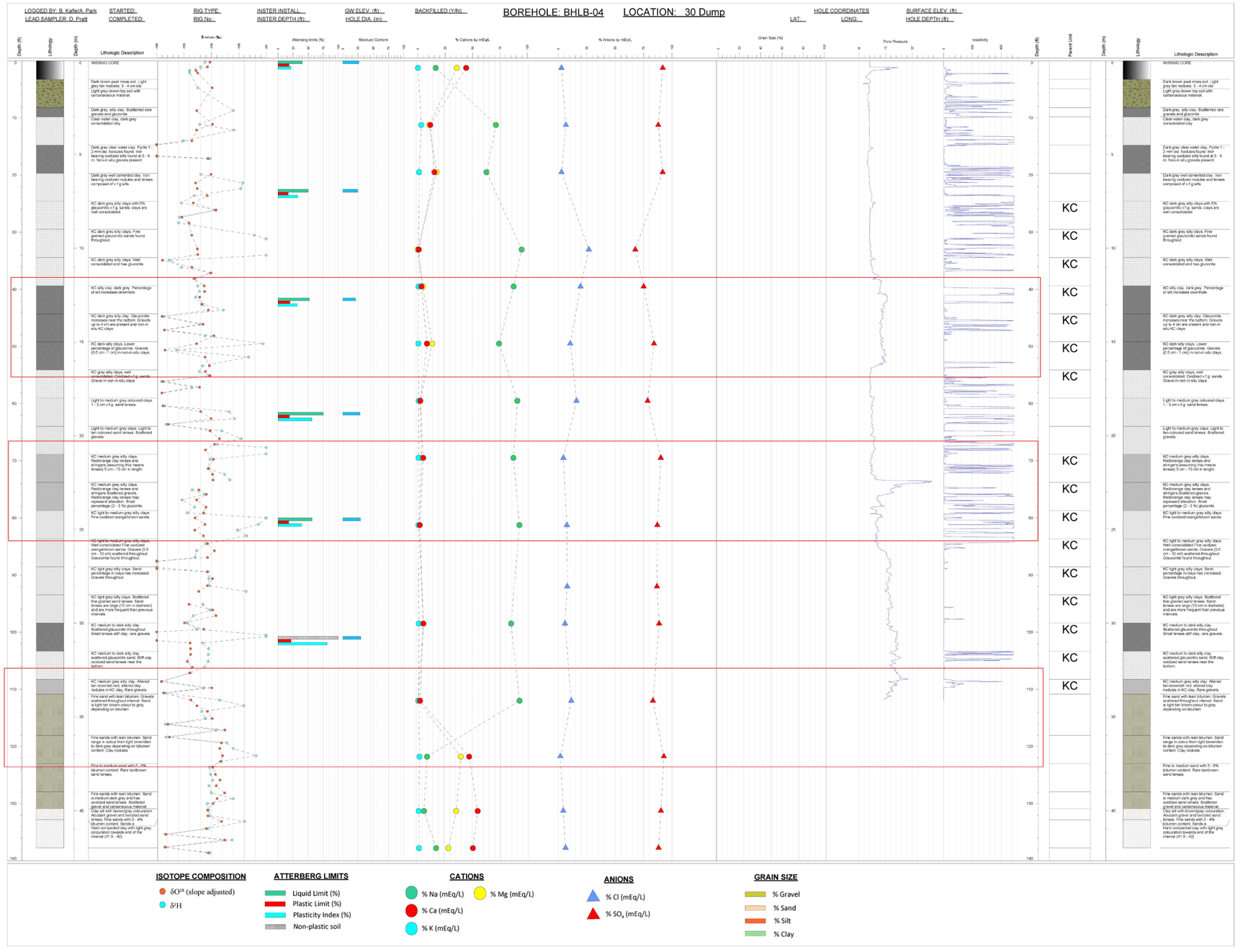
LOGGED BY: B. Kafle/A. Park
LEAD SAMPLER: D. Pratt
STARTED:
COMPLETED:
RIG TYPE:
RIG No.:
INSTER INSTALL.:
INSTER DEPTH (ft):
GW ELEV. (ft):
HOLE DIA. (in):
BACKFILLED (Y/N):
BOREHOLE: BHLB-04
LOCATION: 30 Dump
HOLE COORDINATES
LAT:
LONG:
SURFACE ELEV. (ft):
HOLE DEPTH (ft):
Depth (ft)
Lithology
Depth (m)
Lithologic Description
δ values (‰)
Atterberg limits (%)
Moisture Content
% Cations by mEq/L
% Anions by mEq/L
Grain Size (%)
Pore Pressure
resistivity
Depth (ft)
Parent Unit
Depth (m)
Lithology
Lithologic Description
MISSING CORE
Dark brown peat moss soil. Light grey tan nodules. 3 - 4 cm dia.
Light grey-brown top soil with carbonaceous material.
Dark grey, silty clay. Scattered rare gravels and gluconite.
Clear water clay, dark grey consolidated clay.
Dark grey clear water clay. Pyrite 1 - 2 mm dia. Nodules found. Iron bearing oxidized silts found at 5 - 6 m. Non-in situ gravels present.
Dark grey well cemented clay. Iron bearing oxidized nodules and lenses composed of v f g silts.
KC dark grey silty clays with 5% glauconitic v f g. sands. clays are well consolidated.
KC dark grey silty clays. Fine grained glauconitic sands found throughout.
KC dark grey silty clays. Well consolidated and has gluconite.
KC silty clay, dark grey. Percentage of silt increases downhole.
KC dark grey silty clay. Glauconite increases near the bottom. Gravels up to 4 cm are present and non-in situ KC clays.
KC dark silty clays. Lower percentage of glauconite. Gravels (0.5 cm - 1 cm) in non-in situ clays.
KC grey silty clays, well consolidated. Oxidized v f g. sands. Gravel in non in situ clays.
Light to medium grey coloured clays 1 - 3 cm v f g. sand lenses.
Light to medium grey clays. Light to tan coloured sand lenses. Scattered gravels.
KC medium grey silty clays. Red/orange clay lenses and stringers (assuming this means lenses) 5 cm - 10 cm in length.
KC medium grey silty clays. Red/orange clay lenses and stringers Scattered gravels. Red/orange clay lenses may represent alteration. Small percentage (2 - 3 %) gluconite.
KC light to medium grey silty clays. Fine oxidized orange/brown sands.
KC light to medium grey silty clays. Well consolidated Fine oxidized orange/brown sands. Gravels (0.5 cm - 10 cm) scattered throughout. Glauconite found throughout.
KC light grey silty clays. Sand percentage in clays has increased. Gravels throughout.
KC light grey silty clays. Scattered fine grained sand lenses. Sand lenses are large (10 cm in diameter) and are more frequent than previous intervals.
KC medium to dark silty clay. Scattered glauconite throughout. Small lenses stiff clay, rare gravels.
KC medium to dark silty clay scattered glauconitic sand. Stiff clay oxidized sand lenses near the bottom.
KC medium grey silty clay. Altered tan brownish red, altered clay nodules in KC clay, Rare gravels.
Fine sand with lean bitumen. Gravels scattered throughout interval. Sand is light tan brown colour to grey depending on bitumen
Fine sands with lean bitumen. Sand range in colour from light brown/tan to dark grey depending on bitumen content. Clay nodules
Fine to medium sand with 5 - 6% bitumen content. Rare tan/brown sand lenses.
Fine sands with lean bitumen. Sand is medium dark grey and has oxidized sand lenses. Scattered gravel and carbonaceous material.
Clay silt with brown/grey colouration. Clay silt with brown/grey colouration. Sand lenses. Fine sands with 3 - 4% bitumen content. Sands a Hard compacted clay with light grey colouration towards end of the interval (41.9 - 42).
Parent Unit
KC
ISOTOPE COMPOSITION
δO18 (slope adjusted)
δ2H
ATTERBERG LIMITS
Liquid Limit (%)
Plastic Limit (%)
Plasticity Index (%)
Non-plastic soil
CATIONS
% Na (mEq/L)
% Mg (mEq/L)
% Ca (mEq/L)
% K (mEq/L)
ANIONS
% Cl (mEq/L)
% SO4 (mEq/L)
GRAIN SIZE
% Gravel
% Sand
% Silt
% Clay

LOGGED BY: B. Kafle/A. Park
LEAD SAMPLER: D. Pratt

STARTED: July 30, 2013
COMPLETED: August 1, 2013

RIG TYPE: Sonic
RIG No.: 89

INSTER INSTALL.: VWP
INSTER DEPTH (ft): 59.93

GW ELEV. (ft): No GW
HOLE DIA. (in): 6

BACKFILLED (Y/N): Y

BOREHOLE: BHLB-05

LOCATION: 30 Dump

HOLE COORDINATES
LAT: 56.993365 LONG: -111.617678

SURFACE ELEV. (ft): 1049
HOLE DEPTH (ft): 70

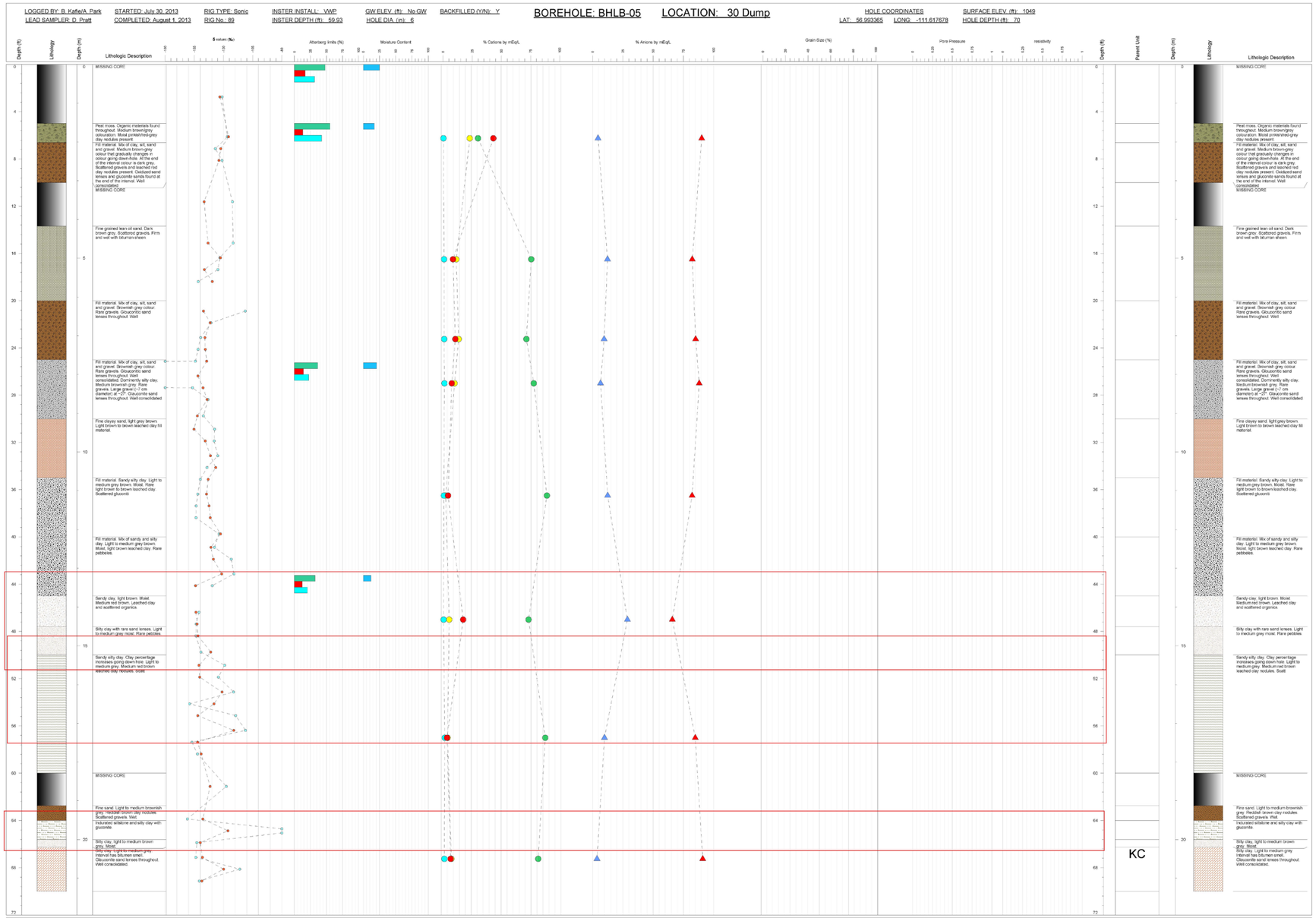

ISOTOPE COMPOSITION
- δO^{18} (slope adjusted)
- δ^2H

ATTERBERG LIMITS
- Liquid Limit (%)
- Plastic Limit (%)
- Plasticity Index (%)
- Non-plastic soil

CATIONS
- % Na (mEq/L)
- % Mg (mEq/L)
- % Ca (mEq/L)
- % K (mEq/L)

ANIONS
- % Cl (mEq/L)
- % SO_4 (mEq/L)

GRAIN SIZE
- % Gravel
- % Sand
- % Silt
- % Clay

LOGGED BY: B. Kafle/A. Park
LEAD SAMPLER: D. Pratt

STARTED: June 25, 2013
COMPLETED: June 26, 2013

RIG TYPE: Sonic
RIG No.: 89

INSTER INSTALL.: N/A
INSTER DEPTH (ft): N/A

GW ELEV. (ft): No GW
HOLE DIA. (in): 4

BACKFILLED (Y/N): N

BOREHOLE: BHLB-06 LOCATION: 30 Dump

HOLE COORDINATES
LAT: 56.996649 LONG: -111.620201

SURFACE ELEV. (ft): 1075
HOLE DEPTH (ft): 100

ISOTOPE COMPOSITION
- δO^{18} (slope adjusted)
- δ^2H

ATTERBERG LIMITS
- Liquid Limit (%)
- Plastic Limit (%)
- Plasticity Index (%)
- Non-plastic soil

CATIONS
- % Na (meEq/L)
- % Mg (meEq/L)
- % Ca (meEq/L)
- % K (meEq/L)

ANIONS
- % Cl (meEq/L)
- % SO_4 (meEq/L)

GRAIN SIZE
- % Gravel
- % Sand
- % Silt
- % Clay

LOGGED BY: B. Kafle/A. Park
LEAD SAMPLER: D. Pratt

STARTED: July 1, 2013
COMPLETED: July 3, 2013

RIG TYPE: Sonic
RIG No.: 89

INSTER INSTALL.: VWP
INSTER DEPTH (ft): 149

GW ELEV. (ft): No GW
HOLE DIA. (in): 6

BACKFILLED (Y/N): Y

BOREHOLE: BHLB-07 LOCATION: SWSS - Nest 15

HOLE COORDINATES
LAT: 56.992896 LONG: -111.738956

SURFACE ELEV. (ft): 1277
HOLE DEPTH (ft): 150

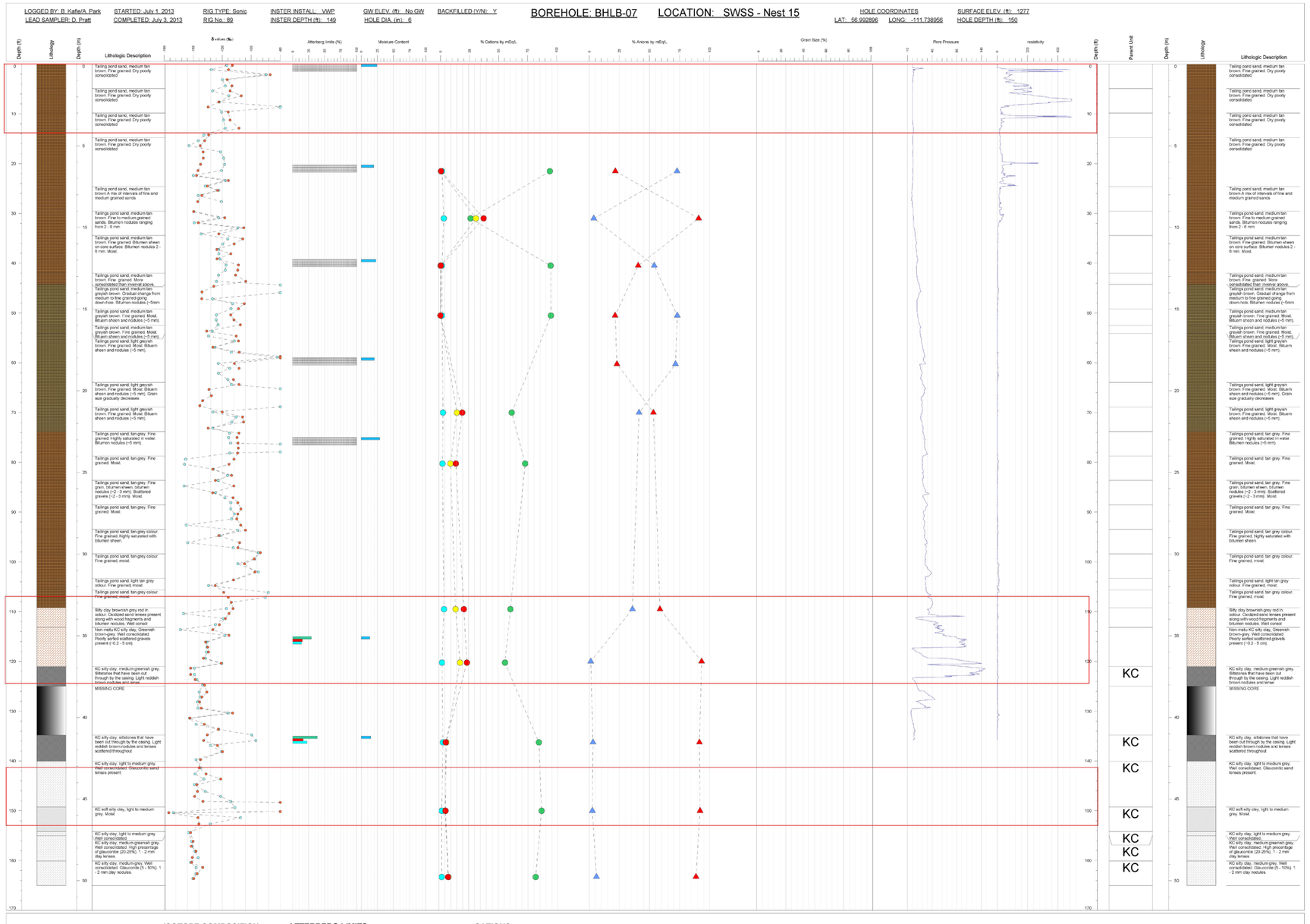

ISOTOPE COMPOSITION
- δO^{18} (slope adjusted)
- δ^2H

ATTERBERG LIMITS
- Liquid Limit (%)
- Plastic Limit (%)
- Plasticity Index (%)
- Non-plastic soil

CATIONS
- % Na (meQ/L)
- % Mg (meQ/L)
- % Ca (meQ/L)
- % K (meQ/L)

ANIONS
- % Cl (meQ/L)
- % SO_4 (meQ/L)

GRAIN SIZE
- % Gravel
- % Sand
- % Silt
- % Clay

LOGGED BY:
LEAD SAMPLER:

STARTED:
COMPLETED:

RIG TYPE:
RIG No.:

INSTER INSTALL.:
INSTER DEPTH (ft):

GW ELEV. (ft):
HOLE DIA. (in):

BACKFILLED (Y/N):

BOREHOLE:

LOCATION:

HOLE COORDINATES
LAT:
LONG:

SURFACE ELEV. (ft):
HOLE DEPTH (ft):

Depth (ft) | Lithology | Depth (m) | Lithologic Description | $ values (‰) | Atterberg limits (%) | Moisture Content | % Cations by mEq/L | % Anions by mEq/L | Grain Size (%) | Pore Pressure | resistivity | Depth (ft) | Parent Unit | Depth (m) | Lithology | Lithologic Description

Tailing pond sand, medium tan brown. Fine grained. Dry poorly consolidated

Tailing pond sand, medium tan brown. Fine grained. Dry poorly consolidated

Tailing pond sand, medium tan brown. Fine grained. Dry poorly consolidated

Tailing pond sand, medium tan brown. Fine grained. Dry poorly consolidated

Tailing pond sand, medium tan brown. A mix of intervals of fine and medium grained sands

Tailings pond sand, medium tan brown. Fine to medium grained sands. Bitumen nodules ranging from 2 - 6 mm

Tailings pond sand, medium tan brown. Fine grained. Bitumen sheen on core surface. Bitumen nodules 2 - 6 mm. Moist.

Tailings pond sand, medium tan brown. Fine grained. More consolidated than inverval above.

Tailings pond sand, medium tan brown. Fine grained. Change from medium to fine grained going down-hole. Bitumen nodules (~5mm

Tailings pond sand, medium tan greyish brown. Fine grained. Moist. Bitumen sheen and nodules (~5 mm).

Tailings pond sand, medium tan greyish brown. Fine grained. Moist. Bitumen sheen and nodules (~5 mm).

Tailings pond sand, light greyish brown. Fine grained. Moist. Bitumen sheen and nodules (~5 mm). Grain size gradually decreases

Tailings pond sand, light greyish brown. Fine grained. Moist. Bitumen sheen and nodules (~5 mm).

MISSING CORE

Tailing sand, light tan grey. Fine grained. Highly saturated. Bitumen sheen present.

Tailing sand, light tan grey. Fine grained. Moist.

Tailings sand, light tan grey. Fine grained, highly saturated. Bitumen sheen.

Tailings sand, light tan grey. Fine grained, highly saturated. Bitumen sheen. Bitumen nodules (~2 - 5 mm).

Tailings sand, light tan grey. Fine grained. Moist. Bitumen nodules (~2 - 4 mm).

Tailings sand, light tan grey. Fine grained, highly saturated. Bitumen sheen. Bitumen nodules (~2 - 3 mm). Fine grained. Moist. Bitumen nodules (~2 - 10 mm).

Tailings sand, light tan grey colour. Fine grained. Moist bitumen nodules (~2 - 3 mm).

Tailings sand, light tan grey colour. Fine grained. Highly saturated. Bitumen nodules (~2 - 3 mm).

Non-insitu KC silty clay. Brownish greyhed. Well consolidated. light grey to tan yellow. Fine grained oxidized sand lenses. Fe

Non-insitu KC silty clay. Reddish brown/grey. Well consolidated. Light red clay nodules. Oxidized sand lenses. Scattered gravel

Non-insitu KC silty clay. Light brownish grey. Well consolidated Oxidized sand lenses. Scattered gravels.

Non-insitu KC silty clay. Light to medium grey. Well consolidated. Scattered gravels (~5 - 20 mm dia.)

KC silty clay. Light to medium grey. Well consolidated. Glauconitic sands towards end of interval.

Indurated siltstone.

KC silty clay, medium greenish grey. Well consolidated. Glauconitic sands throughout interval.

Siltstone
KC silty clay, medium greenish grey. Well consolidated. Glauconitic sands.

KC
KC
KC
KC
KC
KC
KC

Tailing pond sand, medium tan brown. Fine grained. Dry poorly consolidated

Tailing pond sand, medium tan brown. Fine grained. Dry poorly consolidated

Tailing pond sand, medium tan brown. Fine grained. Dry poorly consolidated

Tailing pond sand, medium tan brown. Fine grained. Dry poorly consolidated

Tailing pond sand, medium tan brown. A mix of intervals of fine and medium grained sands

Tailings pond sand, medium tan brown. Fine to medium grained sands. Bitumen nodules ranging from 2 - 6 mm

Tailings pond sand, medium tan brown. Fine grained. Bitumen sheen on core surface. Bitumen nodules 2 - 6 mm. Moist.

Tailings pond sand, medium tan brown. Fine grained. More consolidated than inverval above.

Tailings pond sand, medium tan brown. Fine grained. Change from medium to fine grained going down-hole. Bitumen nodules (~5mm

Tailings pond sand, medium tan greyish brown. Fine grained. Moist. Bitumen sheen and nodules (~5 mm).

Tailings pond sand, medium tan greyish brown. Fine grained. Moist. Bitumen sheen and nodules (~5 mm).

Tailings pond sand, light greyish brown. Fine grained. Moist. Bitumen sheen and nodules (~5 mm). Grain size gradually decreases

Tailings pond sand, light greyish brown. Fine grained. Moist. Bitumen sheen and nodules (~5 mm).

MISSING CORE

Tailing sand, light tan grey. Fine grained. Highly saturated. Bitumen sheen present.

Tailing sand, light tan grey. Fine grained. Moist.

Tailings sand, light tan grey. Fine grained, highly saturated. Bitumen sheen.

Tailings sand, light tan grey. Fine grained. Moist. Bitumen nodules (~2 - 5 mm).

Tailings sand, light tan grey. Fine grained. Moist. Bitumen nodules (~2 - 4 mm).

Tailings sand, light tan grey. Fine grained, highly saturated. Bitumen sheen. Bitumen nodules (~2 - 3 mm). Fine grained. Moist. Bitumen nodules (~2 - 10 mm).

Tailings sand, light tan grey colour. Fine grained. Moist bitumen nodules (~2 - 3 mm).

Tailings sand, light tan grey colour. Fine grained. Highly saturated. Bitumen nodules (~2 - 3 mm).

Non-insitu KC silty clay. Brownish greyhed. Well consolidated. light grey to tan yellow. Fine grained oxidized sand lenses. Fe

Non-insitu KC silty clay. Reddish brown/grey. Well consolidated. Light red clay nodules. Oxidized sand lenses. Scattered gravel

Non-insitu KC silty clay. Light brownish grey. Well consolidated Oxidized sand lenses. Scattered gravels.

Non-insitu KC silty clay. Light to medium grey. Well consolidated. Scattered gravels (~5 - 20 mm dia.)

KC silty clay. Light to medium grey. Well consolidated. Glauconitic sands towards end of interval.

Indurated siltstone.

KC silty clay, medium greenish grey. Well consolidated. Glauconitic sands throughout interval.

Siltstone
KC silty clay, medium greenish grey. Well consolidated. Glauconitic sands.

ISOTOPE COMPOSITION
- δO^{18} (slope adjusted)
- δ^2H

ATTERBERG LIMITS
- Liquid Limit (%)
- Plastic Limit (%)
- Plasticity Index (%)
- Non-plastic soil

CATIONS
- % Na (mEq/L)
- % Mg (mEq/L)
- % Ca (mEq/L)
- % K (mEq/L)

ANIONS
- % Cl (mEq/L)
- % SO_4 (mEq/L)

GRAIN SIZE
- % Gravel
- % Sand
- % Silt
- % Clay

LOGGED BY: B. Kafle/A. Park
LEAD SAMPLER: D. Pratt

STARTED: July 9, 2013
COMPLETED: July 12, 2013

RIG TYPE: Sonic
RIG No.: 89

INSTER INSTALL: VWP
INSTER DEPTH (ft): 96.8

GW ELEV. (ft): No GW
HOLE DIA (in): 6

BACKFILLED (Y/N): Y

BOREHOLE: BHLB-08 LOCATION: SWSS - Nest 7

HOLE COORDINATES
LAT: 56.994184 LONG: -111.732216

SURFACE ELEV. (ft): 1211
HOLE DEPTH (ft): 98

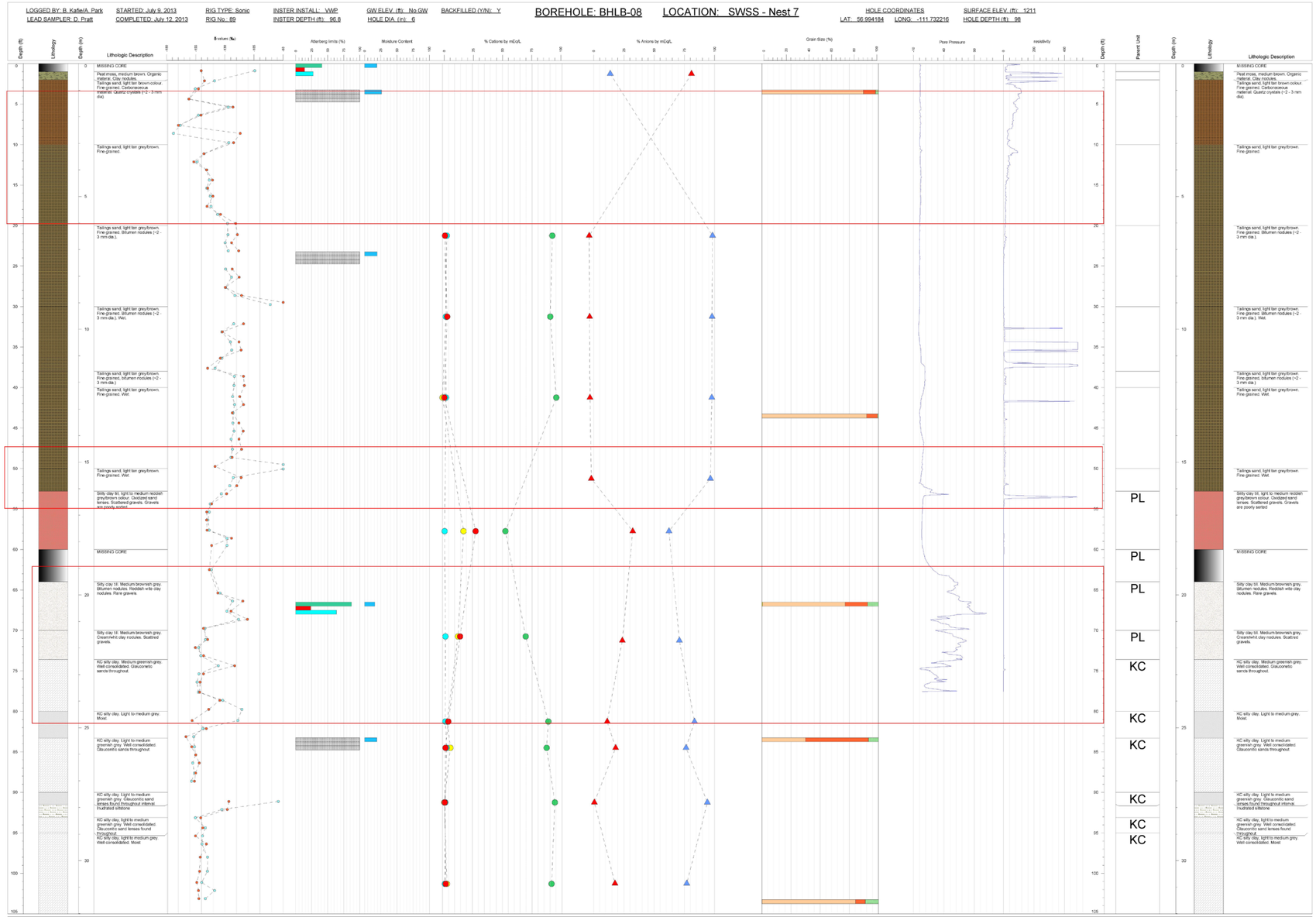

ISOTOPE COMPOSITION
- δO^{18} (slope adjusted)
- δ^2H

ATTERBERG LIMITS
- Liquid Limit (%)
- Plastic Limit (%)
- Plasticity Index (%)
- Non-plastic soil

CATIONS
- % Na (meEq/L)
- % Mg (meEq/L)
- % Ca (meEq/L)
- % K (meEq/L)

ANIONS
- % Cl (meEq/L)
- % SO_4 (meEq/L)

GRAIN SIZE
- % Gravel
- % Sand
- % Silt
- % Clay

LOGGED BY: B. Kafle/A. Park
LEAD SAMPLER: D. Pratt

STARTED: July 7, 2013
COMPLETED: July 10, 2013

RIG TYPE: Sonic
RIG No.: 89

INSTER INSTALL: N/A
INSTER DEPTH (ft): N/A

GW ELEV. (ft): No GW
HOLE DIA. (in): 6

BACKFILLED (Y/N): N

BOREHOLE: BHLB-09 LOCATION: SWSS - Nest 4

HOLE COORDINATES
LAT: 56.994502 LONG: -111.730115

SURFACE ELEV. (ft): 1183
HOLE DEPTH (ft): 80

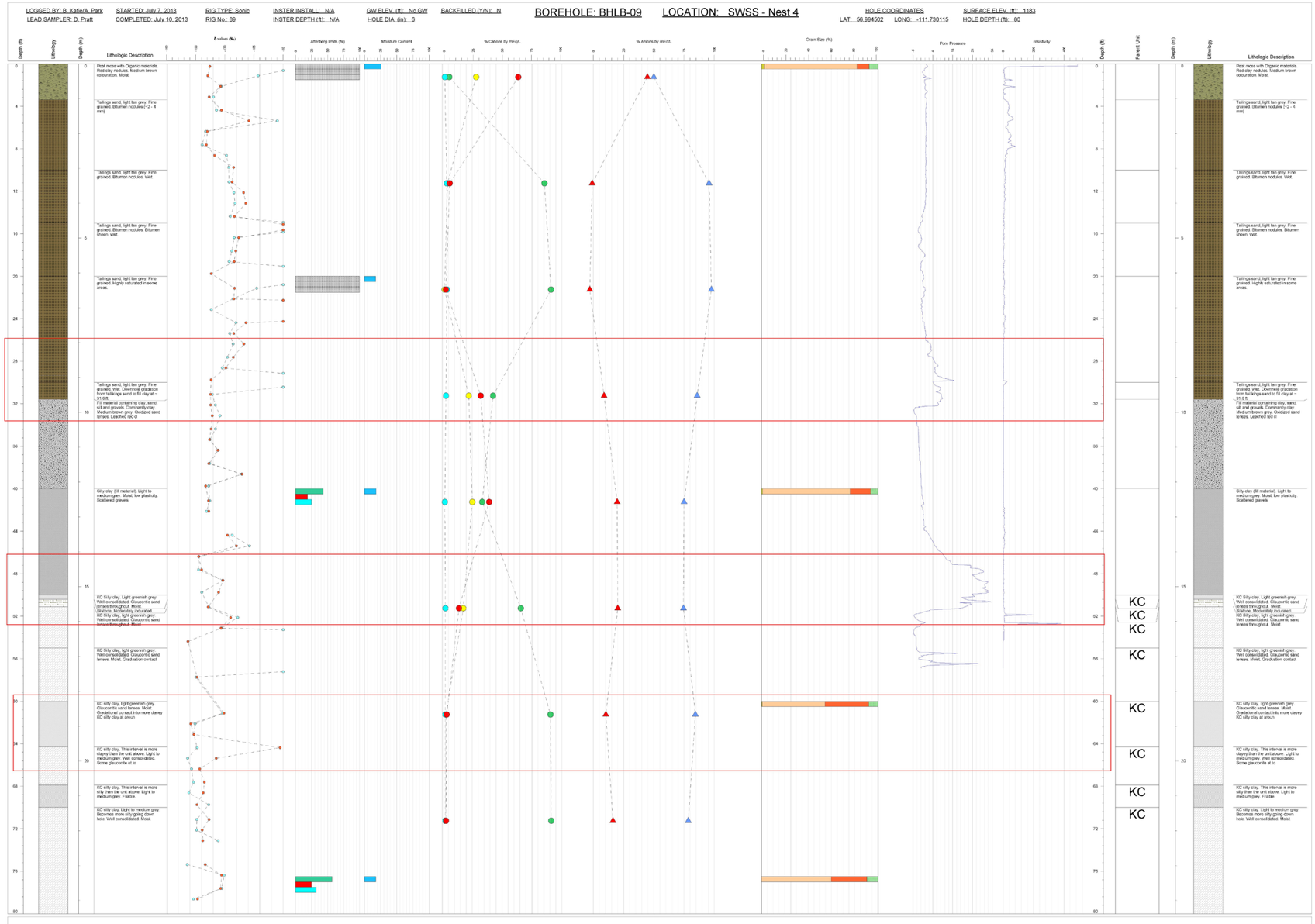

ISOTOPE COMPOSITION
- δO^{18} (slope adjusted)
- $\delta^2 H$

ATTERBERG LIMITS
- Liquid Limit (%)
- Plastic Limit (%)
- Plasticity Index (%)
- Non-plastic soil

CATIONS
- % Na (mEq/L)
- % Mg (mEq/L)
- % Ca (mEq/L)
- % K (mEq/L)

ANIONS
- % Cl (mEq/L)
- % SO_4 (mEq/L)

GRAIN SIZE
- % Gravel
- % Sand
- % Silt
- % Clay

Syncrude
Securing Canada's Energy Future
Geotechnical Division

Instrumentation Central File
Check List

Instrument no. SI/VP080069R

		Initials
	Office Documentation	
☐	Request sheet and installation schematic	
☐	All email correspondence related to instrumented hole	
	Field Documentation	
☐	Borehole construction report sheet	
☑	Installation sheet including as-built information	SK
☐	Borehole sampling and test sheets	
	☐ SPT sheet SS	
	☐ Core log sheet CS	
	☐ Grab sample log sheet GS	
	☐ Auger sample sheet AS	
	☐ Other i.e. shelby TO/TP	
	☐ Gamma ray log report sheet	
	☐ Other log type	
☐	Field commissioning sheet	
	☐ SI intialization print out sets 1&2	
	☐ Field book readings	
☐	Photo copy of all calibration sheets **including tip check sheet**	
☐	Instrument extension sheet **(vertical / horizontal)**	
	☐ 1st extension	
	☐ 2nd extension	
	☐ 3rd extension	
	Lab Documentation	
☐	Copy of lab request sheet	
☐	Copy of lab test results	
☐	**Instrument abandonment sheet or decommissioning sheet**	

Geotechnical Instrumentation

Slope Inclinometer & Vibrating Wire Piezometer

Commissioning Sheet

Instrument Location (Structure): W1 Dump

Instrument Number (SI) 080069R

Installation Date: _____

Monitor _____

Proposed Coordinates:

Northing _____

Easting _____

Elevation _____

Azimuth _____

Re- Commissioning Date: 2009 MAY 03

Monitor: RCD / NA

As-Built Coordinates:

Northing 49069.56

Easting 45595.92

Elevation 355.443m

Azimuth 170°

Survey As-built (Top Of Pipe)

Survey Request No. 90667

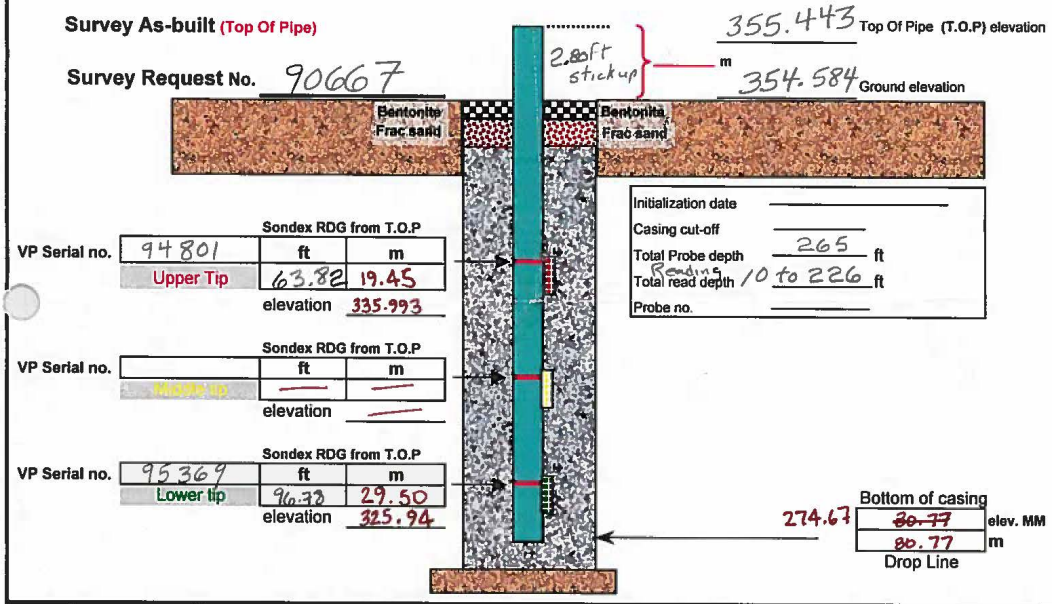

Final Check List:

Grout Settlement	☐ Yes ☐ No	**Quadro-pod Labeled**	☑ Yes ☐ No
Depth of Settlement	_____ m	**End Cap on Casing**	☑ Yes ☐ No
Hole Topped up	☐ Yes ☐ No	**Does Area require remedial work**	☐ Yes ☐ No

Date	Rdg Hz²/Therm.	Date	Rdg Hz²/Therm.	Date	Rdg Hz²/Therm.	Date	Rdg Hz²/Therm.	Date	Rdg Hz²/Therm.
	u		u		u		u		u
	m		m		m		m		m
	L		L		L		L		L
Date	Rdg Hz²/Therm.	Date	Rdg Hz²/Therm.	Date	Rdg Hz²/Therm.	Date	Rdg Hz²/Therm.	Date	Rdg Hz²/Therm.
	u		u		u		u		u
	m		m		m		m		m
	L		L		L		L		L

Comments:

Slope Inclinometer
Commissioning Sheet

Instrument Location (Structure): W1 DUMP

Instrument Number (SI) 080069R

Installation Date: _____

Monitor _____

Proposed Coordinates:
Northing _____
Easting _____
Elevation _____
Azimuth _____

Commissioning Date: OCT.21/08

Monitor: D.WHEELER

As-Built Coordinates:
Northing 49069.95
Easting 45595.95
Elevation 352.956
Azimuth 170°

Survey As-built (Top Of Pipe)

Survey Request No. 90149

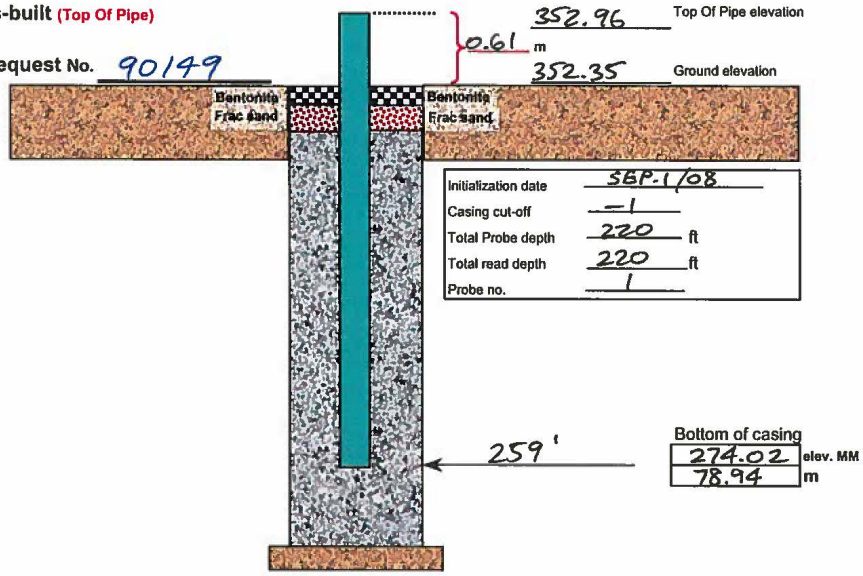

Final Check List:

Grout Settlement	☐ Yes	☑ No	Quadro-pod Labeled	☑ Yes	☐ No
Depth of Settlement	_____ m		End Cap on Casing	☑ Yes	☐ No
Hole Topped up	☐ Yes	☐ No			
Grout	_____ Volume		Does Area require		
Frac Sand	_____ No. Bags		remedial work	☐ Yes	☑ No
Bentonite	_____ No. Bags				

Comments:

Vibrating Wire Piezometer

Commissioning Sheet

Instrument Location (Structure): W1 DUMP

Instrument Number (VP) 080069R

Installation Date: _____

Requestor: _____

Proposed Coordinates:
Northing _____
Easting _____
Elevation _____

Commissioning date OCT.21/08

Monitor: DW / AS

As-Built Coordinates:
Northing 49069.82
Easting 45596.24
Elevation 352.348

As- Built

Survey Request no. 90149

Note: Survey will always pick Top of Pipe or conduit. Measure stick-up of conduit to calculate ground elevation

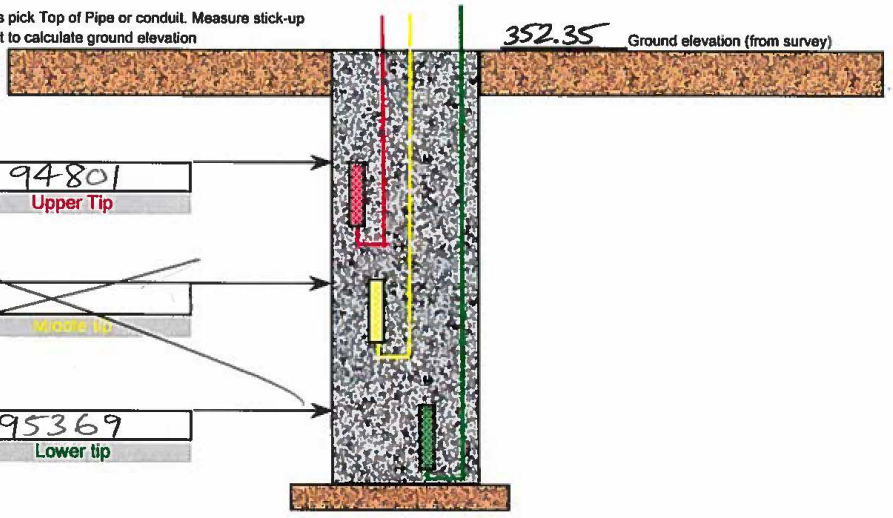

Daily Instrument Readings until Stabilized

Date	Rdg Hz²/Therm.	Date	Rdg Hz²/Therm.	Date	Rdg Hz²/Therm.	Date	Rdg Hz²/Therm.	Date	Rdg Hz²/Therm.
	u		u		u		u		u
	m		m		m		m		m
	L		L		L		L		L
Date	Rdg Hz²/Therm.	Date	Rdg Hz²/Therm.	Date	Rdg Hz²/Therm.	Date	Rdg Hz²/Therm.	Date	Rdg Hz²/Therm.
	u		u		u		u		u
	m		m		m		m		m
	L		L		L		L		L

Check List

☑	**Hole Topped up** (bentonite chips)	Does area require additional remedial work	☐ Yes	☑ No
☐	**Protective Conduit** around leads	Is instrument in an active construction zone	☐ Yes	☑ No
☑	Quadro-pod labeled	Access	☑ good	☐ poor

Comments: BUGGY WHIP INSTALLED

Slope Inclinometer
Extension Sheet

Instrument Location (Structure): W1 Dump

Instrument Number (SI) OB0069R

Installation Date: _____

Monitor _____

Extension Date: Between MAY 8/09 and JUNE 26/09

Monitor: R. DECOURVILLE

Proposed Coordinates:
Northing 49069
Easting 45596
Elevation 355.4
Azimuth 170°

As-Built Coordinates:
Northing 49069.82
Easting 45596.19
Elevation 354.04
Azimuth ~~170~~ 170°

Cut Down

Survey As-built (Top Of Pipe)
Request No. 110596

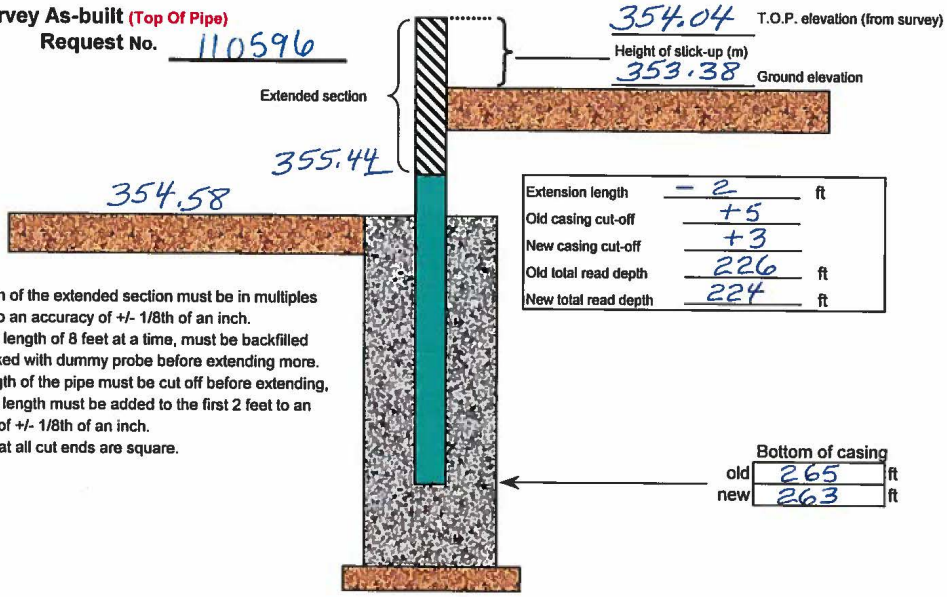

Extension length	-2	ft
Old casing cut-off	+5	
New casing cut-off	+3	
Old total read depth	226	ft
New total read depth	224	ft

1. The length of the extended section must be in multiples of 2 feet to an accuracy of +/- 1/8th of an inch.
2. Maximum length of 8 feet at a time, must be backfilled and checked with dummy probe before extending more.
3. If any length of the pipe must be cut off before extending, that exact length must be added to the first 2 feet to an accuracy of +/- 1/8th of an inch.
4. Ensure that all cut ends are square.

Bottom of casing
old 265 ft
new 263 ft

Summary Check List:

Length of extended section	☑ Yes	☐ No	Quadro-pod Labeled	☑ Yes	☐ No
Height of stick-up	☑ Yes	☐ No	End Cap on Casing	☑ Yes	☐ No
Cutoff labels updated	☑ Yes	☐ No	Remedial work required	☐ Yes	☑ No
DMM database updated	☑ Yes	☐ No	As-built survey request	☑ Yes	☐ No
Original copy in central files	☑ Yes	☐ No			

Comments:

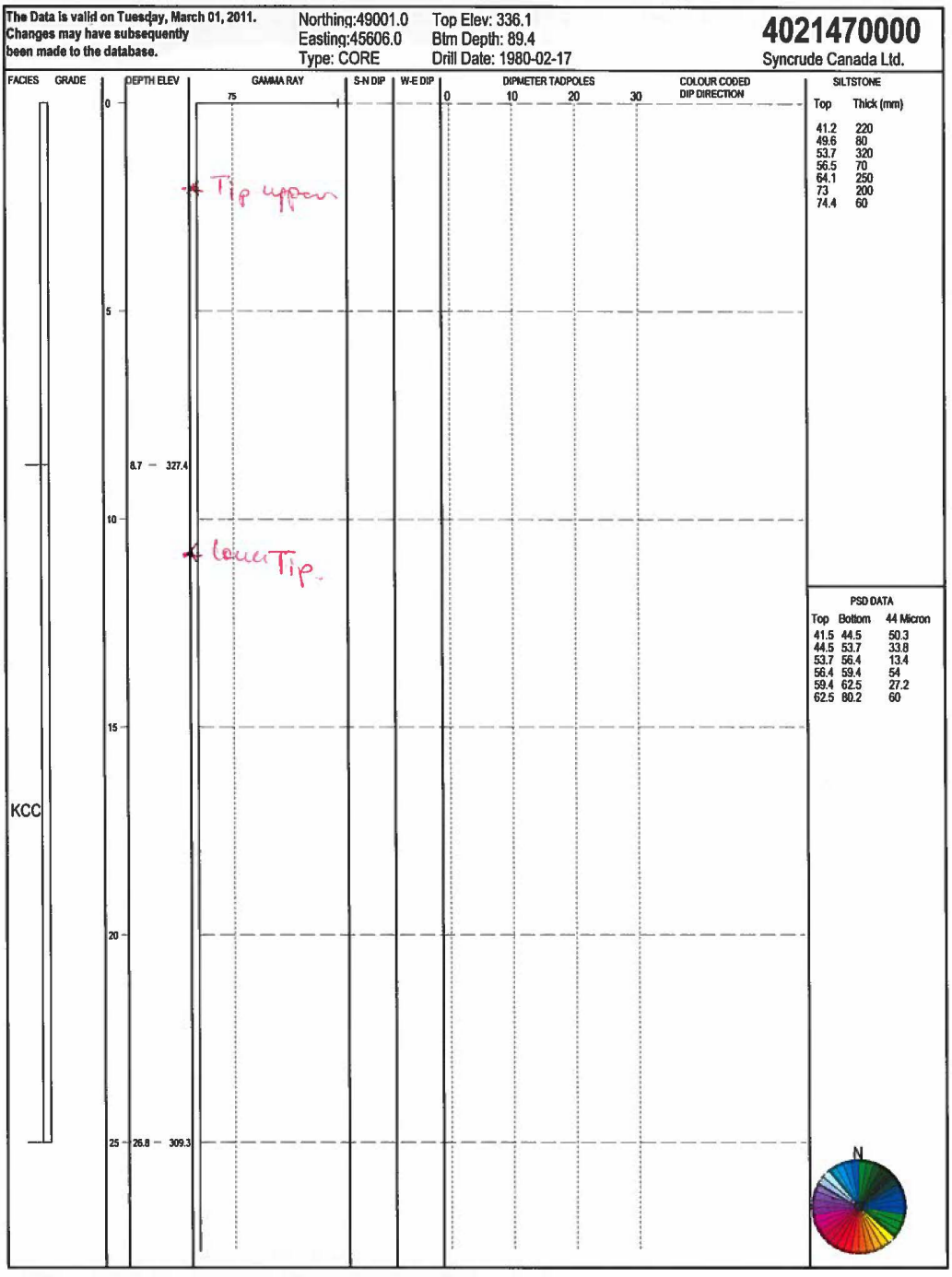
The Data is valid on Tuesday, March 01, 2011.
Changes may have subsequently been made to the database.
Northing:49001.0
Easting:45606.0
Type: CORE
Top Elev: 336.1
Btm Depth: 89.4
Drill Date: 1980-02-17
4021470000
Syncrude Canada Ltd.
FACIES
GRADE
DEPTH ELEV
GAMMA RAY
75
S-N DIP
W-E DIP
DIPMETER TADPOLES
0
10
20
30
COLOUR CODED DIP DIRECTION
SILTSTONE
Top Thick (mm)
41.2 220
49.6 80
53.7 320
56.5 70
64.1 250
73 200
74.4 60
Tip upper
Lower Tip.
0
5
8.7 — 327.4
10
15
20
25
26.8 — 309.3
KCC
PSD DATA
Top Bottom 44 Micron
41.5 44.5 50.3
44.5 53.7 33.8
53.7 56.4 13.4
56.4 59.4 54
59.4 62.5 27.2
62.5 80.2 60
N

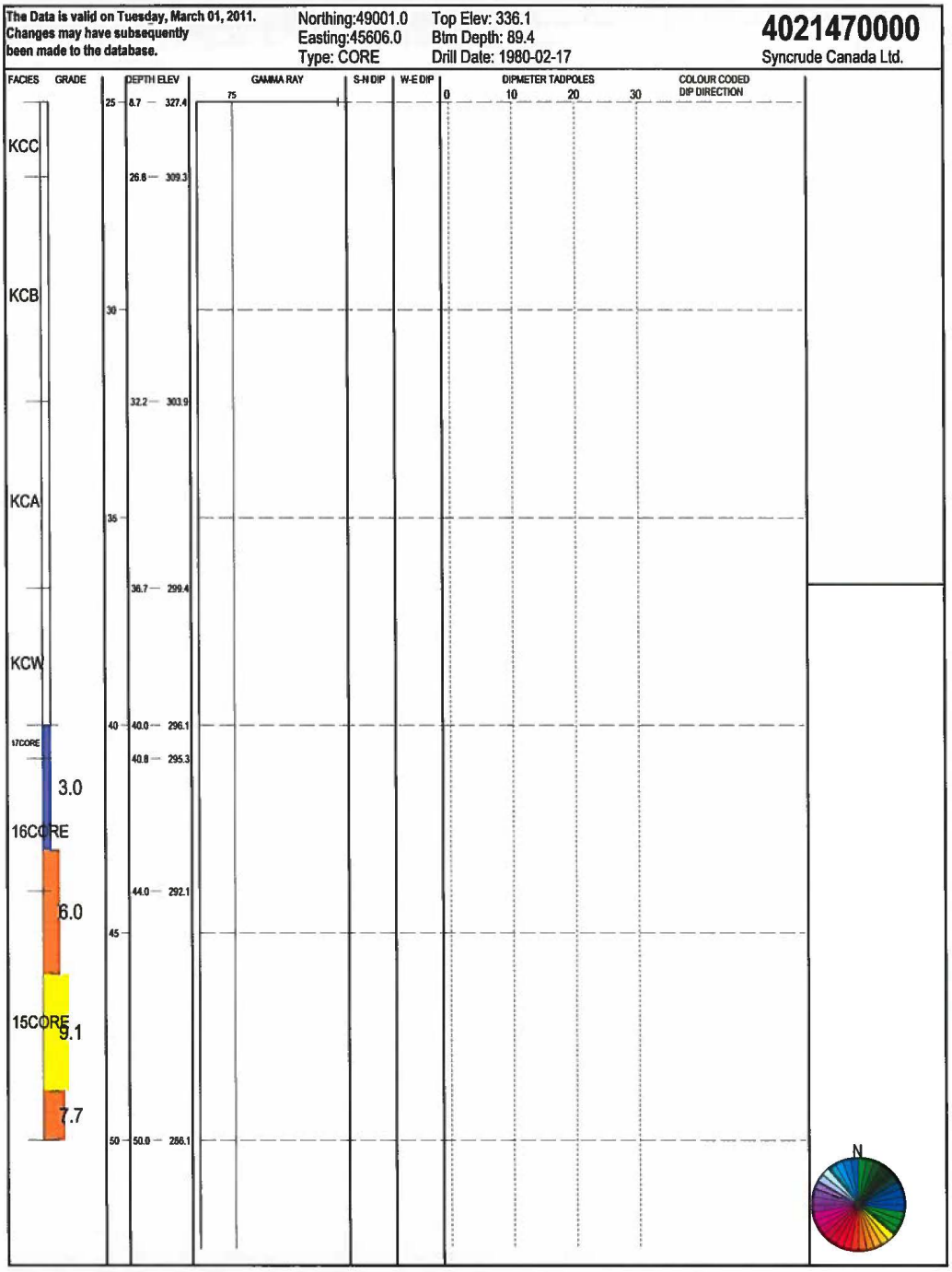
The Data is valid on Tuesday, March 01, 2011.
Changes may have subsequently been made to the database.
Northing:49001.0
Easting:45606.0
Type: CORE
Top Elev: 336.1
Btm Depth: 89.4
Drill Date: 1980-02-17
4021470000
Syncrude Canada Ltd.
FACIES
GRADE
DEPTH ELEV
GAMMA RAY
S-N DIP
W-E DIP
DIPMETER TADPOLES
COLOUR CODED DIP DIRECTION
KCC
KCB
KCA
KCW
17CORE
3.0
16CORE
6.0
15CORE
9.1
7.7
25
30
35
40
45
50
8.7 327.4
26.8 309.3
32.2 303.9
36.7 299.4
40.0 296.1
40.8 295.3
44.0 292.1
50.0 286.1
75
0
10
20
30
N

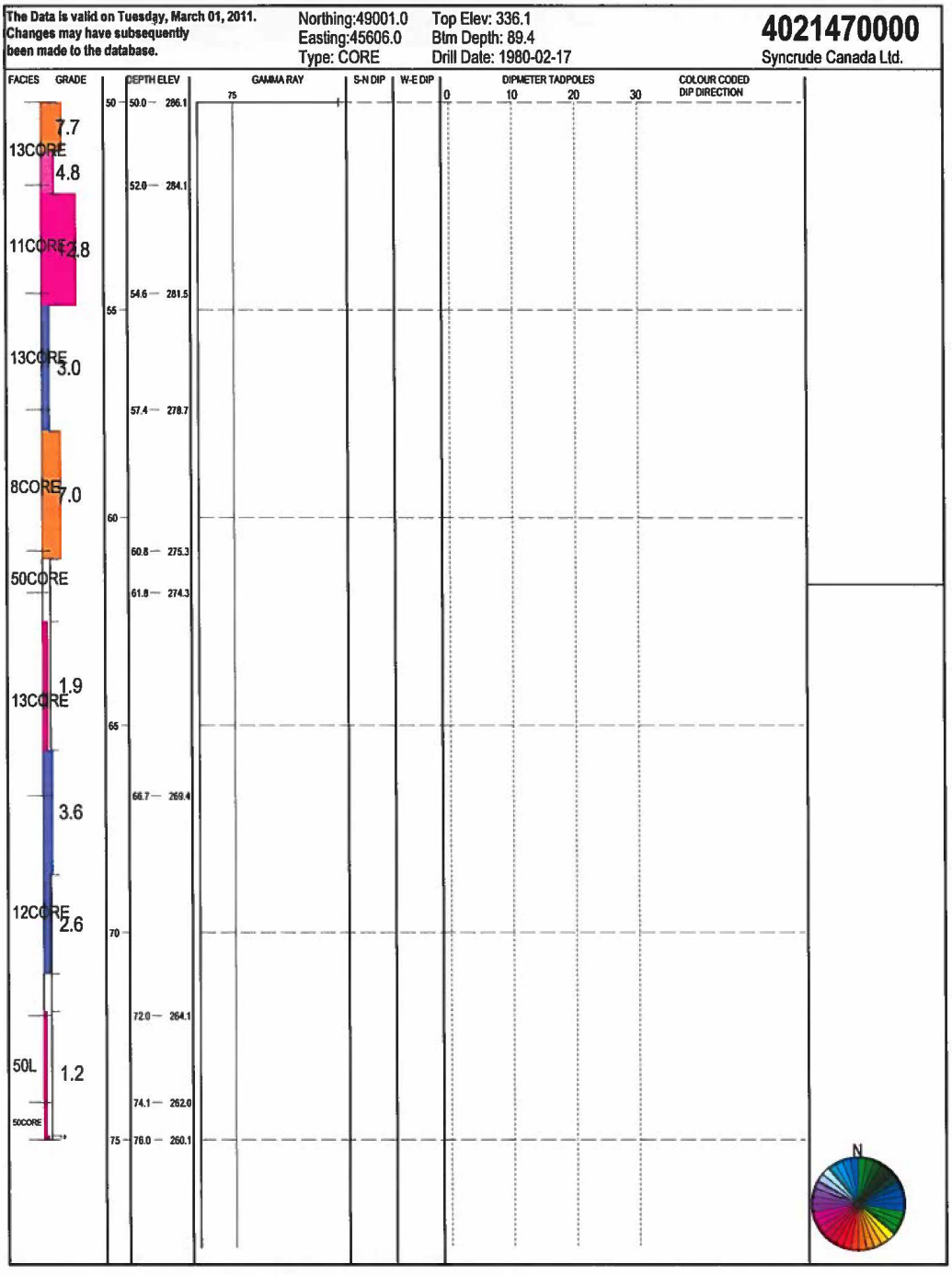
The Data is valid on Tuesday, March 01, 2011.
Changes may have subsequently been made to the database.
Northing:49001.0
Easting:45606.0
Type: CORE
Top Elev: 336.1
Btm Depth: 89.4
Drill Date: 1980-02-17
4021470000
Syncrude Canada Ltd.
FACIES
GRADE
DEPTH ELEV
GAMMA RAY
S-N DIP
W-E DIP
DIPMETER TADPOLES
COLOUR CODED DIP DIRECTION
7.7
13CORE
4.8
11CORE
12.8
13CORE
3.0
8CORE
7.0
50CORE
1.9
13CORE
3.6
12CORE
2.6
50L
1.2
50CORE
50.0 286.1
52.0 284.1
54.6 281.5
57.4 278.7
60.8 275.3
61.8 274.3
66.7 269.4
72.0 264.1
74.1 262.0
76.0 260.1
N

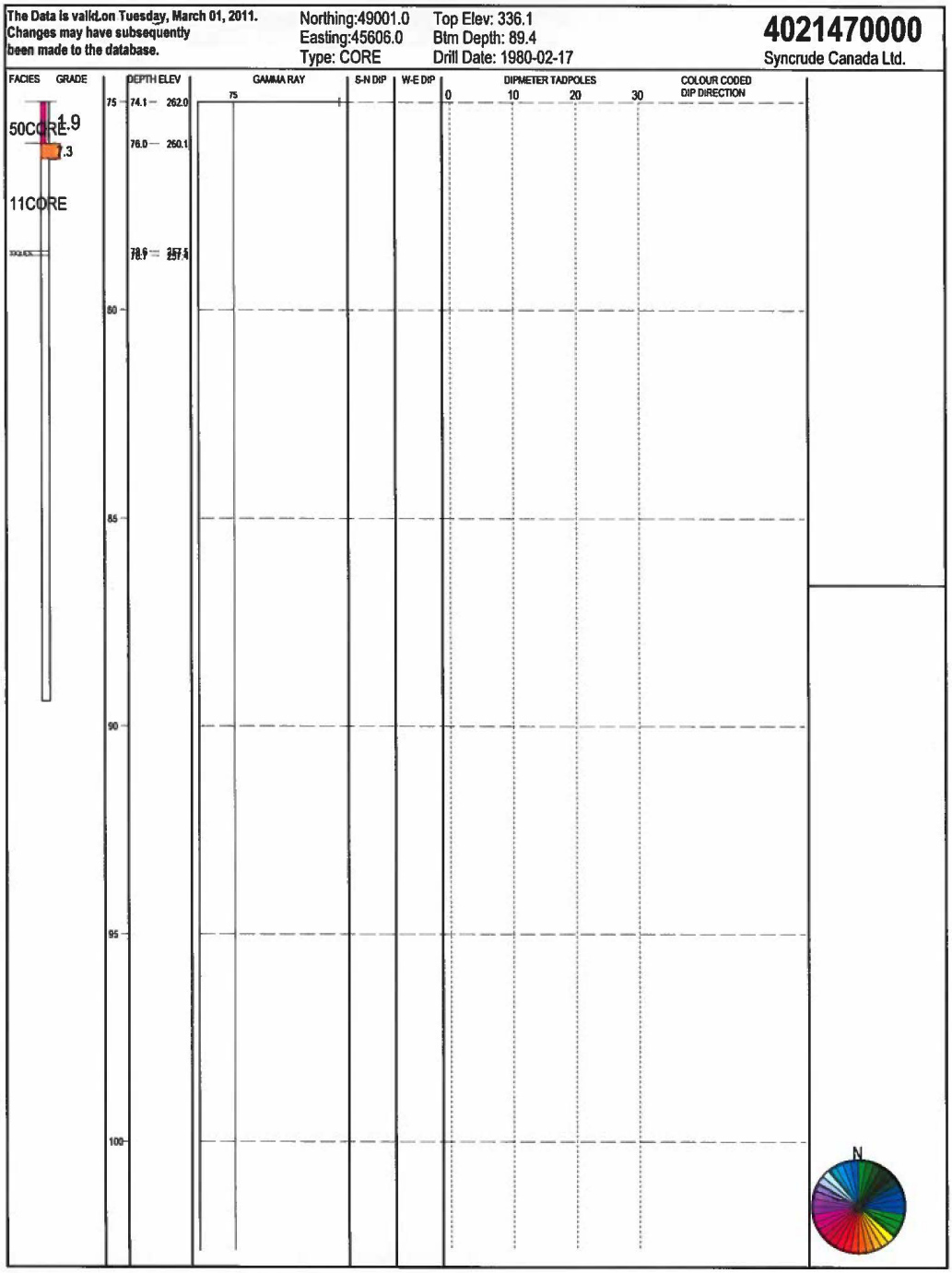
The Data is valid.on Tuesday, March 01, 2011.
Changes may have subsequently been made to the database.
Northing:49001.0
Easting:45606.0
Type: CORE
Top Elev: 336.1
Btm Depth: 89.4
Drill Date: 1980-02-17
4021470000
Syncrude Canada Ltd.
FACIES
GRADE
DEPTH ELEV
GAMMA RAY
S-N DIP
W-E DIP
DIPMETER TADPOLES
COLOUR CODED DIP DIRECTION
50CORE
11CORE
75
74.1
262.0
76.0
260.1
80
85
90
95
100
0
10
20
30
N

Syncrude
GEOTECHNICAL ENGINEERING (www.syncrude.com)

PROJECT #	
PROJECT:	BY
SUBJECT: SI/VP 080069R (SI replaced & additional tips added)	DATE / PAGE OF

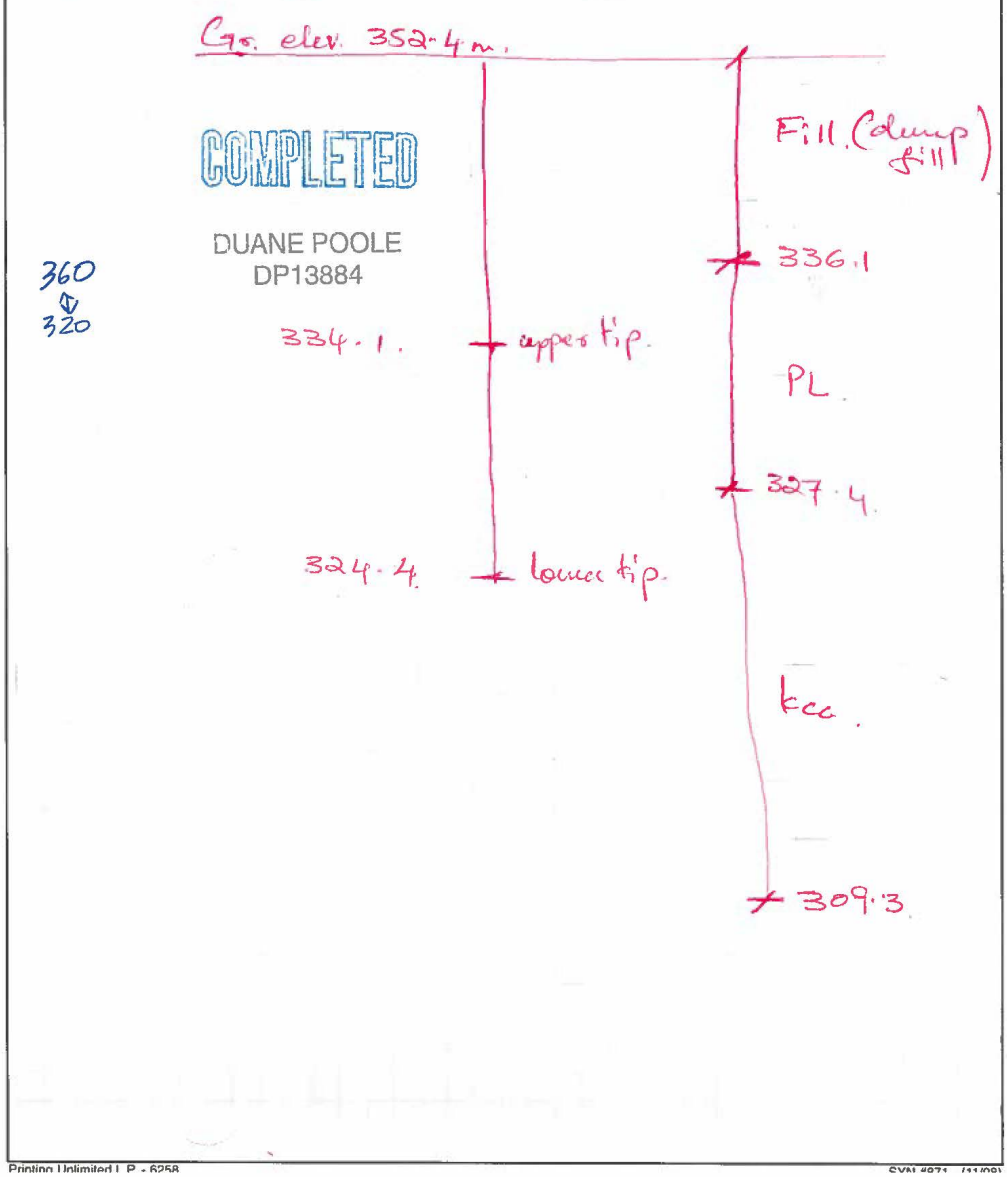

Printing Unlimited L.P. - 6258

Syncrude
Securing Canada's Energy Future
Geotechnical Division

Instrumentation Central File
Check List

Instrument no. SI/VP080046

	Office Documentation	Initials
☐	Request sheet and installation schematic	
☐	All email correspondence related to instrumented hole	
	Field Documentation	
☑	Borehole construction report sheet	EK
☑	Installation sheet including as-built information	EK
☑	Borehole sampling and test sheets	EK
	☑ SPT sheet SS	
	☐ Core log sheet CS	
	☐ Grab sample log sheet GS	
	☐ Auger sample sheet AS	
	☐ Other i.e. shelby TO/TP	
	☐ Gamma ray log report sheet	
	☑ Other log type Drill log	
☐	Field commissioning sheet	
	☐ SI initialization print out sets 1&2	
	☐ Field book readings	
☑	Photo copy of all calibration sheets including tip check sheet	EK
☐	Instrument extension sheet (vertical / horizontal)	
	☐ 1st extension	
	☐ 2nd extension	
	☐ 3rd extension	
	Lab Documentation	
☐	Copy of lab request sheet	
☐	Copy of lab test results	
☐	**Instrument abandonment sheet or decommissioning sheet**	

Geotechnical Instrumentation

Slope Inclinometer Casing
Vibrating Wire Piezometer Installation

Instrument Location (Structure): W1 Dump

Instrument Number (SI) 080046

Proposal Date: 3-Apr-08

Installation Date: June 25/08

Requestor: Duane Poole / Murray Danku

Monitor: DPrue

Proposed Coordinates:
- Northing 49270
- Easting 45575
- Elevation 367
- Azimuth 180

As-Built Coordinates:
- Northing
- Easting
- Elevation
- Azimuth

Design

Ground elevation: 367

meters
- 47.0 — 46.4/152 320 m — upper VP tip — serial number
- 59.0 — 58.4/191 308 m — middle VP tip — serial number
- 63.0 — 62.4/204 304 m — lower VP tip — serial number

Bottom of casing: 277 elev. / 90.4/293 90 m

276 elev. / 90.4/296' 91 m — Bottom of Hole

2nd's
U 45.7m
L 910' bttm
Spt@150
SpbE 190
SpbE 210'

210' SPT + 2nd ok'd by Duane P.

As- Built

367.33 Top Of Pipe elevation

366.4 Ground elevation (from survey stake)

Metal sondex ring strap 1" from top of inverted VWP

Metal sondex ring strap 1" from top of inverted VWP

Metal sondex ring strap 1" from top of inverted VWP

Bottom of casing: 270 elev. MM / 96.3 m

elev. MM / 96.3 m — Bottom of Hole — Total depth

NQ Sauger

Initialization date	
Casing cut-off	
Total Probe depth	ft
Probe no.	

Installation of Instrument Instructions:

Very hard drilled by crew.

Grout mix ratio: 1.0 Water : 1.0 Cement : 0.2 Bentonite (mix ratio is by weight)

Stage Grout required	Yes ☐ No ■	
Anchor Required	Yes ■ No ☐	
Settlement Rings	Yes ■ No ☐	(Every 10 feet)
Dry drilling required	Yes ☐ No ■	(Prevent Hydraulic fracturing)

Sampling Requirements

Type	Interval	from (m)	To (m)	Comments
SPT				Obtain a representative sample at each tip location. Sample size approx. 400g
Core (triple tube)				
Core (Split tube)				
Auger				
Other				

Drill Method

■ Dual Rotary	☐ Wet Rotary	☐ Air Rotary	☐ Auger	☐ Sonic
■ Casing and drill string only	☐ Open Hole	☐ Conventional	☐ Solid Stem	☐ Dry
☐ Auger flight with air-sub	☐ Cased hole	☐ Reverse Circulation	☐ Hollow Stem	☐ Wet

SIVP

mcrude

GEOTECHNICAL
Drilling & Instrumentation Installation
BOREHOLE CONSTRUCTION REPORT

Project / Structure: W1 Dump Hole No. SIVP0840046 Monitor: Bruce

Survey Stake Information: 49270 Northing 45575 Easting 3664 Ground Elevation

Contractor: Beck

Rig Type: Barlin DR-12

Rig Number: 46

Drill bit diameter: Walmar in.
Casing Depth: 96.3 m
Casing diameter: BOD in.
Shoe bit diameter: BOD in.
Total Drill Depth: 96.3 m

Drill Crew

Driller	☐	____ hours	Name	Ryan Neelson
Helper 1	☐	____ hours	Name	Ryan Moore
Helper 2	☐	____ hours	Name	Jared Lumbar
Other	☐	____ hours	Name	Eddy Helped it installed

Normen to end Sept 10:15

Drill Shiningtly

Drill Method

☒ Dual Rotary	☐ Wet Rotary	☐ Air Rotary	☐ Auger	☐ Sonic
☐ Dry	☐ Open Hole	☐ Conventional	☐ Solid Stem	☐ Dry
☐ Wet	☐ Cased hole	☐ Reverse Circulation	☐ Hollow Stem	☐ Wet
☐ Air-sub / Auger				

Drill Rig Operating Time

Date	Start Time (A)	Down Time (B)	Hours (A + B)	Description
	Total Hours	→		

Other Support Equipment

Date	Hours	Unit no.	Description
	Total Hours		

Inclinometer Installation Notes

Grout Mix Ratio:

water	cement	bentonite
1.0	1.0	.12

Material Used:

litres	# bags (25kg)	bag

Casing Stick-up

Cut-Off

Casing Type used:

☐

☐

Casing Size: ☒ 3.34" ☐ 2.75"

SI Anchor: ☒ Yes ☐ No

Bottom of Casing: 96.3

Bottom of hole: 96.3

Drilling Consumables

BCL Supplied	Driller Supplied	Amount / QTY	Installation Materials
☐	☐		Bags Cement
☐	☐	N/A	Bags Frac Sand
☐	☐		Bags Quick Gel
☐	☐	N/A	Bags Kim Mud
☐	☐	N/A	Bags of Bentonite Chips (Volclay)
☐	☐	N/A	Buckets of Coated Bentonite Pellets
☐	☐	340'	1" Length Grout Hose
☐	☐	33	Couplers
☒	☐	33	10' Casing Lengths installed

Description of other material and equipment used during installation

3 VP's also installed

Red @ 45.7, Yellow @ 57.9

Green @ 64m

Will Bring Grout up To 140' from surface

Grout to Surface Tomorrow.

This will avoid making Sip pressure

OK'd by Duane Poole.

Check List

☐ Yes	☒ No	Hole Topped up (bentonite chips)	Does area require additional remedial work	☐ Yes	☒ No
☐ Yes	☒ No	Hole Topped up (grout)	Is instrument in an active construction zone	☐ Yes	☒ No
☐ Yes	☐ No	Protective Conduit around leads	Quadro-pod labeled	☒ Yes	☐ No

Duane Poole
Mine Geotech
780 0834 / 780 8606

crew: Ryan Needham, Ryan Wade, Gord Dumba.

Normby this A.M. dropped off SI casing.

Syncrude

Geotechnical Drill Log

DATE YR/MO/DD	TIME From	TIME To	CONDITIONS	Drill Depth meter	Drill Depth feet	DESCRIPTION
08/06/24						Vezan Rig Rig Truck out + Clean Access
	10:00	12:00			70	
		3:10			150	First Spt Sample. chrotic Kc
	3:10	4:45			190'	Will do Spt in A.M.
08/06/25	8:30					Spt up Kc
						Cont. drill to next Spt location @ 210'/64m, OK'd by Duane Poole. Design proposed Spt @ 190+200' (Sip middle + upper) Zip only 10' apart.
		12:35			320'	1 D in outboard, Rubber Rolled 20' over shrinking no haul to T n in limestone. Ryan called before cont. dn hold. Talk to Duane about 20' and decided she was OK with that Andrew will still be in outboard.
	1:00	2:30				Trip inner Pipe + install SI + UP
	2:30					Start Trip Casing
		3:35				Casing pulled, help cleaning up tools
						wait for Norm to Island.

Slope Inclinometer
Commissioning Sheet

Instrument Location (Structure): W1 DUMP

Instrument Number (SI) 080046

Installation Date: _____

Monitor _____

Proposed Coordinates:
Northing _____
Easting _____
Elevation _____
Azimuth 180

Commissioning Date: AUG. 1/08

Monitor: D. WHEELER

As-Built Coordinates:
Northing 49269.28
Easting 45573.04
Elevation
Azimuth 178 (35° OFFSET)

Survey As-built (Top Of Pipe)

Survey Request No. 81072

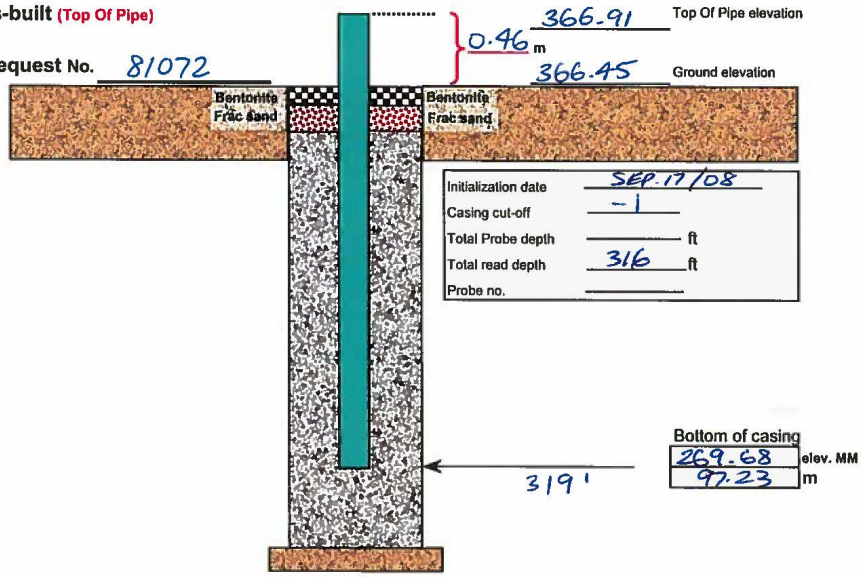

Final Check List:

Grout Settlement	☑ Yes	☐ No	Quadro-pod Labeled	☑ Yes	☐ No
Depth of Settlement	_____ m		End Cap on Casing	☑ Yes	☐ No
Hole Topped up	☑ Yes	☐ No			
Grout	_____ Volume		Does Area require		
Frac Sand	_____ No. Bags		remedial work	☐ Yes	☑ No
Bentonite	_____ No. Bags				

Comments:

Slope Inclinometer
Extension Sheet

Instrument Location (Structure): W1 DUMP

Instrument Number (SI) 080046

Installation Date: _____

Monitor _____

Proposed Coordinates:
Northing _____
Easting _____
Elevation _____
Azimuth _____

Extension Date: AUG-5/10

Monitor: D. WHEELER

As-Built Coordinates:
Northing _____
Easting _____
Elevation _____
Azimuth _____

Survey As-built (Top Of Pipe)
Request No. _____

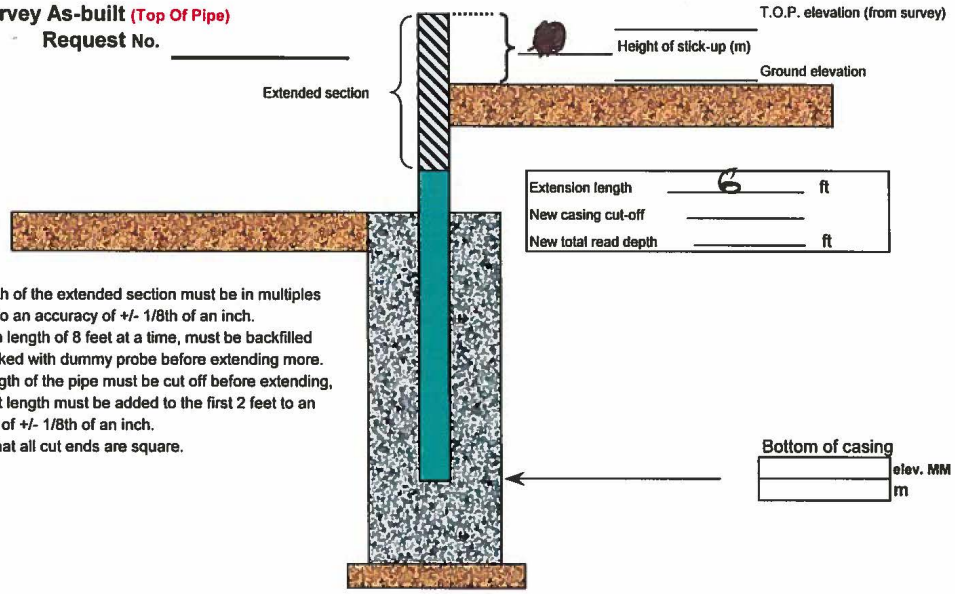

1. The length of the extended section must be in multiples of 2 feet to an accuracy of +/- 1/8th of an inch.
2. Maximum length of 8 feet at a time, must be backfilled and checked with dummy probe before extending more.
3. If any length of the pipe must be cut off before extending, that exact length must be added to the first 2 feet to an accuracy of +/- 1/8th of an inch.
4. Ensure that all cut ends are square.

Summary Check List:

Length of extended section	☑ Yes	☐ No	Quadro-pod Labeled	☑ Yes	☐ No
Height of stick-up	☐ Yes	☑ No	End Cap on Casing	☑ Yes	☐ No
Field book updated	☑ Yes	☐ No	Remedial work required	☐ Yes	☑ No
Database updated	☑ Yes	☐ No	As-built survey request	☐ Yes	☑ No
Original copy in central files	☑ Yes	☐ No			

Comments:

Slope Inclinometer
Extension Sheet

Instrument Location (Structure): W1 DUMP

Instrument Number (SI) 080046

Installation Date: _____

Monitor _____

Proposed Coordinates:
Northing 49269.
Easting 45573
Elevation 366
Azimuth _____

Extension Date: AUG. 5/10

Monitor: D. WHEELER

As-Built Coordinates:
Northing 49269.32
Easting 45573.09
Elevation 368.65
Azimuth 178°

Survey As-built (Top Of Pipe)
Request No. 110596

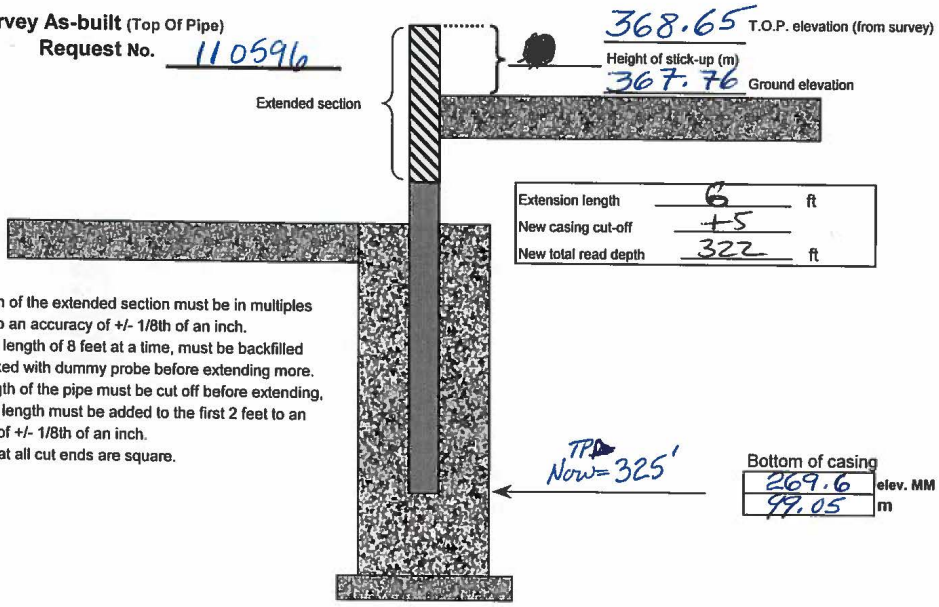

1. The length of the extended section must be in multiples of 2 feet to an accuracy of +/- 1/8th of an inch.
2. Maximum length of 8 feet at a time, must be backfilled and checked with dummy probe before extending more.
3. If any length of the pipe must be cut off before extending, that exact length must be added to the first 2 feet to an accuracy of +/- 1/8th of an inch.
4. Ensure that all cut ends are square.

Summary Check List:

Length of extended section	☑ Yes	☐ No	Quadro-pod Labeled	☑ Yes	☐ No
Height of stick-up	☐ Yes	☑ No	End Cap on Casing	☑ Yes	☐ No
Field book updated	☑ Yes	☐ No	Remedial work required	☐ Yes	☑ No
Database updated	☑ Yes	☐ No	As-built survey request	☑ Yes	☑ No
Original copy in central files	☑ Yes	☐ No			

Comments:
Survey Request submitted Mar 2/11 By K. DeCourville

Slope Inclinometer Casing
Vibrating Wire Piezometer Installation

Instrument Location (Structure): W1 Dump

Instrument Number (SI) 080046

Proposal Date: 3-Apr-08

Requestor: Duane Poole / Murray Danku

Proposed Coordinates:
Northing 49270
Easting 45575
Elevation 367
Azimuth 180

Installation Date: _____

Monitor: _____

As-Built Coordinates:
Northing _____
Easting _____
Elevation
Azimuth _____

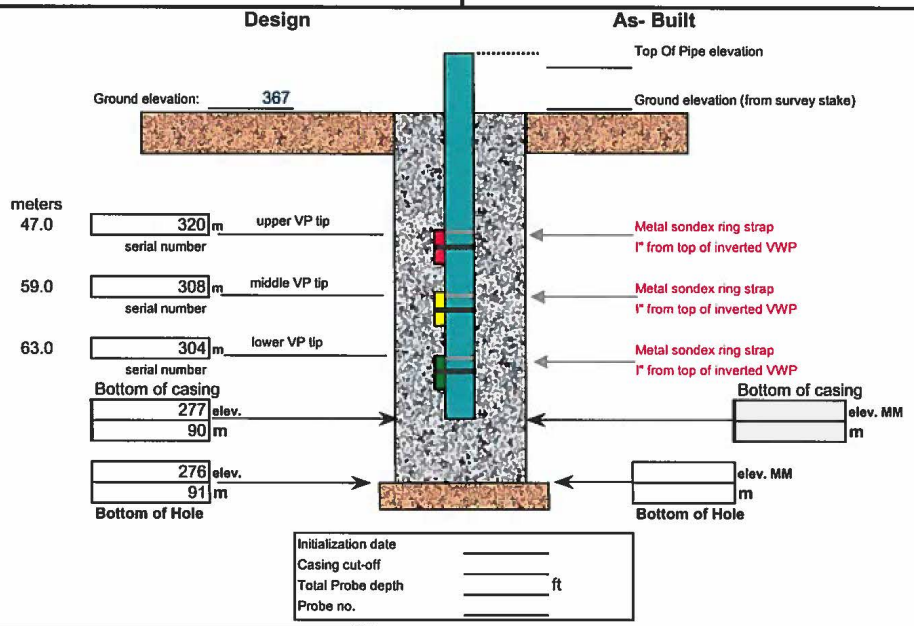

Installation of Instrument Instructions:

Grout mix ratio 1.0 Water 1.0 Cement 0.2 Bentonite
mix ratio is by weight

Stage Grout required	Yes ☐	No ■	
Anchor Required	Yes ■	No ☐	
Settlement Rings	Yes ■	No ☐	(Every 10 feet)
Dry drilling required	Yes ☐	No ■	(Prevent Hydraulic fracturing)

Sampling Requirements

Type	Interval	from (m)	To (m)	Comments
SPT				Obtain a representative sample at each tip location. Sample size approx. 400g
Core (triple tube)				
Core (Split tube)				
Auger				
Other				

Drill Method

■ **Dual Rotary**	☐ **Wet Rotary**	☐ **Air Rotary**	☐ **Auger**	☐ **Sonic**
■ Casing and drill string only	☐ Open Hole	☐ Conventional	☐ Solid Stem	☐ Dry
☐ Auger flight with air-sub	☐ Cased hole	☐ Reverse Circulation	☐ Hollow Stem	☐ Wet

Vibrating Wire Piezometer

Commissioning Sheet

Instrument Location (Structure): W1 Dump

Instrument Number (VP) 080046

Installation Date: _____

Requestor: _____

Proposed Coordinates:
Northing _____
Easting _____
Elevation _____

Commissioning date Aug 1/08

Monitor: David Forrest

As-Built Coordinates:
Northing 49269.28
Easting 45573.04
Elevation 366.91 (TOP.)

As- Built

Survey Request no. 81072

Note: Survey will always pick Top of Pipe or conduit. Measure stick-up of conduit to calculate ground elevation

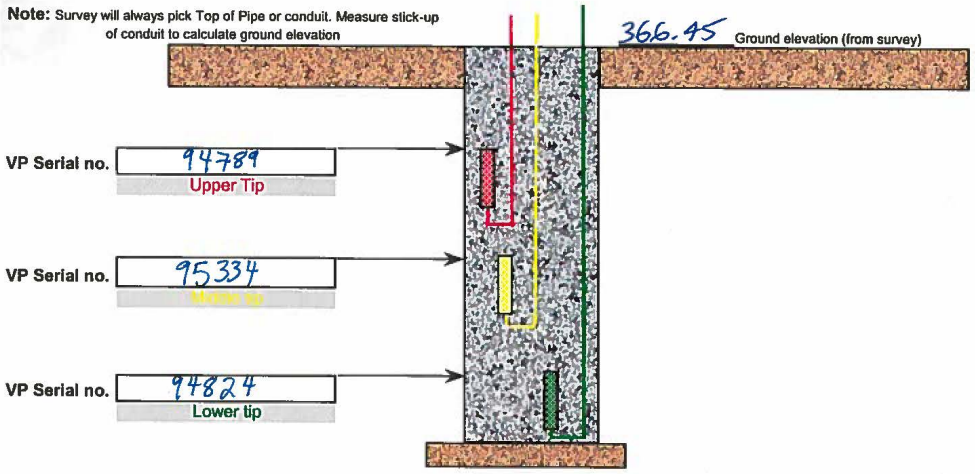

Daily Instrument Readings until Stabilized

Date	Rdg Hz²/Therm.	Date	Rdg Hz²/Therm.	Date	Rdg Hz²/Therm.	Date	Rdg Hz²/Therm.	Date	Rdg Hz²/Therm.
	u		u		u		u		u
	m		m		m		m		m
	L		L		L		L		L
Date	Rdg Hz²/Therm.	Date	Rdg Hz²/Therm.	Date	Rdg Hz²/Therm.	Date	Rdg Hz²/Therm.	Date	Rdg Hz²/Therm.
	u		u		u		u		u
	m		m		m		m		m
	L		L		L		L		L

Check List

- ☑ **Hole Topped up** (bentonite chips)
- ☐ **Protective Conduit** around leads
- ☑ Quadro-pod labeled

Does area require additional remedial work ☐ Yes ☑ No
Is instrument in an active construction zone ☑ Yes ☐ No
Access ☑ good ☐ poor

Comments:

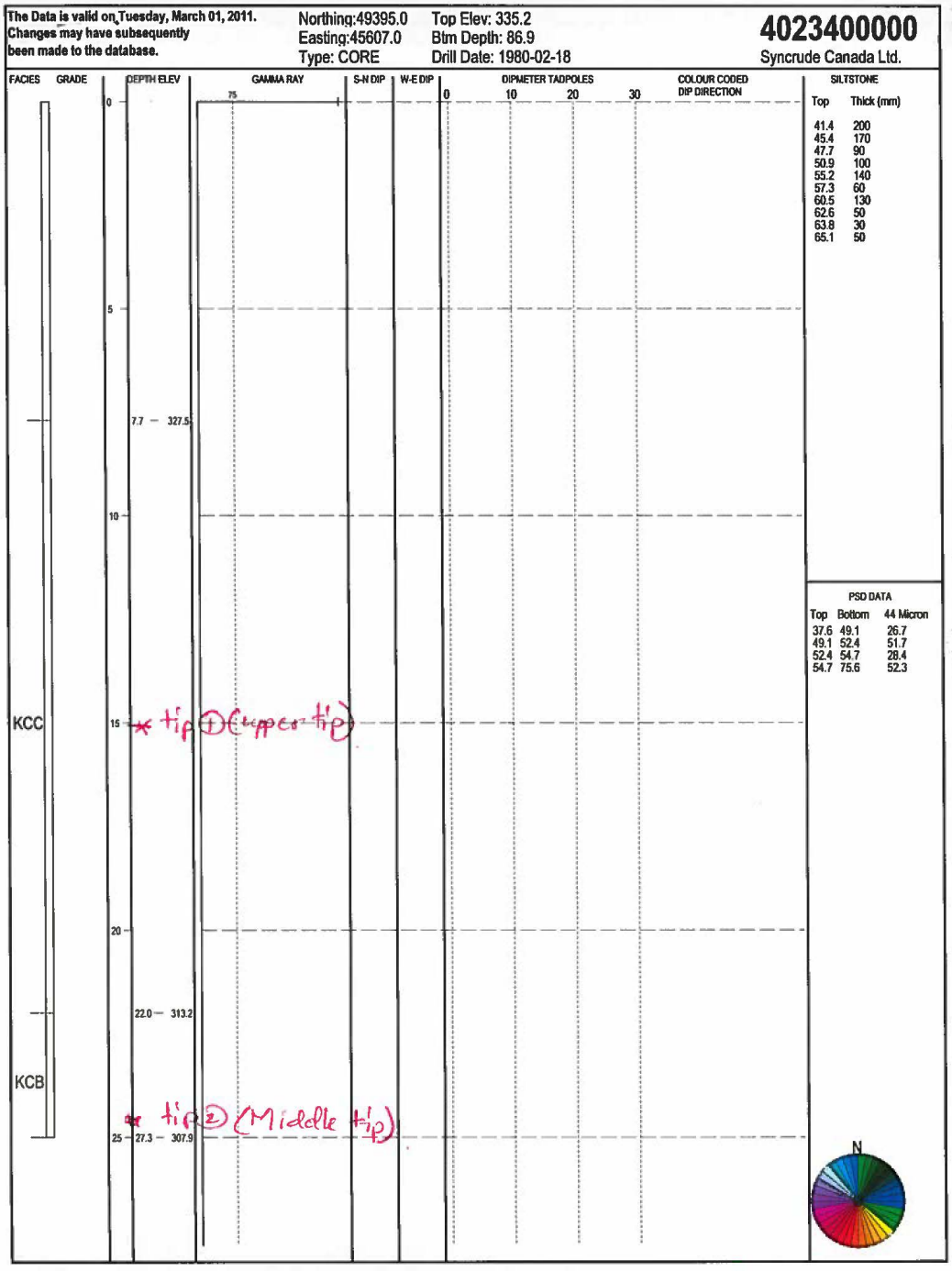
The Data is valid on Tuesday, March 01, 2011.
Changes may have subsequently been made to the database.
Northing:49395.0
Easting:45607.0
Type: CORE
Top Elev: 335.2
Btm Depth: 86.9
Drill Date: 1980-02-18
4023400000
Syncrude Canada Ltd.
FACIES
GRADE
DEPTH ELEV
GAMMA RAY
S-N DIP
W-E DIP
DIPMETER TADPOLES
COLOUR CODED DIP DIRECTION
SILTSTONE
Top Thick (mm)
41.4 200
45.4 170
47.7 90
50.9 100
55.2 140
57.3 60
60.5 130
62.6 50
63.8 30
65.1 50
PSD DATA
Top Bottom 44 Micron
37.6 49.1 26.7
49.1 52.4 51.7
52.4 54.7 28.4
54.7 75.6 52.3
KCC
KCB
7.7 — 327.5
22.0 — 313.2
27.3 — 307.9
tip 1 (Upper tip)
tip 2 (Middle tip)
N

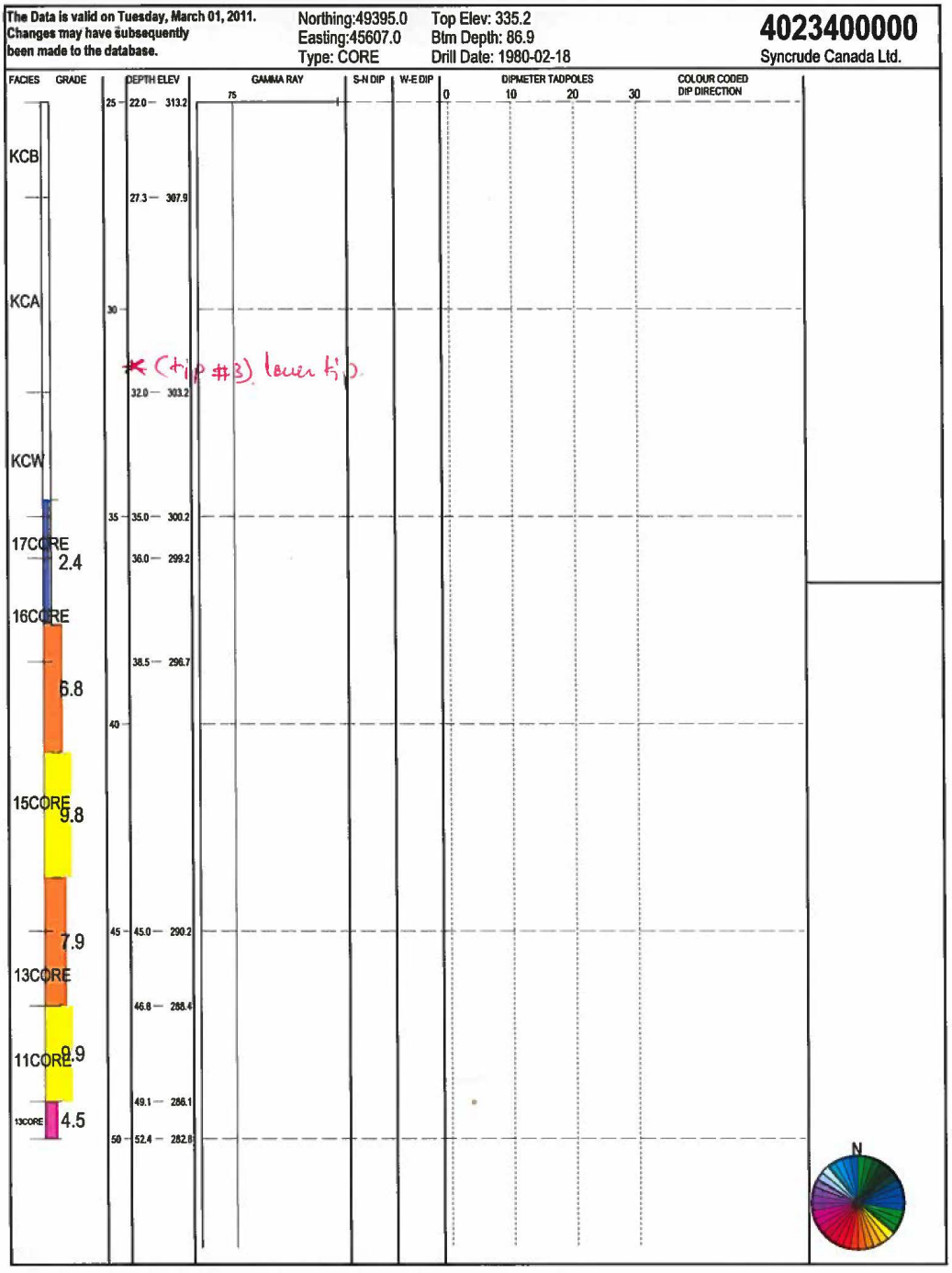
The Data is valid on Tuesday, March 01, 2011.
Changes may have subsequently been made to the database.
Northing:49395.0
Easting:45607.0
Type: CORE
Top Elev: 335.2
Btm Depth: 86.9
Drill Date: 1980-02-18
4023400000
Syncrude Canada Ltd.
FACIES
GRADE
DEPTH ELEV
GAMMA RAY
S-N DIP
W-E DIP
DIPMETER TADPOLES
COLOUR CODED DIP DIRECTION
KCB
KCA
KCW
17CORE
2.4
16CORE
6.8
15CORE
9.8
7.9
13CORE
11CORE
9.9
13CORE
4.5
22.0 313.2
27.3 307.9
32.0 303.2
35.0 300.2
36.0 299.2
38.5 296.7
45.0 290.2
46.8 288.4
49.1 286.1
52.4 282.8
* (tip #3) lower tip
N

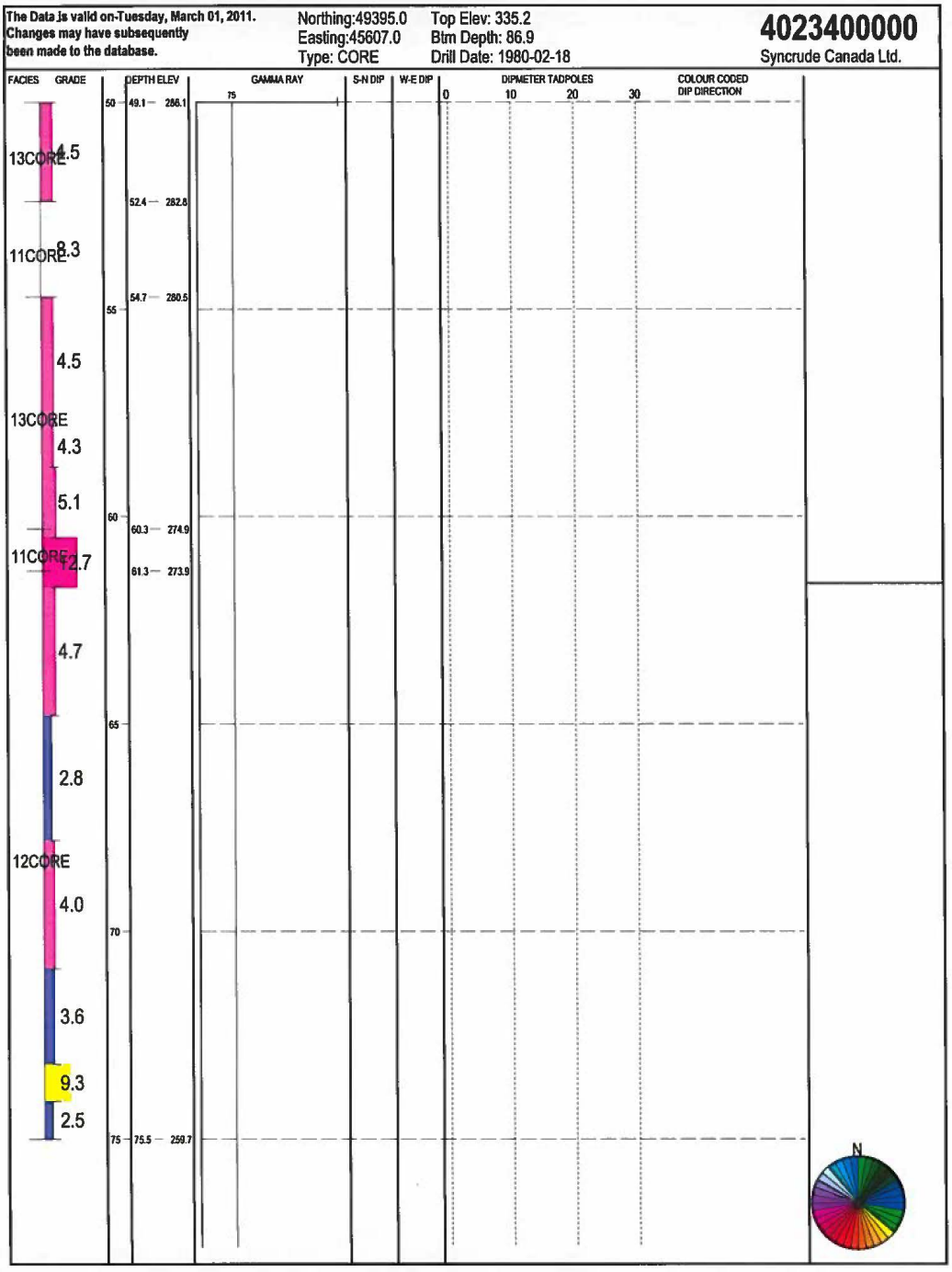
The Data is valid on-Tuesday, March 01, 2011.
Changes may have subsequently been made to the database.
Northing:49395.0
Easting:45607.0
Type: CORE
Top Elev: 335.2
Btm Depth: 86.9
Drill Date: 1980-02-18
4023400000
Syncrude Canada Ltd.
FACIES
GRADE
DEPTH ELEV
GAMMA RAY
S-N DIP
W-E DIP
DIPMETER TADPOLES
COLOUR CODED DIP DIRECTION
13CORE
4.5
11CORE
8.3
4.5
13CORE
4.3
5.1
11CORE
12.7
4.7
2.8
12CORE
4.0
3.6
9.3
2.5
50
49.1 — 286.1
52.4 — 282.8
54.7 — 280.5
55
60
60.3 — 274.9
61.3 — 273.9
65
70
75
75.5 — 259.7
75
0
10
20
30
N

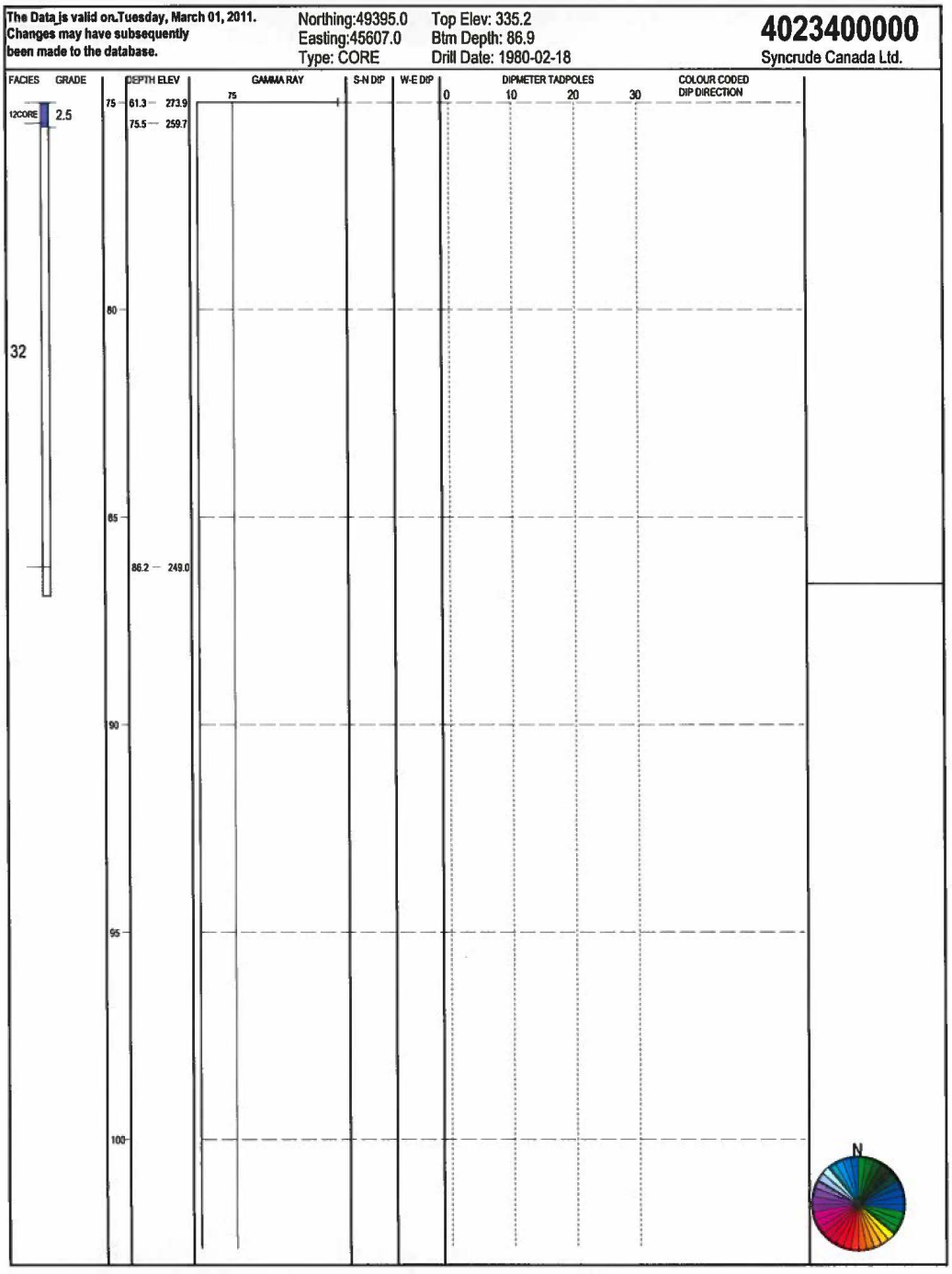
The Data is valid on:Tuesday, March 01, 2011.
Changes may have subsequently been made to the database.
Northing:49395.0
Easting:45607.0
Type: CORE
Top Elev: 335.2
Btm Depth: 86.9
Drill Date: 1980-02-18
4023400000
Syncrude Canada Ltd.
FACIES
GRADE
DEPTH ELEV
GAMMA RAY
S-N DIP
W-E DIP
DIPMETER TADPOLES
COLOUR CODED DIP DIRECTION
12CORE
2.5
32
75
61.3 — 273.9
75.5 — 259.7
80
85
86.2 — 249.0
90
95
100
0
10
20
30
N

Ryan notes
Bead Number

SYNCRUDE CANADA LTD FIELD BOREHOLE LOG

SYNCRUDE CANADA LTD
EOTECHNICAL ENGINEERING

PROJECT:

BOREHOLE NO. : SIUP080046

PAGE 1 OF

BOREHOLE LOC. (m) 49270 N 45575 E

RIG TYPE: DR-12 Barber

DATE DRILLED: June 24 - 25TH

ROUND ELEV (m) 366.4 CASING ELEV (m)

CONTRACTOR: Beck

HAMMER WEIGHT (lbs) 140LBS

SAMPLE CONDITION: LOST DISTURBED GOOD FAIR POOR

DROP (in): 18

SAMPLE TYPE: A.S. - AUGER P.B - PITCHER BRL. T.O. - THIN WALLED OPEN D.C. - DYNAMIC CONE G.S. - GRAB SAMPLE
C.S. - CORE S.S. - SPLIT SPOON T.P. - THIN WALLED PISTON S.C. - STATIC CONE

TOTAL DEPTH (ft)

LOGGED BY: J. Bruce

DRILL INTERVAL		SAMPLE/LOG INTERVAL		SAMPLE TYPE	SPT BLOWS 0-6" A	SPT BLOWS 6-12" B	SPT BLOWS 12-18" C	SPT BLOWS N B+C	PENETRATION TOTAL LENGTH (inches)	RECOVERY WORDS ALLOWED (inches)	SAMPLE CONDITION	SAMPLE NUMBER	STRATIGRAPHY & PIEZO TIPS	DESCRIPTION
(ft)	(ft)	(ft)	(ft)	SS	BLOWS	BLOWS	BLOWS	BLOWS						Group name, gradation, colour, moisture, bitumen, consistency or compactness, plasticity, structure, local name, other - detailed clay layer description
0	150	150	151.5	SS	26	19/4"	R	19	9	6		160843	Upper Tip	Kc clay, Dark brn/grey clay in light to medium clay, Soft Tenacious, Trace Siltstone / Shale fragments in Shear, Very Stiff, moderate to high plastic, Drilled & Refusal @ 19 Blows from 6-12", Natural, Soil Boundary, moist
150	190	190	191.5			55/6"	R	R	6"	6"		160844	Mid Tip	Kc clay, med. to Dark brn/grey, Silty Tenacious, Very hard, low plastic, moist
190	210	210	211.5			5"/5"			5"	5"		160751	Low Tip	Calcareous F.G. Silty, Brown to Black, Very dense, moist, minor clay beds, moist, Low Grade.
210														

Insitu

NOTES: (gas, water level, weather, drilling rates, site notes, location, ...)

V2.7

Syncrude
GEOTECHNICAL ENGINEERING (www.syncrude.com)

PROJECT:	BY	
SUBJECT: SI/VP 080046	DATE	PAGE OF

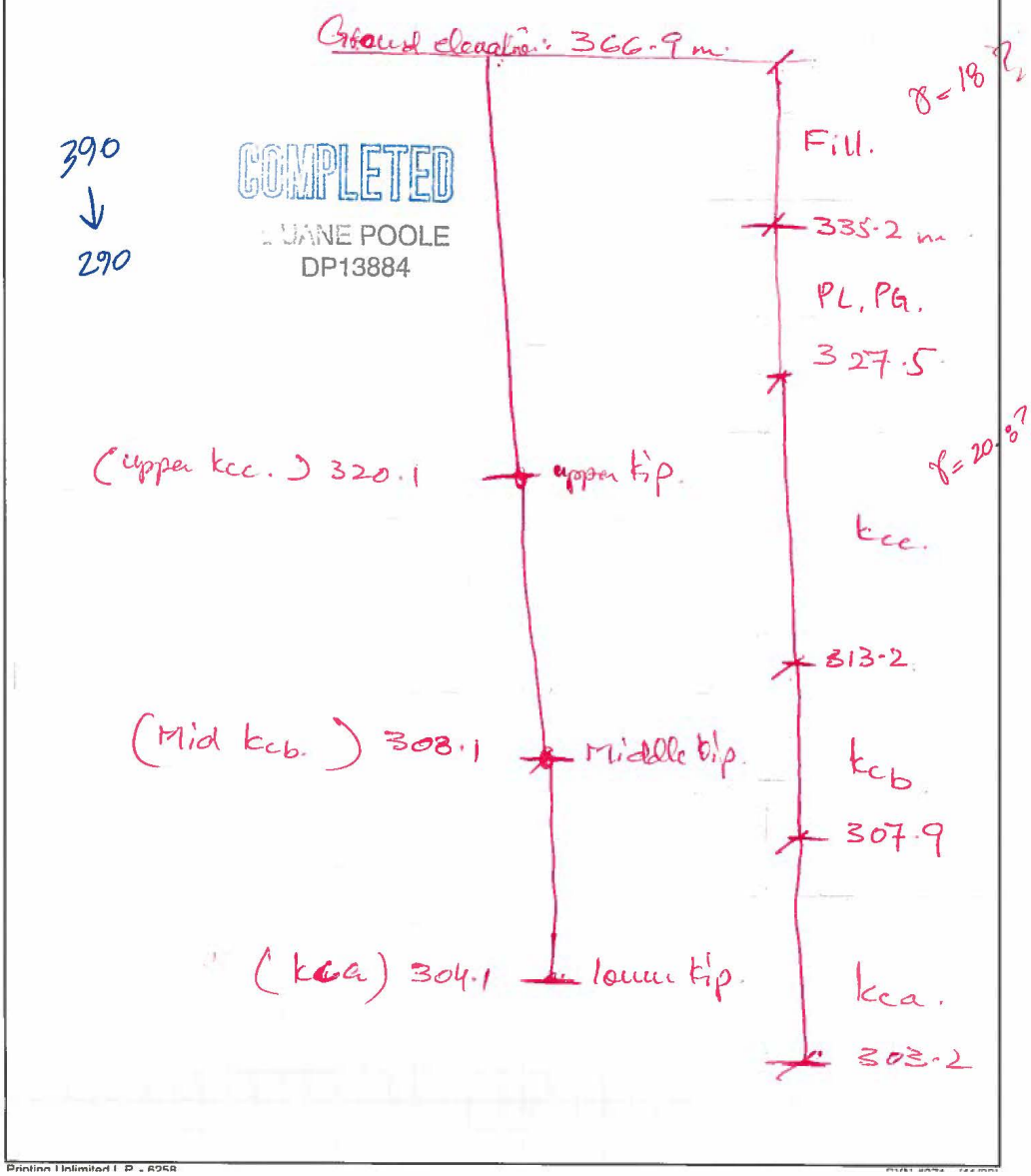

APPENDIX B – EDDY COVARIANCE INSTRUMENTATION DETAILS

(This statement provided by Dr. Sean Carey)

A CSAT3 sonic anemometer (Campbell Scientific Ltd., Logan, UT (CSI)) and an open-path infrared gas analyzer (LI-7500, LI-COR) were mounted 6.9 m above the surface and logged at 10 Hz to a CR3000 data logger (CSI). Calculations of friction velocity (u*), sensible and latent heat fluxes (H and LE) were carried out on the logger using ambient air temperature and pressure measurements. ET was calculated from latent heat fluxes and the latent heat of vaporization using measured air temperature.

High frequency data collected by the CR3000 were processed by means of Eddy Pro software (v 5.2.1, LI-COR) using 30-min bulk averaging, the maximization of the covariance with a default time delay, Moncrief spectral corrections, coordinate rotation in two dimensions, no self-heating correction on the LI-7500, and de-spiking. All data underwent a QA/QC procedure using Matlab (v 8.6, Mathworks, USA). Measurements were removed when they were associated with equipment malfunction, rain events which obstructed the open-path gas analyzer windows, statistics of eddy covariance input variables were outside of a reasonable value range, or when computed fluxes were greater than three standard deviations from the monthly daytime or nighttime average for a trace. The midday growing season flux footprint representing 90 % of the flux source area is on average 130 ± 2 m (± 1 SE). The predominant wind direction is southwest (180 ° - 210 °). Small gaps (up to two half-hour measurements) in the LE and H energy fluxes were filled using linear interpolation. Larger gaps were filled using a linear relationship between LE and net radiation (Rn) with a subsequent adjustment using a data window of 100 half-hour measurements incremented in steps of 20 half-hour measurements to adjust for seasonality.

APPENDIX C – WEATHER STATION DETAILS

(This statement provided by Amy Heidman – O'Kane Consultants)

[OKC has] weather stations in SWSS Cell 32 and 46. Each have one of each of these sensors:

- HMP45C air temperature / relative humidity sensor with radiation shield
- R.M. Young Model 05103 wind monitor
- NR-Lite net radiometer
- TE525 tipping bucket rain gauge, resolution 0.254 mm/tip
- SR50 sonic ranging sensor to measure snow height

All sensors were purchased with Campbell Scientific Canada.

APPENDIX D - SWSS CROSS SECTION

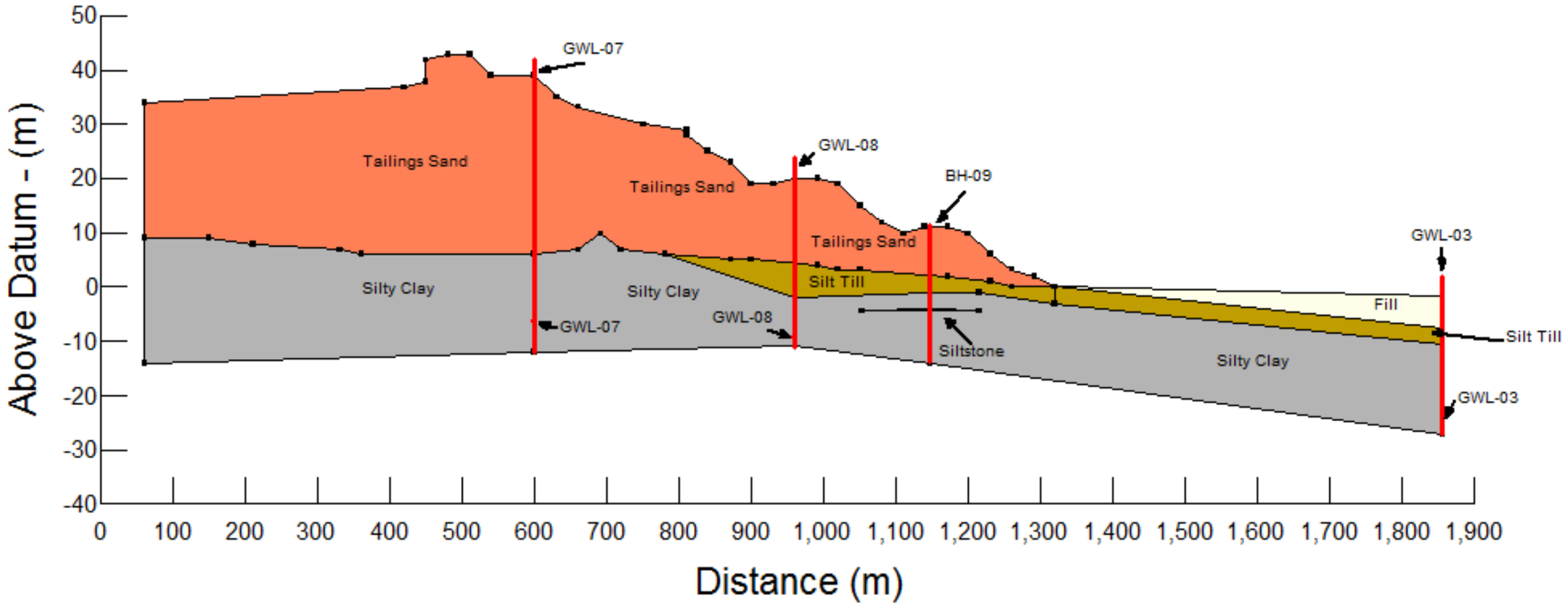
Above Datum - (m)
50
40
30
20
10
0
-10
-20
-30
-40
0
100
200
300
400
500
600
700
800
900
1,000
1,100
1,200
1,300
1,400
1,500
1,600
1,700
1,800
1,900
Distance (m)
GWL-07
GWL-08
BH-09
GWL-03
Tailings Sand
Tailings Sand
Tailings Sand
Silty Clay
Silty Clay
Silty Clay
Silt Till
Fill
Silt Till
Siltstone
GWL-07
GWL-08
GWL-03